UNIVERSIDADE ESTADUAL DE CAMPINAS

FACULDADE DE CIÊNCIAS MÉDICAS

JEANY DELAFIORI

ALTERAÇÕES METABÓLICAS INDUZIDAS PELO VÍRUS DA ZIKA EM CÉLULAS DA PRÓSTATA: METABOLÔMICA E POTENCIAL ONCOLÍTICO

METABOLIC ALTERATIONS INDUCED BY ZIKA VIRUS IN PROSTATE CELLS: METABOLOMICS AND ONCOLYTIC POTENTIAL

CAMPINAS

2022

JEANY DELAFIORI

ALTERAÇÕES METABÓLICAS INDUZIDAS PELO VÍRUS DA ZIKA EM CÉLULAS DA PRÓSTATA: METABOLÔMICA E POTENCIAL ONCOLÍTICO

METABOLIC ALTERATIONS INDUCED BY ZIKA VIRUS IN PROSTATE CELLS: METABOLOMICS AND ONCOLYTIC POTENTIAL

Tese apresentada à Faculdade de Ciências Médicas da Universidade Estadual de Campinas como parte dos requisitos exigidos para a obtenção do título de Doutora em Ciências.

Thesis presented to the School of Medical Sciences from the University of Campinas as part of the requisites to obtain the title of Ph.D. in Sciences

ORIENTADOR: RODRIGO RAMOS CATHARINO

ESTE TRABALHO CORRESPONDE À VERSÃO
FINAL DA TESE DEFENDIDA PELA
ALUNA JEANY DELAFIORI, E ORIENTADA PELO
PROF. DR. RODRIGO RAMOS CATHARINO.

CAMPINAS

2022

Ficha catalográfica
Universidade Estadual de Campinas
Biblioteca da Faculdade de Ciências Médicas
Maristella Soares dos Santos - CRB 8/8402

D371a

Delafiori, Jeany, 1993-
Alterações metabólicas induzidas pelo vírus da Zika em células da próstata : metabolômica e potencial oncolítico / Jeany Delafiori. – Campinas, SP : [s.n.], 2022.

Orientador: Rodrigo Ramos Catharino.
Tese (doutorado) – Universidade Estadual de Campinas, Faculdade de Ciências Médicas.

1. Espectrometria de massas. 2. Metabolômica. 3. Zika virus. 4. Próstata. 5. Neoplasias. 6. Metabolismo dos lipídeos. I. Catharino, Rodrigo Ramos, 1977-. II. Universidade Estadual de Campinas. Faculdade de Ciências Médicas. III. Título.

Informações Complementares

Título em outro idioma: Metabolic alterations induced by Zika virus in prostate cells : metabolomics and oncolytic potential
Palavras-chave em inglês:
Mass spectrometry
Metabolomics
Zika virus
Prostate
Neoplasms
Lipid metabolism
Área de concentração: Fisiopatologia Médica
Titulação: Doutora em Ciências
Banca examinadora:
Rodrigo Ramos Catharino [Orientador]
William Marciel de Souza
Daisy Machado
Catarina Raposo Dias Carneiro
Daniel Fabio Kawano
Data de defesa: 25-11-2022
Programa de Pós-Graduação: Fisiopatologia Médica

Identificação e informações acadêmicas do(a) aluno(a)
- ORCID do autor: https://orcid.org/0000-0003-2481-0465
- Currículo Lattes do autor: http://lattes.cnpq.br/9913984857291706

COMISSÃO EXAMINADORA DA DEFESA DE DOUTORADO

JEANY DELAFIORI

ORIENTADOR: RODRIGO RAMOS CATHARINO

MEMBROS TITULARES:

1. PROF. DR. RODRIGO RAMOS CATHARINO

2. PROF. DR. WILLIAM MARCIEL DE SOUZA

3. PROFA. DRA. DAISY MACHADO

4. PROFA. DRA. CATARINA RAPOSO DIAS CARNEIRO

5. PROF. DR. DANIEL FABIO KAWANO

Programa de Pós-Graduação em Fisiopatologia Médica da Faculdade de Ciências Médicas da Universidade Estadual de Campinas.

A ata de defesa com as respectivas assinaturas dos membros encontra-se no SIGA/Sistema de Fluxo de Dissertação/Tese e na Secretaria do Programa da FCM.

Data de Defesa: 25/11/2022

DEDICATÓRIA

Aos meus pais,

Edson Delafiori e Santina Pereira Delafiori,

meu eterno amor e gratidão.

AGRADECIMENTOS

Agradeço à **Deus** por iluminar meu caminho.

À toda minha família, em especial meus pais, **Edson** e **Santina**, e meu irmão **Jean**, por me incentivarem desde sempre e proporcionarem todo o carinho e apoio emocional necessários nessa jornada.

Ao meu amigo e esposo, meu amor, **Mayko**, por ser porto-seguro quando me faltava ânimo e confiança, por estar presente em todos os momentos sendo paciente e prestativo.

Ao **Prof. Dr. Rodrigo Ramos Catharino**, por me acolher no Laboratório Innovare desde 2013. Obrigada pela confiança, por me ouvir e aconselhar nos momentos certos e proporcionar uma vivência completa do que é ciência, a qual vai muito além do disposto nesta tese.

Aos amigos do Laboratório Innovare de Biomarcadores por proporcionarem um ambiente leve, alegre e de partilha. Obrigada **Diogo**, **Flávia**, **Arthur**, **Geovana**, **Estela**, **Carlos**, **Tatiane**, **Cibele**, **Mônica** e **Mohamed** pelos anos de convivência, ensinamentos, discussões e conselhos.

Ao **Me. Luiz Navarro** e à **Dra. Alessandra Faria** pelo companheirismo e ajuda em planejamentos, experimentos, análise de dados e reflexões. A todos os **colaboradores** deste trabalho, em especial **Profa. Dra. Carmen Veríssima Ferreira-Halder**, **Prof. Dr. José Luiz Proença-Módena**, **Prof. Dr. Marcelo Lancellotti**, **Dra. Ana Lúcia Tasca Gois Ruiz**, **Profa. Dra. Estela de Oliveira Lima** que ofereceram a infraestrutura de seus laboratórios e expertises permitindo a execução desta tese.

Ao **Dr. Theodore Alexandrov** e a todo **A-team** do *European Molecular Biology Laboratory* pela oportunidade e por me ensinarem tanto em tão pouco tempo, proporcionando meu crescimento profissional e contribuindo indiretamente na elaboração deste trabalho.

Por fim, agradeço o apoio da **Coordenação de Aperfeiçoamento de Pessoal de Nível Superior – Brasil (CAPES)** Código de Financiamento 001, e da **Fundação de Amparo a Pesquisa do Estado de São Paulo (FAPESP)** Bolsa no país processo n° 2019/05718-3 na concretização deste trabalho.

RESUMO

O vírus da Zika (ZIKV) é um flavivírus da família *Flaviviridae*. No período de 2015 a 2016 ocorreu a introdução da infecção por ZIKV nas Américas e nas ilhas do Pacífico, sendo a epidemia associada a complicações neurológicas, como a síndrome de Guillain-Barré e a síndrome congênita associada à infecção pelo vírus Zika. Dada a importância clínica e epidemiológica do ZIKV, estudos são necessários para a elucidação dos mecanismos de infecção celular pelo ZIKV. Em células de alta proliferação, como células progenitoras neurais, glioblastoma e neuroblastoma, o ZIKV promove efeito antiproliferativo, sendo sugerido o potencial oncolítico desse arbovírus na intervenção tumoral. Adicionalmente, o ZIKV apresenta tropismo por células do sistema reprodutor masculino, em especial células da próstata permissíveis à infecção persistente, sugerindo a próstata como reservatório de replicação viral e potencial implicância na infertilidade masculina durante a infecção. A persistência da replicação viral em células epiteliais da próstata resulta em significativas alterações no transcriptoma celular. Entretanto, novas investigações são necessárias para determinar a influência da infecção persistente pelo ZIKV no metaboloma celular. Considerando a característica patogênica multifatorial da infecção pelo ZIKV, o presente estudo propôs utilizar uma abordagem metabolômica não-direcionada na investigação das alterações metabólicas induzidas pelo ZIKV em células da próstata, buscando a identificação de marcadores de infecção persistente e elucidação do seu potencial oncolítico. Observou-se que o ZIKV afeta de maneira diferente a viabilidade e o metabolismo de células normais (PNT1a) e tumorais da próstata (PC-3), sendo as células PC-3 mais suscetíveis à inibição de crescimento. Em termos metabólicos há alterações em marcadores lipídicos que explicam o efeito antiproliferativo do ZIKV em células PC-3. A infecção persistente em células PNT1a é mediada por alterações nos níveis de glicerolipídios, acilcarnitinas, ácidos graxos, oxilipinas, e pequenos metabólitos resultantes do estresse oxidativo que agem como mediadores de progressão tumoral. A biogênese e o metabolismo lipídico são aspectos importantes na infecção viral, e a perturbação desse metabolismo mostra-se fundamental no resultado da infecção nos tipos celulares analisados demonstrando a dualidade no uso do ZIKV como agente antitumoral.

Palavras-chave: Espectrometria de massas; Metabolômica; Zika virus; Próstata; Neoplasias; Metabolismo dos lipídeos.

ABSTRACT

The Zika virus (ZIKV) is a flavivirus of the *Flaviviridae* family. From 2015 to 2016, the infection was introduced into the Americas and Pacific islands, and the epidemic was associated with neurological complications such as Guillain-Barré syndrome and Congenital Zika syndrome. Given ZIKV clinical and epidemiological importance, studies are necessary to clarify the mechanisms of cellular infection. In highly proliferative cells, such as neural progenitor cells, glioblastoma, and neuroblastoma, ZIKV promotes an antiproliferative effect, suggesting the potential oncolytic effect of this arbovirus in tumor intervention. Additionally, ZIKV has tropism for male reproductive system cells, especially prostate cells that are permissive to persistent infection, suggesting the prostate as a viral replication reservoir and potential implication in male infertility during infection. Persistent ZIKV replication in prostate epithelial cells results in significant changes in cell transcriptome. However, further research is needed to determine the influence of persistent ZIKV infection on the cellular metabolome. Given the multifactor pathogenic characteristic of ZIKV infection, this study used an untargeted metabolomic approach to investigate the metabolic changes induced by ZIKV in prostate cells, seeking the identification of markers of persistent infection and elucidation of its potential oncolytic effect. It was observed that ZIKV affects the viability and metabolism of normal (PNT1a) and tumor (PC-3) prostate cells differently, with PC-3 cells being more susceptible to growth inhibition. In metabolic terms, there are changes in lipid markers that explain the antiproliferative effect of ZIKV in PC-3 cells. Persistent infection in PNT1a cells is mediated by altered levels of glycerolipids, acylcarnitines, fatty acids, oxylipins, and small metabolites resulting from oxidative stress that act as tumor progression mediators. Lipid biosynthesis and metabolism are important aspects of viral infection, and perturbation of this metabolism is shown to be fundamental in the infection outcome of the analyzed cell types, demonstrating the duality in the use of ZIKV as an antitumor agent.

Keywords: Mass spectrometry; Metabolomics; Zika virus; Prostate; Neoplasms; Lipid metabolism.

LISTA DE ABREVIATURAS E SIGLAS

ADA	*ADA Boosting*
CE	Eletroforese capilar (*Capillary electrophoresis*)
DI	Infusão direta (*Direct injection*)
ELISA	Ensaio de imunoabsorção enzimática (*Enzyme-linked immunosorbent assay)*
FA	Ácidos graxos (*Fatty acids*)
FAO	Oxidação de ácidos graxos (*Fatty acids oxidation*)
HRMS	Espectrometria de massas de alta resolução (*High-resolution mass spectrometry*)
IM	Mobilidade de íons (*Ion mobility*)
IT	Armadilha de íons (*Ion trap*)
LD	Gotícula de lipídeo (*Lipid droplet)*
LTQ	Armadilha de íons linear – quadrupolo (*Linear trap quadrupole*)
OXPHOS	Oxidação fosforilativa (*Oxidative phosphorylation*)
ER	Retículo endoplasmático (*Endoplasmic reticulum*)
ESI	Ionização por electrospray (*Electrospray ionization*)
FC	Razão da expressão relativa (*Fold change*)
FTICR	Ressonância ciclotrônica de íons com transformada de fourier (*Fourier-transform ion cyclotron resonance*)
GC	Cromatografia gasosa (*Gas chromatography*)
GDTB	*Gradient tree boosting*
LC	Cromatografia líquida (*Liquid chromatography*)
ML	Aprendizado de máquina (*Machine learning*)
MS	Espectrometria de massas (*Mass spectrometry*)
MSn	Espectrometria de massas sequencial (*Sequential mass spectrometry*)
MTT	Brometo de 3-[4,5-dimetiltiazol-2-il]-2,5 difenil tetrazolio (3-[*4,5-dimethylthiazol-2-yl]-2,5 diphenyl tetrazolium bromide*)
NMR	Ressonância magnética nuclear (*Nuclear magnetic resonance*)
OMV	Vesícula da membrana externa bacteriana (*Outer membrane vesicle*)
PCA	Análise de componentes principais (*Principal component analysis*)

PLS-DA Análise discriminante por mínimos quadrados parciais (*Partial-least squares discriminant analysis*)

PSA Antígeno prostático específico (Prostatic specific antigen)

qTOF Quadrupolo tempo de vôo (*Quadrupole time-of-flight*)

QqQ Triplo quadrupolo (*Triple quadrupole*)

RF Floresta aleatória (*Random forest)*

RT-PCR Reação da transcriptase reversa seguida pela reação em cadeia da polimerase (*Reverse transcription polymerase chain reaction)*

TCA Ciclo do ácido tricarboxílico (*Tricarboxylic acid cycle*)

TG Triacilglicerol (*Triacylglycerol*)

VIP Importância da variável na projeção (*Variable importance in projection*)

ZIKV Vírus da Zika (*Zika virus*)

ZVp Protótipo de vírus da Zika (*Zika virus prototype*)

SUMÁRIO

1. INTRODUÇÃO

1.1 O vírus da Zika

O vírus da Zika (ZIKV) é um flavivírus da família *Flaviviridae*, isolado pela primeira vez na Floresta de Zika em Uganda em 1947 durante análises de sangue de primatas sentinela. O vírus foi detectado em mosquitos *Aedes africanus* na década subsequente sendo encontrados indícios da infecção de humanos pelo ZIKV devido à presença de imunidade serológica nos habitantes de regiões africanas e asiáticas próximas a Uganda. Entretanto, apenas 13 casos da doença foram confirmados no período entre sua descoberta até 2007, quando ocorreu um surto na Micronésia (1,2). Novos surtos da infecção pelo ZIKV ocorreram posteriormente, sendo os mais significativos na Polinésia Francesa (2012-2014) e na América Central e do Sul, especialmente no Brasil (2015-2016). Estima-se que 4 milhões de pessoas foram infectadas nas Américas, com declaração de emergência internacional de saúde pública em 2016 pela Organização Mundial da Saúde (3).

A infecção pelo ZIKV pode ser assintomática ou oligossintomática em 80% dos casos, com sintomas inespecíficos caracterizados por febre aguda, erupção cutânea, artralgia e/ou conjuntivite não purulenta, sendo incomum casos de hospitalização e fatalidades (2,3). A não-especificidade dos sintomas reportados torna o diagnóstico clínico de difícil conclusão, muitas vezes sendo confundido com outras arboviroses como a Chikungunya e a Dengue (4). Entretanto, outros desfechos foram posteriormente associados à infecção pelo ZIKV, como aumento da ocorrência da síndrome de Guillain-Barré (paralisia flácida aguda) e a presença da síndrome congênita associada à infecção pelo vírus Zika. Ambas as manifestações são decorrentes do involvimento do sistema nervoso, e no caso da síndrome congênita pelo Zika caracteriza-se pela incidência de neonatos com microcefalia, hipoplasia do tronco encefálico e do cerebelo, mielinização retardada, calcificação grosseira do parênquima cerebral, entre outras consequências (3,5).

A associação da infecção pelo ZIKV a severas consequências neurológicas por estudos epidemiológicos (3) e sua abrangente disseminação resultaram em esforços na investigação das alterações metabólicas celulares frente à infecção por ZIKV. Manifestações neurológicas foram chave para a

investigação do tropismo do ZIKV por células neuronais em diferenciação. Nesses estudos, observou-se que o vírus promove impedimentos no desenvolvimento neuronal através de interrupções do ciclo celular e indução de morte celular (6–10). Evidências da associação entre a infecção por ZIKV e malformações fetais foram comprovadas através de estudos com modelos animais (8,11). A desregulação da expressão de moléculas pro-apoptóticas, como caspase-3 e p53, de mecanismos autofágicos como a via PI3K-Akt-mTOR, e a interação celular com proteínas virais têm sido apontados como mediadores de morte celular e genotoxicidade induzidos pelo ZIKV (7,10,12–14). Além disso, foi observado que o ZIKV induz expressão diferencial de proteínas e genes (6,15), e que possíveis miRNAs produzidos durante a infecção podem estar associados à patogênese viral e no retardo do desenvolvimento fetal e neurológico (16). Durante a replicação viral, o retículo endoplasmático (ER) é essencial para glicosilação de proteínas virais e lipídeos. Entretanto, o estresse do ER devido à sua vacuolização pode acarretar a ativação da resposta a proteínas mal enoveladas, sendo apontados como mecanismos contribuintes aos defeitos da microcefalia congênita (17–19).

Durante a epidemia, testes para diagnóstico laboratorial basearam-se na detecção do vírus e/ou dos componentes virais, como o uso de ensaios imunológicos e RT-PCR (Reverse Transcription Polimerase Chain Reaction) para a detecção do RNA viral. Embora seja considerado padrão ouro pela sua especificidade, sua sensitividade está condicionada a fase aguda da infecção, a qual é evidenciada pelas manifestações clínicas da doença (4). Outro tipo de exame empregado foi a sorologia, que visa a detecção de imunoglobulinas por ELISA (Enzyme-Linked Immunosorbent Assay) como IgM; porém o mesmo apresenta como limitação a recorrência de reação cruzada como outros flavivírus (1,4). De forma geral, flavivírus promovem significativas alterações lipídicas nas células dos hospedeiros, resultando em perfis característicos da infecção nos fluidos biológicos. Tais alterações podem ser exploradas por métodos alternativos para diagnóstico de infecções virais (20–24).

1.1.1 Infecção e lipídeos

Devido à sua semelhança com outros flavivírus, no ambiente urbano o ZIKV é transmitido pelo ciclo humano-mosquito-humano, sendo os mosquitos *Aedes aegypti* e *Aedes albopictus*, vetores predominantes nas Américas (1). Acredita-se que o fato do ZIKV ser detectado em diferentes fluidos corporais, como sangue, saliva, urina e esperma pode ter contribuído para sua rápida disseminação por vias independentes do vetor; transfusão sanguínea, transmissão sexual e migração transplacentária durante o primeiro trimestre de gestação foram reportadas como vias de transmissão (3,25).

Virus são partículas dependentes das células do hospedeiro para sua replicação (Figura 1). No processo de infecção por *flavivirus* as partículas virais interagem com receptores de membrana promovendo sua internalização. No caso do ZIKV, receptores AXL, TIM-1, TYRO3, e TLR3 foram reportados como mediadores da infecção viral e lipídeos do envelope viral como fosfatidilserinas e fosfatidiletanolaminas apresentaram importante papel no reconhecimento viral. A partícula é então digerida no endossomo levando à liberação do RNA viral para dentro da célula. Partículas viras de ZIKV são formadas por RNA de fita simples positiva, a qual codifica ao final 9 proteínas virais, sendo 3 estruturais (C, M, e E) e 7 não-estruturais (NS1, NS2A, NS2B, NS3, NS4A, NS4B, and NS5)(12,24). No ER ocorre a formação de complexos de replicação para multiplicação do genoma viral. Nesse complexo, o virus promove um extenso remodelamento lipídico sendo os esfingolipídeos essenciais (24). Ceramidas, uma subclasse de esfingolipídeos, são recrutadas pelo vírus ao sítio de replicação para estabelecer adequada curvatura de membrana. A diminuição dos níveis de esfingolipídeos celulares afetam diretamente a replicação viral (24,26). Após a replicação, as proteínas virais são traduzidas, glicosiladas, e em conjunto com o RNA viral e membrana lipídica do hospedeiro dão origem a uma nova partícula. Essa é transportada ao Complexo de Golgi onde ocorre sua maturação. Novas partículas virais são exocitadas permitindo a infecção de novas células (12). Todo esse processo de reconhecimento, internalização, replicação, montagem e liberação é altamente mediado por lipídeos, os quais encontram-se significativamente alterados com a infecção.

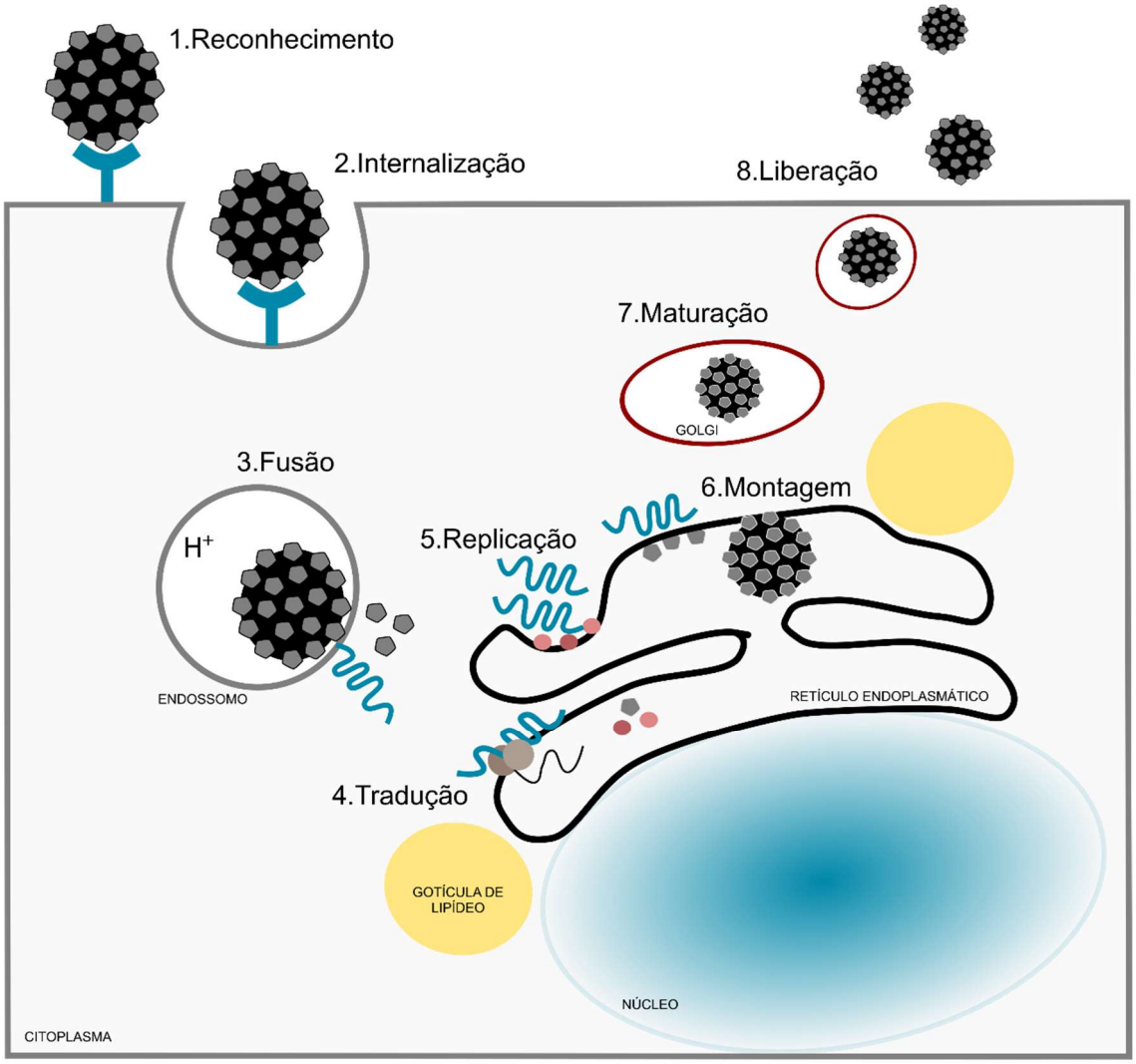

Figura 1. Processo de replicação de flavivírus composto por 8 fases: 1. Reconhecimento da partícula viral por receptores de membrana; 2. Internalização mediada por receptores de membrana; 3. Fusão da partícula viral com endossomo que culmina na liberação do RNA viral para dentro da célula; 4. Tradução do RNA viral com a formação de proteínas estruturais e não-estruturais no retículo endoplasmático (ER); 5. Replicação do RNA viral no retículo endoplasmático; 6. Montagem de nova partícula viral com sequestro de lipídeos da membrana do ER; 7. Maturação da partícula viral no complexo de Golgi; e 8. Liberação do vírus infectante.

Flavivírus não apenas sequestram e realocam lipídeos da célula hospedeira, como também promovem o aumento da síntese de ácidos graxos através da indução de enzimas envolvidas com a lipogênese e posteriormente formação de lipídeos mais complexos (24). A infecção por Zika induz de forma

transiente a formação e acúmulo de gotículas de lipídeos, em inglês denominadas *lipid droplets* (LD), as quais são ricas em lipídeos complexos como triacilglicerois (TG)(24,27). Esse aumento de LD impulsiona a resposta imune mediada por interferons do tipo I e III (28). Entretanto, lipofagia e uso dos ácidos graxos para geração de energia e suporte à replicação também são reportados como mechanismos mediados por infecção por flavivírus (24,27).

A patogênese induzida pelo ZIKV mostra-se multifatorial, e com extenso comprometimento de metabólitos do metaboloma celular. Os estudos dos mecanismos celulares (8,9,13–15,29,30) envolvidos na infecção pelo ZIKV impulsionam o desenvolvimento de novas formas de diagnóstico rápido e preciso da infecção viral (1,4,21) e novas estratégias para o combate e prevenção da disseminação do vírus, como a compreensão de fatores relacionados a transmissão e manifestações clínicas (1,3,22), e ao desenvolvimento de vacinas e tratamentos (31–33). O uso de técnicas de biologia molecular clássica e até a aplicação de ômicas, como genômica, transcriptômica, proteômica e metabolômica são fundamentais para uma compreensão abrangente dos efeitos induzidos pelo ZIKV.

1.1.2 ZIKV e tropismo celular

Recentes estudos demonstraram o tropismo do ZIKV para uma ampla gama de tecidos em mamíferos, sendo os mais característicos os tecidos neural, ocular, testicular e placentário, devido ao perfil de persistência e propagação (34,35). Diferentes tipos de células do sistema nervoso, como as células progenitoras neurais, neurônios, astrócitos e células da glias são permissíveis à infecção pelo ZIKV. Seu efeito danoso ao desenvolvimento cerebral, como a inibição do crescimento celular e a morte celular por apoptose e consequente microcefalia também foram confirmados (6–10,13–15,36). Além do sistema nervoso, células placentárias, da córnea, da retina e nervo óptico, células do sistema reprodutor masculino e feminino, renal, fibroblastos e células mononucleares sanguíneas também são susceptíveis à infecção pelo ZIKV (34,35,37–39). Esse extenso tropismo explica a presença do vírus e/ou RNA viral (e de possíveis metabólitos) em fluidos como lágrimas, saliva, líquido

cefalorraquidiano, fluido amniótico, sêmen, muco cervical e urina (34,35). A presença da partícula viral nos diferentes fluidos representa os riscos e as nuances envolvidas na transmissão do ZIKV, que pode ocorrer através do contato sexual (25).

A susceptibilidade e persistência do ZIKV no sistema reprodutor masculino foi estudada por diversos autores (37–42). Kumar et al. (2018) demonstrou a susceptibilidade de células de Sertoli à infecção por ZIKV e a persistência da infecção nos testículos (40). Além disso, o ZIKV foi capaz de infectar testículos de ratos levando a um intenso estresse oxidativo e comprometimento da espermatogênese, evidenciando o possível impacto da infecção por ZIKV na fertilidade masculina (41). Em homens infectados com ZIKV além de hematospermia, os mesmos apresentaram prostatite o que sugere a inflamação da próstata como fator contribuinte (37,42). Células epiteliais e mesenquimais da próstata são susceptíveis à infecção, replicação e produção de partículas virais infecciosas, confirmando o tropismo do ZIKV por esse tecido e levantando a possibilidade da próstata se apresentar como um reservatório de replicação (37–39,42). Izuagbe et al. (2019) observou através de estudos *in vitro* o estabelecimento de infecção persistente em células epiteliais da próstata; a infecção persistente foi acompanhada de alterações na transcrição de genes envolvidos na resposta imune e antiviral ao Zika (39). Adicionalmente, Machado et al. (2021) demonstrou que a cepa brasileira induz a expressão de miRNAs potencialmente envolvidos com processos inflamatórios, imunológicos, de proliferação e carcinogênese (38). Células de câncer de próstata infectadas a curto prazo também demonstraram título viral alto e consistente (Kaid et al. 2018; Spencer et al. 2018). Embora não haja evidências de infertilidade masculina em humanos devido ao ZIKV (42), recente estudo publicado com macacos demonstra a persistência do RNA viral no sistema reprodutor, incluindo a glândula prostática, com observações de inflamação e lesão tecidual que poderiam impactar a fertilidade (44).

Considerando a persistência das partículas de ZIKV nas células da próstata, incluindo relatos de prostatite durante infecção, e a abrangência do seu tropismo incluindo células tumorais, torna-se relevante investigar as potenciais

alterações metabólicas envolvidas nesses processos (37,42,45). Tais mecanismos podem ser investigados através de estudos metabolômicos.

1.1.3 Efeito oncolítico

O câncer é uma das doenças mais devastadoras já descritas, apresentando crescente incidência e mortalidade todos os anos. Devido à sua heterogeneidade e difícil prognóstico, o estudo do câncer tornou-se um dos campos da ciência com maiores investimentos, levando a grandes avanços e contribuições científicas nas últimas décadas. De forma simplificada, células cancerígenas podem ser caracterizadas por possuírem um metabolismo disruptivo em relação às células normais, um metaboloma passível de ser profundamente explorado. Embora a metabolômica ainda seja uma área emergente, seus métodos auxiliam na investigação dos mecanismos bioquímicos centrais que contribuem para o desenvolvimento e manutenção dos tumores, contribuindo para o processo de identificação de biomarcadores que auxiliem no diagnóstico, prognóstico e intervenções terapêuticas (46).

Diferentes tipos de amostras podem ser utilizados em um estudo metabolômico em câncer, sendo o estudo de células tumorais *in vitro* parte essencial dos ensaios preliminares para obtenção de dados. O crescimento de células tumorais *in vitro* permite o desenvolvimento de testes científicos sem a interferência das características individuais dos sujeitos de pesquisa, e são propícios para testes de novos produtos e intervenções terapêuticas, como o uso de vetores virais (46). O conhecimento de que certos vírus possuem tropismo por células tumorais e possível capacidade de erradicá-las data do início do século 20. Diversos tipos de agentes virais já foram identificados por sua atividade oncolítica, como adenovírus sorotipo 4 responsável pela doença de Newcastle, o vírus do Oeste do Nilo, dentre outros. Além de serem utilizados como carreadores para terapia gênica em câncer, a lise de células tumorais por vírus oncolítico pode ocorrer pela direta ação da replicação viral e/ou pelo reconhecimento das células infectadas como alvo para o sistema imune (47,48). Alguns tumores apresentam poucos infiltrados de células do sistema imune e mutações necessários para a ativação de resposta imunológica contra o

crescimento tumoral, como é o caso do câncer de próstata, o que leva baixa eficiência de imunoterapias. Dessa forma, o uso de virus oncolíticos pode auxiliar no desencadeameno da imunidade antitumor, através da ativação de resposta mediadas por interferons (47).

O ZIKV mostrou potencial oncolítico através da capacidade de desregular o ciclo celular e promover a morte de células neurais *in vitro* e *in vivo*, e prejudicar a formação de neuroesferas (6–11,13–15). Tais evidências reforçam a atividade oncolítica do ZIKV para células neurais e de alta proliferação, e seu efeitos antiproliferativos em tumores cerebrais (32,43,49–52). Zhu et al. (2017) observou que o ZIKV, diferentemente de outro flavivírus como o Vírus do Oeste do Nilo, afetava preferencialmente células-tronco de glioblastoma com efeito antiproliferativo em comparação com células neurais normais (51). Já em células de neuroblastoma, o aumento da expressão do marcador CD24 aumenta a permissividade das células à infecção pelo ZIKV (49). A capacidade de infecção e redução dos tumores humanos embrionários agressivos, adicionalmente aos efeitos de aumento de sobrevida, diminuição do tumor, metástases e remissão em modelo animal foram reportados por Kaid et al. (2018) (43).

Recentes estudos sobre os mecanismos envolvidos na interação do Zika com células tumorais, observaram que a proteína viral N5 inibe o crescimento e invasão de células de glioma *in vitro* em comparação a outras 3 proteínas não-estruturais (NS1, NS3 e NS4B) (52); entretanto, as proteínas NS2A, NS2B, NS4A não foram avaliadas, embora NS4A e NS4B tenham sido associadas previamente ao bloqueio do eixo PI3K-Akt-mTOR, via ligada à autofagia (10). Já Iannolo et al. (2019) observou que a infecção de células-tronco de glioblastoma por Zika induz o aumento de expressão de MiR34c, o qual regula diferentes genes, como Bcl2 (apoptose), NOTCH e NUMB (desenvolvimento do sistema nervoso central) (53). Tais informações auxiliam na elucidação dos mecanismos envolvidos na atividade oncolítica do Zika.

Além de cepas infectantes, o uso do vírus modificado/atenuado demonstrou atividade anti-proliferativa contra glioblastoma, com efeitos citopáticos e danos ao DNA (32,50). Análise do transcriptoma de células de glioblastoma sob ação de vírus modificado, sugere um aumento na expressão de genes responsáveis por vias apoptóticas, controle do ciclo celular, sinalização

de fosfatidilinositol 3-quinase (PI3K)-Akt e p53 (32). Não obstante, o envolvimento da via PI3K-AKT-mTOR foi previamente relacionado às alterações metabólicas promovidas pelo Zika através de estudo metabolômico por Melo et al. (2017) (22). Além do glioblastoma, outros tipos de tumores como próstata e ovário são especialmente susceptíveis aos efeitos antiproliferativos do protótipo ZIKV-*Neisseria meningitidis* desenvolvido por Martins et al. (2018), além de efeitos em outras 6 linhagens celulares (33,50). Martins et al. (2018) observou aumento de IL-2, IL-4 e TGF-β em camundongos inoculados com o protótipo, e indução de anticorpos IgG anti-Zika, demonstrando o potencial uso do protótipo como vacina contra Zika (33).

1.2 Próstata e metabolismo

Células da próstata são consideradas energeticamente ineficientes, apresentando um metabolismo peculiar (Figura 2). Essas células possuem um aumento na expressão de transportadores de zinco (54). O aumento nos níveis de zinco intracelular promove a inibição da enzima aconitase mitocondrial, a qual é responsável pela conversão de citrato a isocitrado. Estando inibida, observa-se um acúmulo de citrato intracelular o qual não será reaproveitado no ciclo do ácido tricarboxílico para a geração de energia através da fosforilação oxidativa. O citrato é excretado, compondo o fluido prostático (55,56).

Para o desenvolvimento de novas terapias é essencial o entendimento dos mecanismos envolvidos no metabolismo das células de câncer. Durante o processo de malignificação das células da próstata, a redução das concentrações intracelulares de zinco mostra-se como importante evento. Com isso, a atividade enzimática da m-aconitase promove a utilização do aporte de citrato presente na célula levando ao aumento da oxidação fosforilativa e síntese de ácidos graxos (55,56). A redução dos níveis de zinco e citrato intracelular em câncer de próstata foi observada por estudos metabolômicos (57). Células de câncer de próstata também são marcadas pelo acúmulo de lipídeos mais complexos em LDs e aumento no metabolismo de ácidos graxos (58,59). Estágios mais avançados do tumor possibilitam o aumento da capacidade de

importação de glicose e sua utilização por glicólise anaeróbica, conhecido como efeito Warburg (54).

Alterações do metabolismo celular são essenciais para definição dos diferentes estados metabólicos e heterogeneidade tumoral. Com isso, células normais e tumorais da próstata são predispostas a responder diferencialmente quando submetidas aos mesmos estímulos externos.

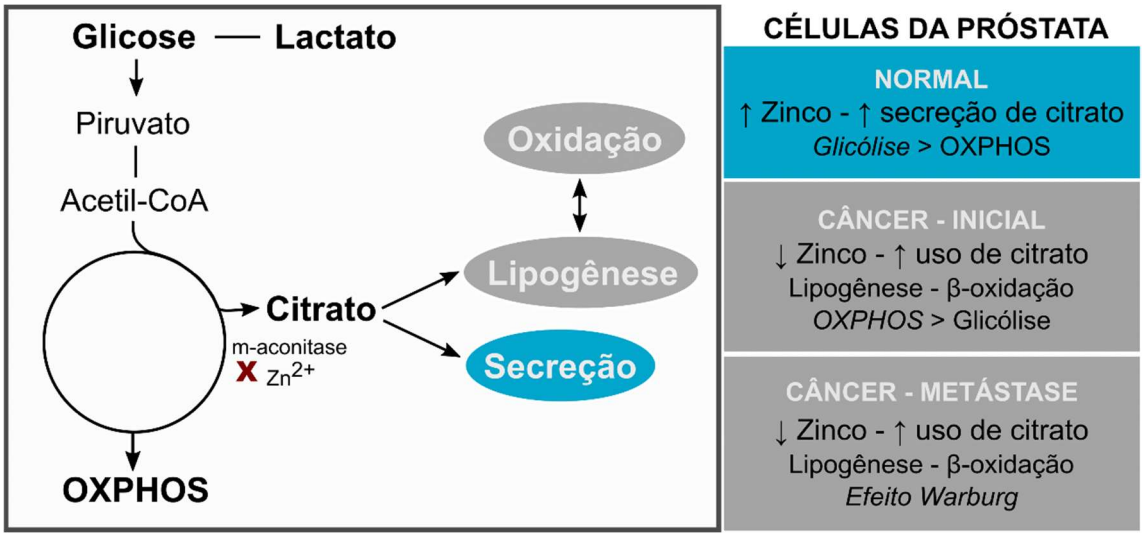

Figura 2. Metabolismo de células da próstata normais e tumorais. Em células normais o influxo de zinco promove a inibição da enzima m-aconitase levando ao acúmulo e secreção de citrato para o fluido prostático. Com menos citrato, essa células tornam-se energeticamente pouco eficientes através da fosforilação oxidativa (OXPHOS). Com o processo de carcinogênese e diminuição no influxo de zinco a célula da próstata passa a utilizar citrato tanto para a produção de energia através de OXPHOS como para síntese lipídica. Células tumorais metastáticas possuem um aporte de glicose que favorece o efeito Warburg além de manter o remodelamento lipídico.

1.2.1 Câncer de próstata

O câncer está entre as doenças mais devastadoras, liderando a causa de mortes no mundo e, consequentemente, exercendo grande impacto na sociedade. Dados estimavam mais de 19.3 milhões de novos cânceres no mundo em 2021 acumulando ambos os sexos e todas as faixas etárias. Desse

total, o câncer de próstata corresponde a uma parcela de 7.3%. Considerando a população masculina, o câncer de próstata é o segundo mais incidente com 14.1%, ultrapassado apenas pelo cancer de pulmão (14.3%). Embora possua crescimento lento, formas agressivas de câncer de próstata podem se espalhar através de metástases levando o câncer de próstata a ocupar a quinta posição em taxas de mortalidade, precedido apenas por cânceres de pulmão, fígado, colorretal e estômago de forma descendente (60). Devido à sua alta incidência, medidas precisas de diagnóstico e tratamento direcionados são necessárias. A realização do exame clínico (toque retal) visando a detecção de nódulos, assimetria e endurecimentos, combinado à dosagem de PSA (antígeno prostático específico) no sangue podem indicar a presença de câncer. Entretanto, tais métodos clínicos e laboratoriais não são conclusivos, sendo o diagnóstico de câncer de próstata feito através da análise histopatológica do tecido prostático após biópsias (61,62). Um novo sistema de graduamento para o tumor foi estabelecido em 2014, auxiliando no diagnóstico e na decisão clínica do tratamento (63).

A vigilância ativa é utilizada quando os malefícios do tratamento se superpõem aos benefícios, sendo o paciente monitorado regularmente. Entretanto, as opções de tratamento são ainda limitadas, e em caso de progressão, a remoção cirúrgica da próstata (prostectomia), seguida de radioterapia, hormonioterapia, quimioterapia, imunoterapia, terapia direcionada e/ou uma combinação dessas abordagens são recomendadas. A resistência a terapias de privação de androgênios é comum, e o tumor pode gerar metástases levando à progressão da doença e necessidade de tratamentos mais efetivos a longo-prazo (62,64,65). Abiraterona e enzalutamide são terapias hormonais que podem ser utilizadas para tratar câncer de próstata em fase metastática. Além desses, outras opções envolvem imunoterapia com vacinas personalizadas contra o câncer, como o Sipuleucel-T, e inibidores de sistema *checkpoint* como o pembrolizumabe que possui como alvo PD-1(64–66).

1.3 Metabolômica

Durante o final do século 20 e o início do século 21, as metodologias clássicas de pesquisa biomédica abriram espaço para uma abordagem holística

introduzida pela genômica, proteômica, transcriptômica e metabolômica. Além de desvendar a sequência de bases nitrogenadas que compõem o DNA e/ou o RNA de um organismo, há um grande desafio em conectar genes com suas funções e relacionar o genótipo com o fenótipo (Figura 3) (67–69).

A metabolômica é o estudo que compreende a análise de moléculas de baixo peso molecular. São elas o resultado do processo metabólico celular, e portanto, consideradas mais próximas ao fenótipo. Dentre os compostos determinados em estudos metabolômicos se destacam os lipídeos, os aminoácidos, as vitaminas, os ácidos nucleicos, os açúcares, os metabólitos de compostos exógenos como medicamentos, toxinas e moléculas de origem vegetal (70). Quando analizadas em conjunto, tais moléculas compreendem o metaboloma; da análise do metaboloma extrai-se importantes informações sobre as características de um determinado grupo de indivíduos, como um recorte global dos processos fisiopatológicos de determinada condição, tratamento ou doença (67,68). A partir do momento que esses compostos tornam-se significativos para a distinção de fenótipos os mesmos são denominados biomarcadores (70).

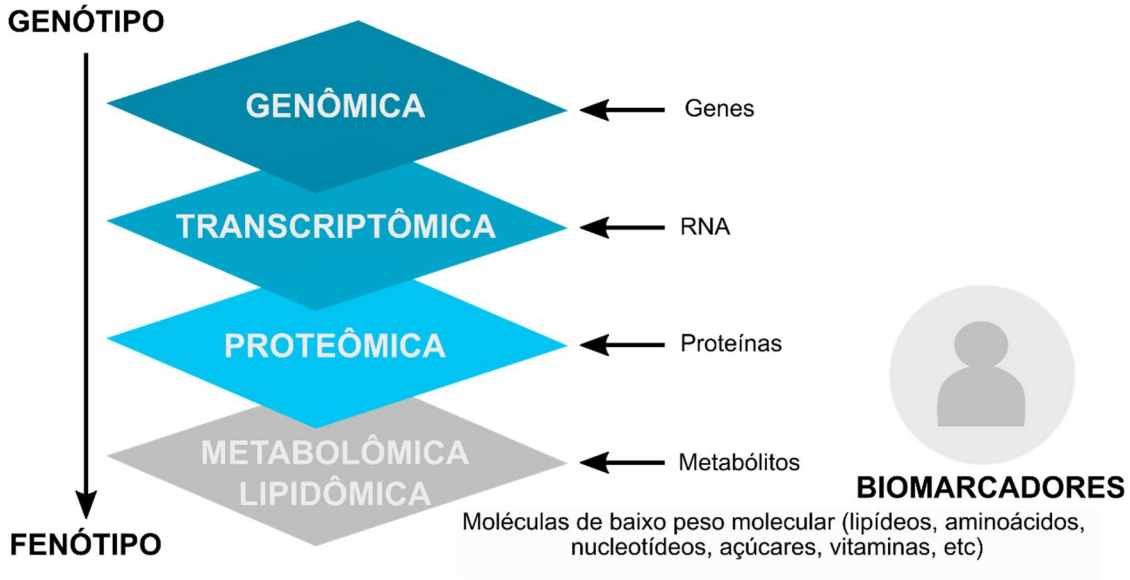

Figura 3. Abordagens multiômicas que englobam genômica, transcriptômica, proteômica, metabolômica e lipidômica relacionam o genótipo ao fenótipo. Moléculas de baixo peso molecular analisadas através da metabolômica podem compor um conjunto de biomarcadores a serem utilizados como novos alvos

moleculares, para elucidação de mecanismos fisiopatológicos, diagnóstico e monitoramento terapêutico. Adaptado de Dettmer et al. (2007) (69).

Diferentes plataformas analíticas podem ser utilizadas para a determinação de biomarcadores, sendo os métodos de detecção mais comuns e robustos baseados em espectrometria de massas (MS) e ressonância magnética nuclear (NMR) (70,71). As análises por espetrometria de massas podem ser precedidas por técnicas análiticas que auxiliam na separação dos compostos presentes na matriz biológica, como a cromatografia gasosa (GC), cromatografia líquida (LC), eletroforese capilar (CE), e mais recentemente uma segunda dimensão de separação por mobilidade de íons (IM) (71). Embora os processos cromatográficos sejam fundamentais para a quantificação e validação de biomarcadores, os mesmos são limitados em relação ao tempo despendido para análise versus o número de amostras, além da necessidade de padrões. Nesse contexto, técnicas de infusão direta (DI) para análises exploratórias, não-alvo específicas e qualitativas são vantajosas para descobertas de biomarcadores de forma abrangente e sistemática (69,71). Essa abordagem exploratória denominada *untargeted*, permite um estudo holístico e não-enviesado dos metabólitos presentes na amostra e, quando acompanhados de processos estatísticos robustos e extensa análise de dados, permitem a criação de hipóteses sobre os processos metabólicos envolvidos nas condições em estudo (67,70,71).

O desenho do estudo e coleta de amostra é variável e depende da condição/doença a ser investigada. De forma geral, as amostras são preparadas através de extração dos metabólitos com solventes orgânicos polares, e os espectros de massas são adquiridos utilizando larga faixa de razão massa-carga *(m/z).* Os dados são filtrados para a remoção sinais inconsistentes e próximos ao ruído, normalizados, e submetidos a testes estatísticos (Wilcoxon), análises multivariadas e/ou de inteligência artificial. Dentre essas destacam-se análises não-supervisionadas como a Análise de Componentes Principais (PCA, *Principal Component analysis*), ou supervisionadas como a Análise Discriminante por Mínimos Quadrados Parciais (PLS-DA, *Partial-Least Squares Discriminant Analysis*) e o Aprendizado de Máquina (ML, *Machine Learning*) (69,71–73). Através das análises estatísticas é possível elencar os valores de *m/z* mais

discriminantes para cada condição, sendo os mesmos posteriormente identificados e investigados em suas funcionalidades através de bancos de dados e análise de vias metabólicas (Figura 4). As abordagens por ML permitem a comparação de uma maior quantidade de dados de grupo de amostras gerados por espectrometria de massas, em comparação com a análise estatística multivariada. Dessa forma, a Inteligência Artificial trouxe novos conceitos e soluções para a resolução de problemas complexos na medicina, ao predizer e classificar diversas doenças, como Zika (21), COVID-19 (20) e câncer de próstata (74).

Consequentemente, a metabolômica associada à espectrometria de massas vem sendo empregada na captação e seleção de biomarcadores para investigação fisiopatológica, diagnóstico, e prognótico de diversas doenças, incluindo infecções virais e câncer (20–22,57,75–77).

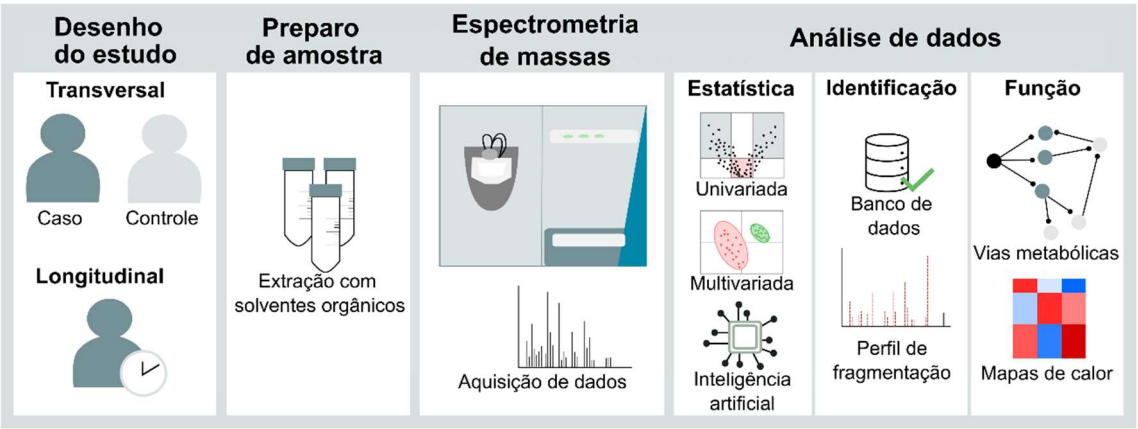

Figure 4. Fluxo de estudo metabolômico exploratório compreendendo quatro estágios principais: desenho do estudo, preparo de amostras, análise por espectrometria de massas e análise de dados. Durante a análise de dados metabolômicos, análises estatísticas auxiliam na observação das variáveis mais importantes e significativas para a distinção entre grupos de amostras, sendo as mesmas identificadas através das informações obtidas nos espectros de massas; metabólitos significativos são relacionados a vias metabólicas para a compreensão funcional.

Embora a metabolômica seja considerada emergente em comparação às demais ômicas na pesquisa em câncer, sua abordagem pode revelar alterações

bioquímicas importantes relacionadas ao desenvolvimento do tumor e potencial terapêutico de novas terapias (75,76). O câncer de próstata vem sendo pesquisado através da metabolômica para a determinação de biomarcadores em fluidos biológicos, tecidos, e células *in vitro* (75,76,78). Em especial nas infecções, a partícula viral é capaz de induzir alterações metabolômicas intracelulares a fim que a célula produza os metabólitos necessários para a replicação e infecção (22–24,26,30). A caracterização dessas alterações através da metabolômica permite verificar quais vias metabólicas estão ativas ou têm sua atividade aumentada ou diminuída, contribuindo para a compreensão do processo de infecção celular pelo vírus em diferentes tipos celulares.

1.3.1 Espectrometria de massas e ionização por electrospray (ESI, electrospray ionization)

A técnica analítica de espectrometria de massas baseia-se na detecção de moléculas ionizadas as quais são traduzidas em espectros de intensidade (abundância) versus a razão massa sobre carga (*m/z*). Tais espectros fornecem informações químicas altamente específicas que estão diretamente relacionadas a fórmula molecular dos compostos detectados. Através da análise dos dados espectrais é possível definir a massa monoisotópica da molécula ionizada com precisão pela utilização de espectrômetro de massas de alta resolução (HRMS, *High-resolution Mass Spectrometry*), pelos padrões de distribuição de isótopos, e experimentos de fragmentação molecular (MS^n) (69,72). Para a obtenção de detecção rápida e sensível e de alta resolução, diferentes métodos de ionização e análise de íons foram desenvolvidos ao longo dos anos (72).

O método ESI permitiu a análise de compostos polares em solução e direto acoplamento do espectrômetro de massas a métodos de separação como a cromatografia líquida. Os analitos em solução são ionizados através da adição de ácidos ou bases à amostra, levando à protonação ($+H^+$) ou desprotonação ($-H^+$) das moléculas, respectivamente. Dependendo da amostra e da condição em estudo, as moléculas podem formar diferentes adutos, compostos pela molécula conjugada a cátions (Na^+, K^+, NH_4^+), ânions (Cl^-), serem desidratadas ($-H_2O$) ou

descarboxiladas (-CO_2) durante o processo de ionização, dentre outros (71,79,80).

Quando o objetivo é analisar moléculas em modo de ionização positivo, a solução acidificada rica em íons com carga positiva, passa por um fino capilar com diferença de potencial positivo. Isso faz com que os íons de carga negativa sejam neutralizados e oxidados (não detectados), enquanto que os íons de carga positiva irão forma um spray eletrolítico em forma de aerossol. Conforme o líquido evapora (dessolvatação) devido à ação de gás inerte e altas temperaturas, e o tamanho das gotículas diminui, ocorre um aumento da repulsão das cargas positivas presentes nas gotículas. A progressiva subdivisão das gotículas devido à repulsão entre as cargas culmina na expulsão dos íons para fase gasosa, os quais serão conduzidos por lentes até o analisador de massas (79,80). Esse processo denominado ESI foi descrito por John Fenn em 1989 (80) (Figura 5).

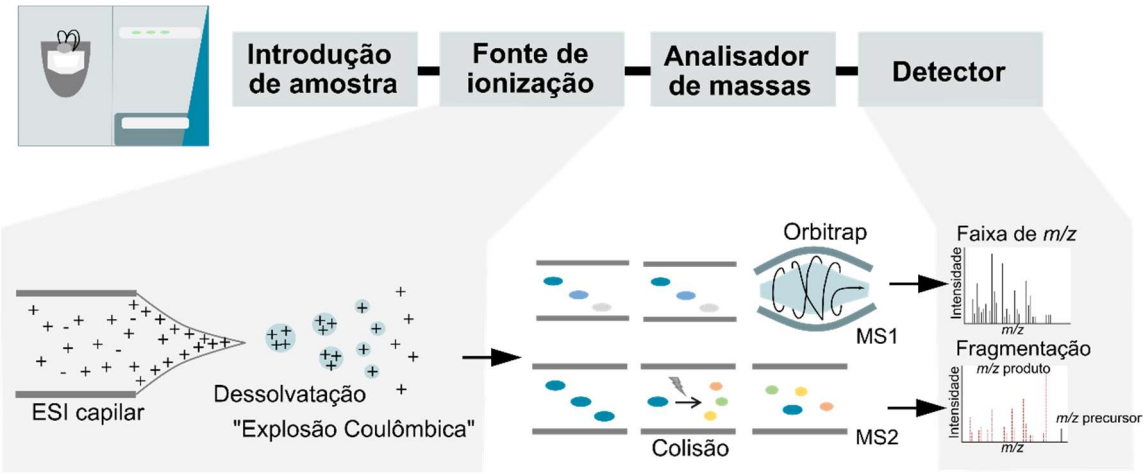

Figura 5. Análise por espectrometria de massas evidenciando a introdução de amostra, ionização, análise de masssas e detecção. O processo de ionização por electrospray (ESI) foi descrito por John Fenn et al. em 1989 (80).

O espectro final será determinado pelos parâmetros definidos para o analisador de massas. Em espectros do tipo MS1, todos íons presentes na amostra são selecionados e detectados ao final do processo, compondo um espectro que se assemelha à impressão digital da amostra. Entretando, dependendo do analisador utilizado é possível obter espectros do tipo MS2, no qual um íon precursor é selecionado, e sobe a ação de um gás inerte (Hélio, He)

é fragmentado; como resultado desse processo obtém-se um espectro no qual observa-se os produtos de fragmentação do íon precursor. Analisadores do tipo *triple quadrupole* (QqQ), *ion trap* (IT), *quadrupole-ion trap* (LTQ) ou *quadrupole-time-of-flight* (qTOF) permitem a realização de reações de fragmentação, obtendo-se espectros de MS2 que auxiliam na identificação estrutural das moléculas (69,79). Diferentes analisadores distinguem-se pelo mecanismo utilizado para a análise das massas, pela performance (velocidade, resolução, exatidão de massa, e faixa de *m/z*) e valor (Quadro 1). Analisadores de alta resolução, como Orbitrap, qTOF e FTICR (*Fourier Transform Ion Cyclotron Resonance*) trazem a possibilidade de analisar amostras com larga faixa de *m/z*, obtendo-se exatidão de massa menor do que 5 ppm, o que auxilia na identificação de compostos por meio do uso de banco de dados de metabolômica (70,72,79).

Quadro 1. Differenças entre os principais analisadores de massas. Adaptado de Hoffmann et al. (2007) e Cunsolo et al. (2014) (79,81).

Analisador	**Resolução (FWHM)**	**Exatidão de massa (ppm)**	**Sensibilidade**	**Faixa de *m/z***
IT	1000-1500	100-1000	picomolar	50-2000; 200-4000
QqQ	1000	100-1500	atomolar	50-4000
LTQ	2000	100-500	fentomolar	50-2000; 200-4000
qTOF	10000-40000	5-50	atomolar	Ilimitado
LTQ-Orbitrap	50000-500000	<5	fentomolar	50-2000; 200-4000
LTQ-FTICR	50000-800000	1-2	fentomolar	50-2000; 200-4000

2. OBJETIVOS

2.1 Objetivo Geral

Investigar através da metabolômica e espectrometria de massas as alterações metabólicas induzidas pelo ZIKV em células normais e tumorais da próstata.

2.2 Objetivos Específicos

- Determinar as alterações metabólicas provocadas pela infecção persistente de células epiteliais da próstata (PNT1a) pelo ZIKV.

- Investigar através da metabolômica os mecanismos e potencial efeito oncolítico do ZIKV em células de câncer de próstata (PC-3).

- Avaliar os efeitos de um protótipo terapêutico baseado no ZIKV (ZVp) no metabolismo de células tumorais da próstata (PC-3) por espectrometria de massas.

- Utilizar algoritmos de Aprendizado de Máquina (*Machine Learning*) para ranquear biomarcadores relacionados com mecanismos gerais da ação do Zika em células da próstata

3. METODOLOGIA

3.1 Vírus e células

A cepa brasileira de ZIKV (BeH823339, GenBank KU729217) foi isolada em 2015 de um paciente no estado do Ceará e generosamente obtida através do Professor Dr. Edison Durigon (Instituto de Ciências Biomédicas, Universidade de São Paulo, USP). Anteriormente aos ensaios, a cepa crescida em células Vero foi titulada atingindo carga viral de 2,25 x 10^6 PFU/mL sendo armazenado a -80°C.

Células de adenocarcinoma de próstata (PC-3) e células normais imortalizadas de epitélio da próstata (PNT1a) são do banco de células do Laboratório de Bioensaios in vitro e Transdução de sinais (Instituto de Biologia, UNICAMP), e rotineiramente crescidas em meio RPMI-1640 suplementado com 100 U/mL penicilina, 100 µg/mL estreptomicina e FBS 10% (Sigma-Aldrich) a 37°C e 5% CO_2. Demais informações sobre as linhagens estão disponíveis no Quadro 2.

Quadro 2. Linhagens celulares PNT1a e PC-3.

Linhagem	**PNT1a**	**PC-3**	**References**
Paciente	35 anos	62 anos	(82)
Órgão	Próstata normal	Próstata	(82)
Doença	Ø	Carcinoma da próstata	(83)
Estágio	Ø	Metastático	(83)
Derivado de	Epitélio	Osso	(83)
Mutação	Ø	TP53	(84)

As linhagens de *N. Meningitidis* (C2135), *Aedes albopictus* (C6/36) foram obtidas do INCQS—FIOCRUZ (Instituto Nacional Controle Qualidade em Saúde — Fundação Oswaldo Cruz Foundation, Rio de Janeiro, RJ).

3.2 Ensaios de viabilidade celular (MTT)

Ensaios de viabilidade celular (MTT) foram realizados em placas de 96 poços plaqueando 2,8x10^3 células/poço. As células foram expostas a

multiplicidade de infecção (MOI) de 0 (controle) e 1 de vírus por 24, 48 e 72 horas, em triplicata para cada condição. Após a remoção do meio, 100 µL de MTT 0,5 mg/mL (Sigma Aldrich) foi adicionado em cada poço e incubado por 3 horas a 37°C. Após o tempo determinado, a solução de MTT foi removida e adicionado 100 µL de etanol para a solubilização dos cristais de formazan. A absorbância da amostra foi medida a $\lambda = 570$ nm utilizando um leitor de microplaca (Synergy HT, BioTek). A representação gráfica dos resultados foi realizada utilizando o software GraphPad Prism 5.0.

3.3 Ensaios de formação de colônia

O ensaio de formação de colônia foi realizado utilizando placa de 6 poços plaqueando 2,8 x 10^3 células/poço. Após aderência (24 horas), as células foram expostas a concentrações de MOI 0 (controle), 1 e 5 de vírus. Após 15 dias, foi feita a remoção do meio, as colônias foram coradas com 1 mL de cristal violeta 5% (água:metanol) (Sigma Aldrich) por 30 minutos. Após a remoção da solução, os poços foram lavados com água, e a placa foi deixada 24 horas em temperatura ambiente para secagem. As colônias de células foram imageadas.

3.4 Protótipo ZVp

A cepa de ZIKV foi replicada em cultura de célula C6/36 após confluência de 70%. O procedimento de cultura e replicação segue conforme descrito por Melo et al. (2016) (85), sendo o estoque de vírus armazenado a -80°C. O protótipo de ZIKV atenuado (ZVp), foi produzido a partir da fusão das partículas virais com OMVs (*Outer Membrane Vesicles*) de *Neisseria meningitidis*. A descrição completa do processo de isolamento das vesículas e preparo do ZVp, assim como caracterização e testes realizados com a partícula encontram-se disponíveis nos estudos de Alves et al. (2013)(86) e Martins et al. (2018) (33). Nano Tracking Analysis (NanoSign, Malvern Instruments Ltd., Reino Unido) foi utilizado na determinação do número de partícula por mL.

3.5 Ensaios para metabolômica com ZIKV

Para avaliação metabolômica de células PNT1a e PC-3 infectadas com o ZIKV, foi seguido o mesmo procedimento do ensaio de formação de colônia, porém em placa de 24 poços. Foi feito plaqueamento a 4,2 x 10^3 células/poço

mantendo a placa a 37°C e 5% CO_2 por 24h. Células foram expostas ao ZIKV em MOI 1, por 5, 10 e 15 dias, em triplicata para cada condição, mantendo-se amostras controles nas mesmas condições. Ao final de cada ponto, células foram coletadas e os metabólitos extraídos conforme disposto no item 3.7.

3.6 Ensaios para metabolômica com ZVp

As células PC-3 foram colocadas em cultura de acordo com os procedimentos descritos por Roman Jr et al (2017) (87). Resumidamente, 5 mL de meio de cultura RPMI-1640 suplementado com 5% de soro fetal bovino (RPMI/FBS 5% Gibco®, EUA) e 1% de antibiótico penicilina: estreptomicina (Nutricell®, Brasil, 1000 U/mL) a 37°C com 5% CO_2, foram usados para crescer as células PC-3 até confluência de 80%. Células foram transferidas para placa de 96 poços (100 µL/poço, densidade de inoculação: $4{,}5 \times 10^4$ células/mL) expostas ao ZVp na concentração de $5{,}9 \times 10^7$ ZVp/mL ou mantidas como controle por 24h a 37°C e 5% CO_2. O ponto de coleta foi definido de acordo com ensaios realizados por Dabaja et al (2018) (50) para a definição do GI50.

3.7 Preparo de amostra para metabolômica

Células obtidas dos ensaios celulares foram extraídas utilizando 200 µL de tetraidrofurano, seguido de homogeneização em vórtex por 30 s. A esta solução foram adicionados 780 µL de metanol com subsequente agitação seguido de centrifugação por 5 min à 3200 rpm. Em seguida, 20 µL do sobrenadante foram diluídos em 980 µL de metanol. Após a homogeneização a solução foi dividida em duas porções de 500 µL cada, nas quais adicionou-se ácido fórmico ou hidróxido de amônio a 0,1% da solução final, para as análises nos modos positivo e negativo.

3.8 Análise por espectrometria de massas

As amostras foram diretamente injetadas no espectrômetro de massas, com resolução variável, a depender do equipamento. Parâmetros específicos utilizados em cada análise encontram-se descritos nos resultados de cada capítulo. De forma geral, definiu-se o número de scans, o fluxo de injeção, a temperatura do capilar, a voltagem da fonte, e o fluxo de gás. As análises foram feitas nos modos positivo e negativo, na faixa de massa-carga (*m/z*) de 50 a

2000. Cada amostra foi analisada com 5 a 10 replicatas técnicas. A confirmação dos marcadores foi feita através de experimentos de espectrometria de massas sequencial (MS^n), usando Hélio como gás de colisão e energia de dissociação (CID) entre 20 e 50 eV.

3.9 Análise estatística e proposta estrutural

Dados coletados foram filtrados e normalizados, seguido de análise multivariadas, podendo essas serem supervisionadas por PLS-DA (Partial Least Square – Discriminant Analysis) ou não-supervisionadas por PCA (Principal Component Analysis). Para tais análises utilizou-se o software online MetaboAnalyst (www.metaboanalyst.ca)(88). Os marcadores foram selecionados utilizando a lista de importância (VIP score – Variable Importance in Projection) e anotados através da comparação entre a *m/z* experimental e a *m/z* teórica disponíveis em bancos de dados de metabolômica, como METLIN (Scripps Center for Metabolomics, La Jolla, CA – www.metlin.scripps.edu) , HMDB (Human Metabolome database - www.hmdb.ca), e LipidMaps (University of California, San Diego, CA - www.lipidmaps.org). Para a confirmação das propostas utilizou-se os dados de MS^n e fragmentação teórica obtidas pelo software Mass Frontier (v. 6.0, Thermo Scientific, San Jose, CA, EUA).

Para validação do modelo utilizou-se PCA com os marcadores identificados e testes de permutação (prediction accuracy during training). As variações de intensidade dos marcadores obtidas através de valores de log_2FC (condição/controle) e teste de wilcoxon com significância p-valor < 0,05 foram projetados em mapas de calor (heatmap).

Análises por aprendizado ML foram realizadas usando os dados dos marcadores identificados para as células PNT1a, seguindo método e software reportados por Delafiori et al. (2021) (89). Dados normalizados com máxima intensidade igual a 1 foram analisados utilizando os seguintes parâmetros:

- Separação dos dados: Treinamento (70%), Validação (30%)
- Número de experimentos de treinamento e validação: 10
- Delta J: seleção de marcadores com variação positiva ou negativa
- Algortimos: ADA, PLS, GDTB e RF
- Modelo de classificação: MCC

Baseados nos testes de validação, métricas são atribuídas para a classificação das amostras (Quadro 3)(20).

Quadro 3. Métricas de performance.

Métrica	**Fórmula**
Sensibilidade (SE)	VP/(VP+FN)
Especificidade (ES)	VN/(VN+FP)
Precisão (PR)	VP/(VP+FP)
Exatidão (EX)	(SE+ES)/2
Matthews' Correlation Coefficient (MCC)	((VP·VN)-(FP·FN))/ sqrt((VP+FP)·(VP+FN)·(VN+FP)·(VN+FN))

VP- Verdadeiro positivo; VN – verdadeiro negativo; FP – falso positivo; FN – falso negativo.

4. RESULTADOS

4.1 Capítulo 1

Artigo publicado na revista *Journal of Proteome Research* (versão publicada)

Delafiori, J., Faria, A. V. de S., de Oliveira, A. N., Sales, G. M., Dias-Audibert, F. L., Catharino, R. R. Unraveling the metabolic alterations induced by Zika infection in prostate epithelial (PNT1a) and adenocarcinoma (PC-3) cell lines. J. Proteome Res. 2023, 22, 193-203. https://doi.org/10.1021/acs.jproteome.2c00630.

(versão submetida)

Unraveling the metabolic alterations induced by Zika infection in prostate epithelial (PNT1a) and adenocarcinoma (PC-3) cell lines

Jeany Delafiori[1], Alessandra Valéria de Sousa Faria[2], Arthur Noin de Oliveira[1], Geovana Manzan Sales[1], Flávia Luísa Dias-Audibert[1], and Rodrigo Ramos Catharino[1,*]

1 Innovare Biomarkers Laboratory, School of Pharmaceutical Sciences, University of Campinas, Campinas/SP, 13083-970, Brazil

2 Department of Biochemistry and Tissue Biology, University of Campinas, Campinas/SP, 13083-862, Brazil

*corresponding author: Rodrigo Ramos Catharino, rrc@unicamp.br, Innovare Biomarkers Laboratory, School of Pharmaceutical Sciences, University of Campinas - Rua Cinco de Junho, 350 - 13083-970 - Cidade Universitária Zeferino Vaz, Campinas/SP – Brazil, Phone: +55 19 3521-9138.

ABSTRACT

The outbreak of Zika virus infection in 2016 led to the identification of its presence in several types of biofluids, including semen. Later discoveries associated Zika infection with sexual transmission, which is explained by viral persistent replication in cells of the male reproductive tract. Several studies demonstrated prostatitis as an associated infection symptom putting the prostate gland as a potential virus reservoir, implicating it in temporary male infertility. Prostate epithelial and carcinoma cells are permissive to virus replication, with studies pointing to transcriptomics alterations of immune and inflammation genes upon persistence. However, metabolome alterations promoted by the Zika virus in prostate cells are unknown. Given its chronic effects and oncolytic potential, we aim to investigate the metabolic alterations induced by the Zika virus in prostate epithelial (PNT1a) and adenocarcinoma (PC-3) cells using an untargeted metabolomics approach and high-resolution mass spectrometry. PNT1a cells were viable up to 15 days post-ZIKV infection, in contrast to its antiproliferative effect in the PC-3 cell lineage. Remarkable alterations in PNT1a cells metabolism were observed upon infection, especially regarding glycerolipids, fatty acids, and acylcarnitines, that could be related to viral cellular resources exploitation, in addition to the overtime increase in oxidative stress metabolites associated with carcinogenesis. The upregulation of FA20:5 at 5-dpi in PC-3 cells corroborates the antiproliferative effect observed since this metabolite was previously reported to induce PC-3 cell death. Overall, Zika virus promotes extensive lipid alterations on both PNT1a and PC-3 cells, promoting different outcomes based on cellular metabolic state.

Keywords: mass spectrometry; Zika virus; prostate cells; prostate cancer; metabolomics.

INTRODUCTION

Zika virus (ZIKV) is a flavivirus from the Flaviviridae family first detected in 1947 in Uganda [1]. A self-limiting febrile disease was reported for this arbovirus until 2015 when the outbreak in the Americas and Pacific Islands. In that occasion, Zika virus infection was associated with several cases of Guillain-Barré syndrome and congenital microcephaly [2,3]. Consequently, Zika infection-related outcomes were for the first time in the spotlight.

The gained visibility of Zika epidemiology importance [3] was supported by reports of Zika virus impact on neuronal growth impairment and its oncolytic potential in neural tumor management [4–8]. Zika neurotropism and replication were characterized by an interruption in the cell cycle and cell death induction [6–10]. In addition to nervous system tropism, ZIKV can be transmitted sexually; viral RNA was detected in semen for more than 60 days after symptoms onset, being accompanied by prostatitis in some cases [11–13]. In this context, the assessment of male reproductive systems' cells to ZIKV infection susceptibility was amplified; finds of the potential involvement of human prostate cells as Zika replication site have shown stable viral RNA concentrations up to 14 days post-infection [12]. Short-term ZIKV infection in prostate cancer cells DU-145 also demonstrated high and consistent virus titter during 72h [7]. Izuagbe et al. (2019) observed that ZIKV persistent infection in prostate epithelial cells led to transcriptomics alterations in genes involved in antiviral and immune response, such as viral recognition, expression of cytokines, and interferons [14]. Additionally, Machado et al. (2021) presented miRNAs generated during human prostate cell infection with a Brazilian ZIKV strain had genes involved in inflammation, immunity, cell survival and proliferation as in silico predicted targets [15].

Overall, cell machinery is remodeled during flavivirus replication, especially for the use of cell substrates for replication and lipid biogenesis [16]. In metabolic terms, prostate cells are known to have a peculiar inefficient energy metabolism at the basal state. Prostate cells rewire citrate production to excretion by inhibiting citrate conversion to isocitrate in the TCA cycle [17–19]. This results in the accumulation of citrate, and as consequence, less production of energy through oxidative phosphorylation (OXPHOS) and lipid synthesis [18,19].

However, during the malignant process mitochondrial aconitase is less inhibited, leading to the use of accumulated citrate for energy production via OXPHOS, altered fatty acid (FA) metabolism, and lipid droplet (LD) accumulation [17–21]. As the tumor progresses, metastatic cells further decrease the use of OXPHOS, being remarked by glucose consumption and lactate production, known as the Warburg effect [17,19]. Considering the characteristics of prostate normal and cancer cells metabolism and the flavivirus replication, the impact of Zika persistent infection in human epithelial prostate cell and cancer cell metabolism and proliferation needs further investigation.

Studies to assess Zika infection mechanisms are important to propel the understanding of transmission prevention and clinical manifestations [6,8,9,22,23], to surpass the challenges for new approaches for diagnosis, treatment, and vaccines [24–26], and the virus use in Zika-related therapies [4,5,10]. This comprehension can be further extended by metabolomics using high-resolution mass spectrometry [10,16,26–28], which aims to assess, at the low-weight molecular level, the metabolic alterations that result in cell phenotype. Therefore, associating the multifactorial characteristics of Zika infection to the susceptibility of prostate cells to persistent infection, this study aims to employ an untargeted metabolomics approach for the investigation of metabolic alterations induced by Zika virus in epithelial prostate cells (PNT1a) and prostate adenocarcinoma (PC-3) at short- and long-term exposure.

MATERIALS AND METHODS

Zika strain and cell culture

The Brazilian ZIKV strain (BeH823339, GenBank KU729217) was isolated from a patient in 2015 at Evandro Chagas Institute (Pará state, Brazil) and kindly provided by Prof. Dr Edison Durigon (University of São Paulo, USP). The ZIKV strain stock were maintained at -80°C in the Laboratory of Emerging Viruses (Institute of Biology, UNICAMP). Before cellular assays, viral stock titer was determined by plaque assay in Vero cells (PFU/mL).

Human prostatic immortalized cell line (PNT1a) and human prostate adenocarcinoma cell line (PC-3) were kindly provided by the In vitro Bioassays and Signal Transduction lab (Institute of Biology, UNICAMP). Cells were routinely growth at $4x10^4$ cells/cm2 density in RPMI-1640 medium supplemented with 100 U/mL penicillin, 100 µg/mL streptomycin, and fetal bovine serum (FBS) 10% (Gibco, Thermo Fisher Scientific), and propagated at 37°C, 85% humidified and 5% CO_2 atmosphere. All lines were routinely checked for mycoplasma.

Colony formation assay

PNT1a and PC-3 colony formation assays were performed by seeding 2.8 $x10^3$ cells/well in a 6-well plate. Cells were maintained at 37°C, 85% humidified and 5% CO_2 atmosphere for 24h to adhere. Cells were exposed to ZIKV multiplicity of infection (MOI) of 1 and 5, and together with mock cells were cultured for 15 days at incubator (37°C, 85% humidified and 5% CO_2 atmosphere). Culture medium was top-up at days 3, 7 and 10. After 15 days, supernatant was removed, cells washed with PBS, fixed and stained for 30 min with crystal violet 5% (methanol:water). The solution was removed, and cells washed three times with water. Representative images were acquired with phase-contrast microscope (Nikon, Japan), and colonies counted using ImageJ (NIH, USA).

Viability assay

Cell viability assay was conducted by measuring cell capacity in reducing MTT (3-(4,5-dimethylthiazol-2-yl)-2,5-diphenyltetrazolium bromide). PC-3 and PNT1a cells were seeded in a 96-well plate at $2.8x10^3$ cell/well density in triplicate. After 24h at 37°C and 5% CO_2, cells were exposed to ZIKV MOI 1, and together with mock cells were maintained in culture for 1, 2 and 3 days. Cell supernatant was removed and replaced by 100 µl/well of MTT solution (0.5 mg/mL, in an FBS-free culture medium, sterile-filtered). After incubation for 3h at 37°C, 85% humidified and 5% CO_2 atmosphere, medium was removed, and 100 µL/well ethanol were added to solubilize formazan. The microplates were shaken

at a speed of 100 rpm, 10 min (Labnet orbit 1000), for solubilizing the formazan produced. Absorbance was measured at λ = 570 nm in a microplate reader spectrophotometer (Synergy HT, BioTek). Cell viability was calculated using mock cells absorbance as reference and graphs generated using GraphPad Prism 5.0.

Metabolomics assay

PNT1a and PC-3 cells were seeded at $4.2x10^3$ cells/well density in 24-well plates and kept at 37°C, 85% humidified and 5% CO_2 atmosphere. After 24h, cells were exposed to ZIKV strain at MOI 1. Mock cells were kept at the same conditions and timepoints, except by the exposure to ZIKV. Cell culture medium was top-up at days 3, 7 and 10 according to each time point. PNT1a cells were harvested at timepoints 5-, 10- and 15-days post infection (dpi), while PC-3 cells were collected at 5 dpi. Culture medium was carefully removed, cells were washed with a solution of NaCl (0.9%) and scraped from wells to a plastic tube. Cells suspensions were centrifuged for 5 min, 300×g at 4°C to allow pellet formation. The supernatant was discarded, cell pellet resuspended in 200 µL of ice-cold tetrahydrofuran and homogenized for 30 seconds. Additionally, 800 µL of ice-cold methanol was added. Cell suspension was homogenized, sonicated for 5 min and centrifuged for 5 min, 1230×g at 4°C. A 10 µL aliquot of the supernatant was diluted in 980 µL of methanol ionized with 1 µL formic acid. Each sample was diluted into two preparation duplicates for analysis.

Mass spectrometry analysis and metabolites' annotation

The extracted samples were directly infused in a HESI-Q Exactive Orbitrap (Thermo Scientific, Germany), with resolution of 140,000 FWHM. Mass spectral data was acquired for each sample with 5 technical replicates using positive ion mode and mass range from 175 – 1,000 m/z. Instrument was tuned with the following parameters: HESI 33°C, flow rate 10 µL/min, capillary temperature 320°C, spray voltage 3,7 kV, sheath gas flow of 5 (arbitrary units), RF-lens 50, AGC-target 1 x 10^6, and 50 scans/ acquisition. XCalibur 3.0.63 software (Thermo

Scientific, Germany) was used to visualize spectral data. Mass-to-charge (m/z) values were annotated using exact mass with accuracy < 5 ppm when compared to METLIN database (Scripps Center for Metabolomics, La Jolla, CA – www.metlin.scripps.edu). Additional databases such as LIPIDMAPS (University of California, San Diego, CA - www.lipidmaps.org), HMDB (Human Metabolome database - www.hmdb.ca), and Kegg (Kyoto Encyclopedia of Genes and Genomes - www.genome.jp/kegg), and literature search assisted on markers annotation, and biological function assessment.

Statistical analysis

Mass spectra data of cells infected with Zika virus at three different exposure times (5-, 10- and 15-dpi) were compared to their respective mock cells. Mass signals were aligned, filtered (interquartile), normalized by pooled sample from control group (PQN) and transformed (logarithm base 10) prior multivariate statistical analysis using partial least squares discriminant analysis (PLS-DA) on MetaboAnalyst 5.0 web server (www.metaboanalyst.ca) [29]. For each comparison of ZIKV and Mock cells at each timepoint a VIP score list > 1.1 was used to select discriminant *m/z* values for annotation (described in the section above). Annotated datasets were used to project a principal component analysis (PCA) score plot and loadings to observe groups discrimination and markers contribution. The significance of markers' intensity variation was assessed by differential analysis where fold changes (FC) of logarithmic transformed data (ZIKV/Mock cells) at each timepoint were compared, and a p-value (FDR-adjusted) attributed. Volcano plots of markers with FC > 1.5 and p-value < 0.05 illustrate markers considered significant for the conditions. Log_2(FC) values provided for each metabolite and their respective significance allowed the comparison of timepoints through a heat map analysis. Plots were generated with R coding.

RESULTS

Metabolomics of ZIKV infection persistence in PNT1a cells

Zika virus is known to infect several types of human cells. Here we aim to demonstrate how prostate cell viability upon ZIKV infection is cell type-dependent and the metabolic changes during Zika persistent infection, which it is not-well characterized. Therefore, we performed colony formation assays and untargeted metabolomics analysis using high-resolution mass spectrometry as illustrated in Figure 1A. A colony formation assay was used to evaluate the influence of ZIKV multiplicity of infection (MOI) of 1 and 5 in PNT1a cells proliferation when compared to non-infected cells (Mock). Considering a persistent infection of 15 days, we observed cell exposure to ZIKV MOI 1 did not substantially affect proliferation. As a result, a colony count of 104% compared to the control indicates the maintenance of cell viability and function upon persistent infection for 15 days (Figure 1B). However, upon MOI increase to 5, a decrease to 67% in colonies count was observed.

Considering the maintenance of cell viability upon infection with ZIKV MOI 1, we performed a metabolomics assay where harvested PNT1a mock and ZIKV-infected cells were extracted with polar organic solvents, ionized, and directly infused in a high-resolution mass spectrometer. Ion signals ranging from 175 to 1000 *m/z* were processed as described in the methods. Data were analyzed using multivariate statistical analysis through PLS-DA to discriminate between Mock and ZIKV infected groups (Supplementary Figure S1). For each timepoint, 5-, 10- and 15-days post-infection (dpi), a list of ions ranked by importance was used as the basis for metabolite annotation. A total of 62 metabolites were annotated by combining the three timepoints (Table S1). Fatty acids, carnitines, and glycerolipids were among the annotated lipid classes, in addition to small metabolites such as phosphohydroxypyruvate, phosphocreatine, N-lactoylphenylalanine, hydroxyguanosine, and dityrosine.

Together, these annotated markers supported and validated the discrimination of Mock from ZIKV infected PNT1a cells at 5-, 10- and 15-dpi using unsupervised principal component analysis (Figure 1C). At each timepoint, PCA score plot provided high explanation of variability through components, with

78.8% (PC1+PC2) for 5-dpi, 58.2% for 10-dpi, and 67.5% for 15-dpi. PCA loadings (Figure 1D) show the metabolites with the greatest effect on each component (loadings close to -1 or 1). In the first days of infection (5 dpi), ZIKV-infected cells were characterized mainly by the variation of phosphohydroxypyruvate, phosphocreatine, N-lactoylphenylalanine, phosphoguanidinoacetate, and lysophosphatidic acid (LPA 20:1) ions' intensity. In addition to these markers, hydroxylated fatty acids (FA 16:1;O, and FA 14:1;O) influenced the discrimination between PNT1a ZIKV-infected cells and mock cells at 10-dpi. Notably at 15-dpi, we observed a pronounced variation in the intensities of the glycerolipids class.

Aiming to qualitatively assess how much each marker contributed to these results, fold-changes > 1.5 for ZIKV-infected PNT1a cells and PNT1a mock cells at each timepoint were compared and a p-value (FDR-adjusted) attributed, as shown in the volcano plots (Supplementary Figure S2 and Table S1). Log_2FC > 1 indicates metabolite increase in PNT1a ZIKV-infected cells, while log_2FC < 1 indicates a decrease. Heat maps using these results are displayed in Figure 1E. At 5-dpi, phosphohydroxypyruvate (log_2FC 3.33, p-value < 0.05), phosphocreatine (log_2FC 3.07, p-value < 0.05), phosphoguanidinoacetate (log_2FC 3.54, p-value < 0.05), and N-lactoylphenylalanine (log_2FC 4.32, p-value < 0.05) intensities were found elevated in infected cells compared to control. However, the replication persistence promotes a shift in these metabolites' distribution across timepoints, going to normality, while a change from decreased to increased intensities of hydroxyguanosine, dityrosine, and aminotyrosine in infected cells are observed. Remarkably, few species of triacylglycerols (TG), and diacylglycerol (DG) were up regulated at 5-dpi, in contrast to decreased intensities of monoacylglycerols (MG). However, within time, results show a general downregulation of TGs species, while MGs increase.

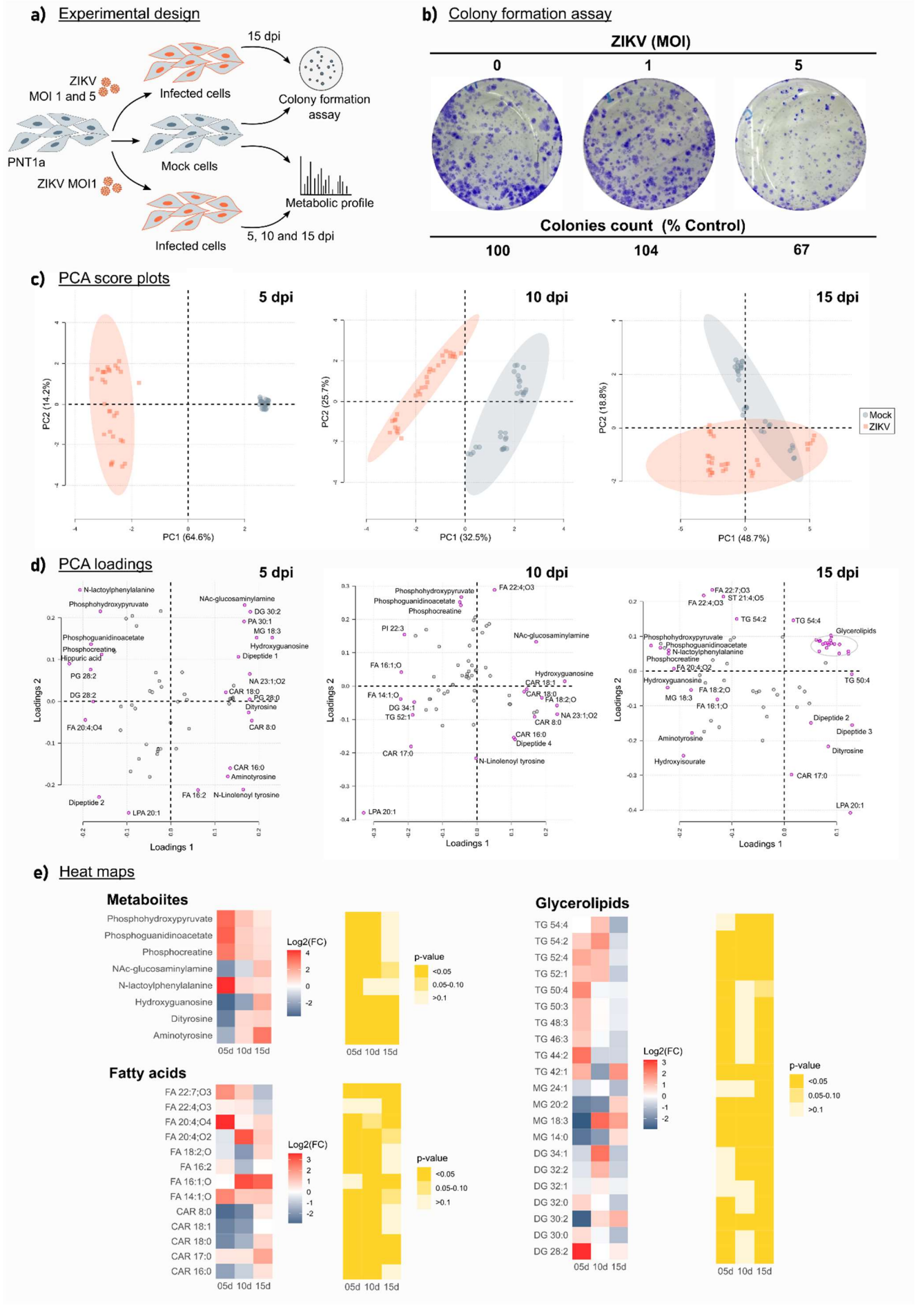
a) Experimental design
15 dpi
ZIKV
MOI 1 and 5
Infected cells
Colony formation assay
PNT1a
Mock cells
ZIKV MOI1
Metabolic profile
Infected cells
5, 10 and 15 dpi
b) Colony formation assay
ZIKV (MOI)
0
1
5
Colonies count (% Control)
100
104
67
c) PCA score plots
5 dpi
10 dpi
15 dpi
PC2 (14.2%)
PC1 (64.6%)
PC2 (25.7%)
PC1 (32.5%)
PC2 (18.8%)
PC1 (48.7%)
Mock
ZIKV
d) PCA loadings
5 dpi
10 dpi
15 dpi
Loadings 2
Loadings 1
N-lactoylphenylalanine
Phosphohydroxypyruvate
Phosphoguanidinoacetate
Phosphocreatine
Hippuric acid
PG 28:2
DG 28:2
FA 20:4;O4
Dipeptide 2
LPA 20:1
NAc-glucosaminylamine
DG 30:2
PA 30:1
MG 18:3
Hydroxyguanosine
Dipeptide 1
NA 23:1;O2
CAR 18:0
PG 28:0
Dityrosine
CAR 8:0
CAR 16:0
Aminotyrosine
FA 16:2
N-Linolenoyl tyrosine
FA 22:4;O3
PI 22:3
FA 16:1;O
FA 14:1;O
DG 34:1
TG 52:1
CAR 18:1
FA 18:2;O
CAR 17:0
Dipeptide 4
FA 22:7;O3
ST 21:4;O5
FA 22:4;O3
TG 54:2
TG 54:4
Glycerolipids
FA 20:4;O2
TG 50:4
MG 18:3
Dipeptide 2
Dipeptide 3
Hydroxyisourate
e) Heat maps
Metaboiites
Phosphohydroxypyruvate
Phosphoguanidinoacetate
Phosphocreatine
NAc-glucosaminylamine
N-lactoylphenylalanine
Hydroxyguanosine
Dityrosine
Aminotyrosine
05d 10d 15d
Log2(FC)
p-value
<0.05
0.05-0.10
>0.1
Fatty acids
FA 22:7;O3
FA 22:4;O3
FA 20:4;O4
FA 20:4;O2
FA 18:2;O
FA 16:2
FA 16:1;O
FA 14:1;O
CAR 8:0
CAR 18:1
CAR 18:0
CAR 17:0
CAR 16:0
Glycerolipids
TG 54:4
TG 54:2
TG 52:4
TG 52:1
TG 50:4
TG 50:3
TG 48:3
TG 46:3
TG 44:2
TG 42:1
MG 24:1
MG 20:2
MG 18:3
MG 14:0
DG 34:1
DG 32:2
DG 32:1
DG 32:0
DG 30:2
DG 30:0
DG 28:2

Figure 1. Metabolomics study to investigate PNT1a cell proliferation and metabolism during ZIKV persistent infection. A) Experimental design comprising a colony formation assay and cell harvesting for metabolomics analysis. B) Colony formation assay of PNT1a upon Zika infection with MOI 1 and 5 compared to mock cells, maintained in culture for 15 days. C) PCA score plots at 5-, 10-, and 15-dpi timepoints showing the discrimination between PNT1a infected cells and mock cells. D). PCA loadings highlighting metabolites that mostly contributed to the conditions discriminated in PCA score plots. E) Heat maps displaying the intensity levels (log_2FC) and significance (p-value < 0.05) of selected metabolites at 5-, 10- and 15-dpi of PNT1a cells. FC ratio compares infected cells over mock cells; positive log_2FC (in red) corresponds to metabolites increased in ZIKV-infected cells, while negative log_2FC (in blue) corresponds to decreased metabolites. Abbreviations: CAR – acylcarnitine; DG – diacylglycerol; FA – fatty acid; MG – monoacylglycerol; TG – triacylglycerol. Metabolites are subjected to isomers.

Differences between PNT1a and PC-3 metabolism upon ZIKV infection

The workflow for the comparison of PNT1a and prostate adenocarcinoma cells (PC-3) response to Zika infection was composed by cell viability assay using MTT, colony formation assay and metabolomics analysis (Figure 2A). Cell viability assay at timepoints 1-, 2-, and 3-dpi shows the trend of decreasing PC-3 cells viability, in contrast to the maintenance of PNT1a cells proliferation (Figure 2B). Considering the colony formation assay with ZIKV MOI1, PC-3 cells proliferation was completely inhibited with 15 days, and cells loosely detached from dish plates upon crystal violet treatment. This observation indicated that in addition to the susceptibility to ZIKV infection, PC-3 cells viability was compromised upon persistent replication. A deeper look into brightfield microscopy at 5-, 10- and 15-dpi (Figure 2C) shows a progressive loss of PC-3 cell characteristic elongated morphology with increasing of dead cells.

Considering the vulnerability of PC-3 cells to ZIKV infection when compared to PNT1a, the timepoint of 5-dpi was considered for metabolomics evaluation. As previously stated, cell extracts were directly infused into a high-

resolution mass spectrometer. Data were processed and analyzed using PLS-DA (Supplementary Figure S3) to discriminate between PC-3 ZIKV-infected cells and Mock cells at 5-dpi timepoint and rank the most important variables (*m/z*) for annotation. A combined table describing annotated markers for PC-3 and PNT1a at 5-dpi is available as Supplementary material Table S2. These markers were important to discriminate Mock from ZIKV-infected cells through unsupervised analysis (PCA) (Figure 2D) with explained variance of 70% (PC1+PC2). PCA loadings show important contribution of fatty acids (FA16:2 and FA18:3;O), N-Acetyl-glucosaminylamine and N-Acetyl-glucosamine, and glycerolipids class in general, especially triacylglycerols (Figure 2E).

A volcano plot using $log_2FC > 1.5$ and p-value < 0.05 (FDR-adjusted) is present as Supplementary Figure S4. Selected metabolites were included in heat maps for qualitative evaluation of the two cell lines response to short-term Zika infection (Figure 2F). N-lactoylphenylalanine, phosphocreatine, and isoxanthopterin/xanthopterin were found less increased in PC-3 when compared to PNT1a. N-acetylglucosamine was found downregulated in both cell types, being more intensively decreased in PC-3 cells. Additionally, FA 20:5 and FA 18:3;0 were differential metabolites when compared to PNT1a, while several other TG species where enhanced at 5-dpi, potentially reflecting the lipid accumulation characteristic of prostate cancer cells.

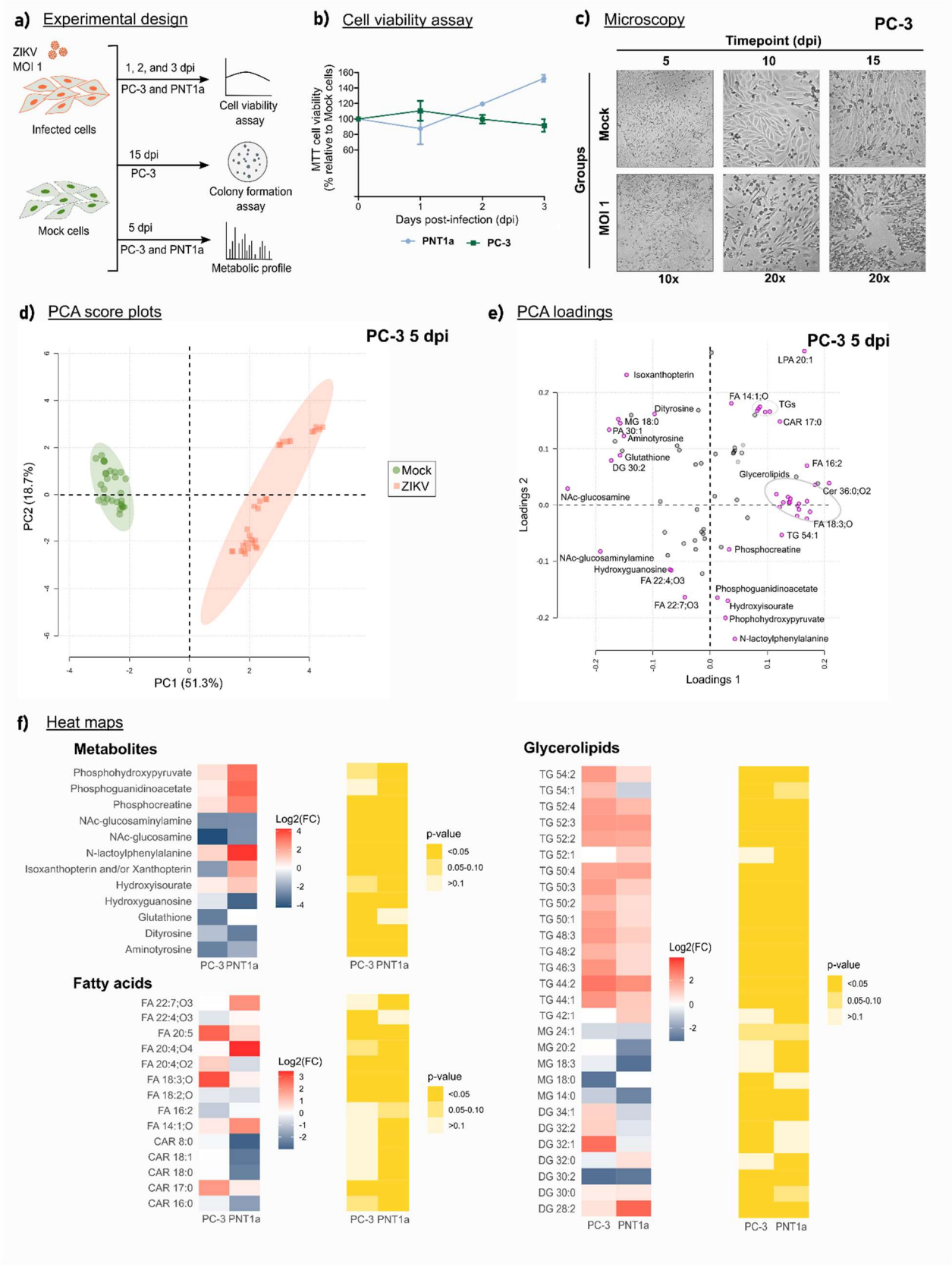

Figure 2. Metabolomics study to compare PNT1a and PC-3 cell proliferation and metabolism upon short-term Zika infection. A) Experimental design comprising

cell viability assay (MTT), colony formation assay and metabolomics analysis. B) Cell viability assay using MTT at 1-, 2- and 3-dpi showing a trend of PC-3 proliferation inhibition. C) Brightfield microscopy images acquired during colony formation assay at 5-, 10-, and 15-dpi, showing PC-3 cell morphology loss and increase in the number of dead cells. D). PCA score plot of PC-3 at 5-dpi showing the discrimination between infected cells and mock cells. E) PCA loadings highlighting metabolites that mostly contributed to the conditions discriminated in PCA score plot. E) Heat maps displaying the intensity levels (log_2FC) and significance (p-value < 0.05) of selected metabolites at 5-dpi for both PNT1a and PC-3 cells. FC ratio compares infected cells over mock cells; positive log_2FC (in red) corresponds to metabolites increased in ZIKV-infected cells, while negative log_2FC (in blue) corresponds to decreased metabolites. Abbreviations: CAR – acylcarnitine; DG – diacylglycerol; FA – fatty acid; MG – monoacylglycerol; TG – triacylglycerol. Metabolites are subjected to isomers.

DISCUSSION

Evidence of Zika virus sexual transmission and long-term viral load in semen generated a series of studies to address the impact of ZIKV replication on the male reproductive system [11–13]. Prostate cells were confirmed to be permissive to ZIKV infection and pointed to as a potential replication reservoir [7,12]; however, only a few studies focused on addressing the mechanism of persistence in prostate cells [14,15]. In this study, our contributions towards understanding ZIKV persistence in prostate cells include: (i) a demonstration of how ZIKV infection impacts cell viability of a prostate epithelial cell line (PNT1a) and a prostate adenocarcinoma cell line (PC-3) at short and long-term; (ii) the metabolic alterations induced by ZIKV persistent replication in PNT1a during a 15-days assay; (iii) the metabolic differences between the short-term infection in PNT1a and PC-3. Therefore, this is the first metabolomic study based on high-resolution mass spectrometry designed to investigate Zika replication persistence in prostate cells.

ZIKV effects on prostate cells is cell-type dependent

Recently, Machado et al. (2021) demonstrated that PNT1a cells are permissive to the Brazilian ZIKV strain [15]. Prostate mesenchymal cells and epithelial adenocarcinoma cells were previously reported as susceptible to Zika persistent replication, with the detection of stable concentrations of viral RNA in a 14-days assay [12]. ZIKV RNA detection in prostate cells was further extended to 30-dpi in vitro. Izuagbe (2019) reported no difference in epithelial cell viability up to 30 days at low MOI infection, regardless of the strain [14]. Similarly, we demonstrated that prolonged in vitro ZIKV infection of PNT1a at low multiplicity (MOI) did not affect cellular proliferation in 15 days. Even though PNT1a ZIKV-infected cell viability was comparable to mock cells, substantial alterations in cell metabolism were observed.

Fatty acids and oxidized fatty acids (oxylipins) were found remarkably altered upon prostate epithelial cells ZIKV-infection (Figure 1E). Oxylipins can be generated enzymatically and non-enzymatically mediated by ROS, showing increased and decreased levels according to molecule specie and timepoint. These bioactive lipids carry out important roles as anti-inflammatory and pro-inflammatory agents. To mention, we observed a significant decrease in FA 18:2;O at 5- and 10-dpi in infected cells compared to control with a slight increase at 15-dpi. This molecule can correspond to 9- and/or 13-HODE (hydroxy-decadienoic acid) which exerts pro-inflammatory and anti-inflammatory properties, respectively. Both oxylipins were found to increase in placenta infected with ZIKV, and plasma of newborns with ZIKV-induced microcephaly [30,31]. In a study with blood donors, Catala et al. (2022) demonstrated that FAs and oxylipins concentrations on red blood cells infected by ZIKV are time-dependent, with HODE intensities increasing after 10-dpi [32].

Moreover, we detected markers associated with enhanced oxidative stress. Dityrosine, aminotyrosine, and hydroxyguanosine intensities in ZIKV-infected cells increase in prolonged cellular infection (15 dpi). The nitration of tyrosine is a protein posttranslational modification promoted by the presence of ROS (reactive oxygen species), leading to functional alterations; their increase is associated with inflammation-related diseases [33,34]. ROS also interacts with guanosine nucleoside from RNA and DNA producing hydroxyguanosine, a

marker associated with prostate cancer and tumor progression [35]. Alterations in tumor-related genes have been reported by previous study. Prostate epithelial cells infected with ZIKV presented altered expression of innate immune response genes, such as interferon at 6-dpi. At 21-dpi, a significant increase in the expression of genes involved in cell cycle functions and prostate tumorigenesis was observed [14]. Additionally, miRNAs differentially expressed upon ZIKV infection in PNT1a cells showed in silico predictions correlated with inflammation, immunity, cell survival and proliferation genes, with these potential targets enriched in Kegg cancer pathways [15]. Regarding immune system, IFN-γ response, increased levels of other inflammatory cytokines (IL-1β, TNF-α), and ROS are related to prostatitis, and ultimately linked to low-quality sperm and infertility [36]. Altogether, this suggests that host cell response to prolonged ZIKV-infection triggers inflammatory processes, which is corroborated by prostatitis being a recurrent symptom associated with ZIKV infection in men [13].

In contrast to PNT1a, we report prostate adenocarcinoma cells (PC-3) as more susceptible to cell death upon ZIKV-persistent infection, showing trends of cell proliferation inhibition already within 72 hours. When comparing PC-3 metabolic alterations to PNT1a at 5-dpi, the increase in FA 18:3;0 and FA 20:5 is more pronounced in PC-3 infected cells. FA 20:5 (eicosapentaenoic acid) is a precursor of oxylipins, markers previously found altered in ZIKV-infected placentas [30]. It inhibits the phosphorylation of proline-rich tyrosine kinases (PYK2) and ERK, and induces overproduction of ROS, exerting anti-proliferative effects in PC-3. This anti-cancer effect has been pointed out by Oono et al. (2020) as dose-dependent, decreasing PC-3 cell proliferation, migration, and invasion [37]. Consistent with a potential increase of ROS species, we have observed a significant decrease in the antioxidant molecule glutathione (log_2FC = -3.02, p-value < 0.05) in PC-3 ZIKV-infected cells, while this marker was not even detected in PNT1a. The reduction of antioxidants may lead to apoptosis signaling [38]. Additionally, the oxylipin FA 18:3;0 could correspond to hydroxy-octadecatrienoic acid (HOTrE). As well as 13-HODE, 13-HOTrE stimulates PPAR-γ receptors, exhibiting anti-inflammatory properties, reducing the accumulation of lipid droplets, and inducing apoptosis [39,40]. Both HODE and HOTrE are metabolites of 15-LOX, an enzyme overexpressed in prostate normal

cells but not in PC-3. However, PC-3 overexpresses PPAR-γ in contrast to normal cells [40]. Therefore, we hypothesize that oxylipins ligands of PPAR-γ may promote inhibition of cell proliferation in prostate cancer cells, but this effect may not be significant for normal cells.

ZIKV-induced metabolic cell fate is dependent on the malignancy behavior of prostate cells

Prostate cell metabolism is heavily influenced by intracellular zinc availability [17]. At a normal metabolic state, high zinc concentrations inhibit mitochondrial aconitase resulting in the accumulation of citrate and its cellular excretion to compose the seminal fluid. Considering that citrate is not available for oxidation in the TCA cycle and further generation of ATP by OXPHOS, prostate epithelial cells are energetically inefficient (Figure 3) [17–19]. This metabolic state is shifted during the early stages of the malignancy process where zinc availability is restricted, and cancer cells can oxidize citrate for energy production. Stocks of acetyl-CoA enable intensive lipid metabolism, promoting de novo lipogenesis and lipid accumulation as lipid droplets (LDs) in balance with increased fatty acids β-oxidation [19–21]. Later, prostate cancer cells will require extra energy input from anaerobic glycolysis to maintain tumoral phenotype [17,18]. Lipid metabolism is a key factor in cancer progression, contributing to energy production, alterations in membrane fluidity for increased invasiveness, and cell signaling, including apoptosis [20,21,41]. Lipid metabolism regulators, such as FASN, DGAT, and SREBP have been found overexpressed in the prostate cancer cells, and therefore, pointed as target to constrain disease progression [21,41].

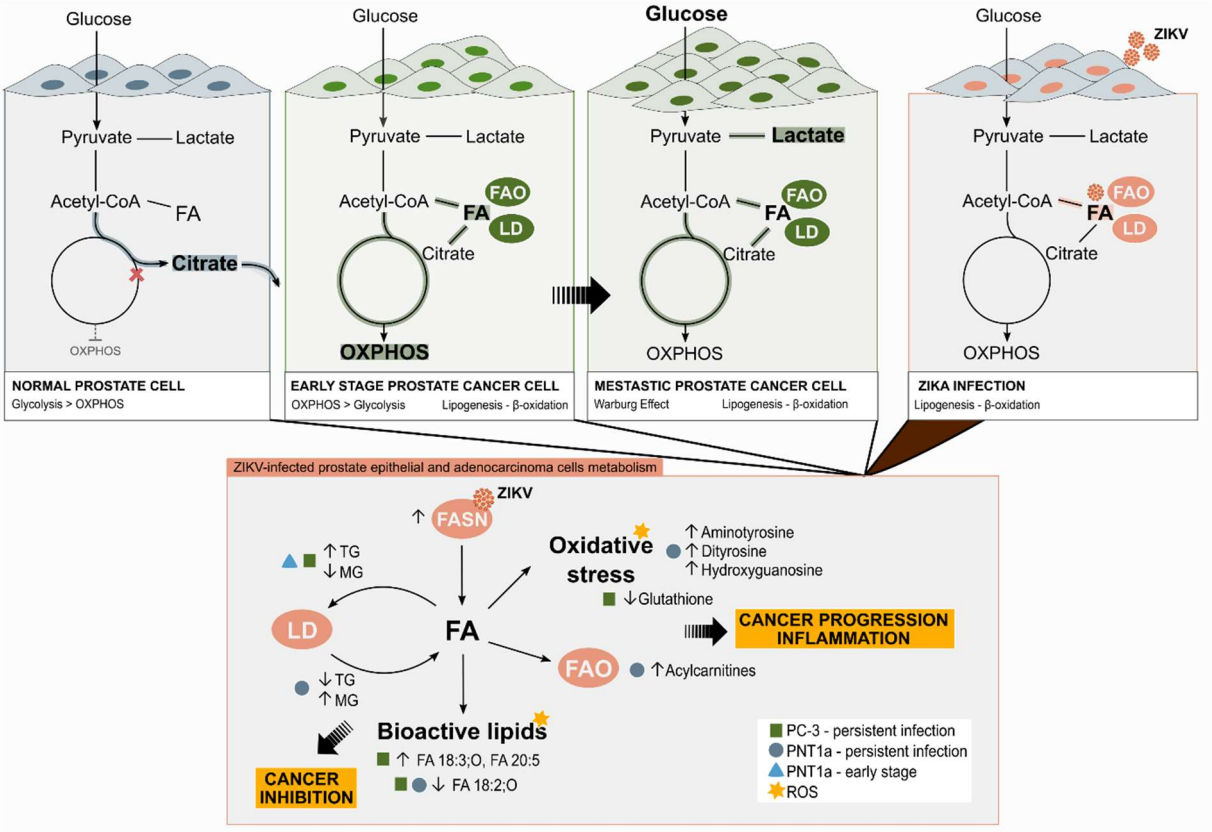

Figure 3. Expected cell metabolic states of normal epithelial prostate cells, early stage and metastatic prostate cancer cells, and ZIKV infection metabolic remodeling highlighting cell energetic state and lipid metabolism (top). Full picture of detected metabolites and their importance to lipid metabolism in PNT1a and PC-3 under short and persistent Zika infection. Abbreviations: FA – fatty acid; FAO – fatty acid oxidation; LD – lipid droplet; MG – monoacylglycerol; OXPHOS – oxidative phosphorylation; ROS – reactive oxygen species TG – triacylglycerol.

Likewise, lipid metabolism is fundamentally altered by flavivirus infection and propagation. Flaviviruses induce cell lipogenesis to create fatty acids as substrates for β-oxidation and biosynthesis of more complex lipids; these will compose membrane rearrangements, as well as accumulate in LDs [16,42]. Conversely, drug therapies targeting key enzymes of lipid metabolism, such as FASN, DGAT and SREBP, and PPAR-γ receptor, have been pointed out as effective for both inhibitions of flavivirus replication and cancer progression [19,21,30,38,41–43]. It has been reported that DENV and ZIKV manipulate

SREBP pathways, regulating FASN, a key enzyme in fatty acid biosynthesis, and perturbing LDs homeostasis [44]. The flavivirus non-structural protein NS3 directly interacts with FASN, promoting its delocalization to sites of viral replication. By co-opting fatty acid biosynthesis to the endoplasmic reticulum (ER), flavivirus establishes an energetic source within replication complexes [45]. In ZIKV-infected placenta, FASN mRNA levels were found increased, suggesting the upregulation of this enzyme upon infection [30]. Fatty acid excess is cytotoxic for cells, and therefore, they are transformed into complex lipids such as triacylglycerols (TGs). TGs are formed by the action of DGAT and stored as lipid droplets derived from ER membranes [30,42,44]. While in infected placentas ZIKV induced DGAT upregulation and accumulation of LDs, other flavivirus and ZIKV are also known to promote lipophagy of LDs, consequently declining TGs levels throughout of the infection [42,44,46]. The initial increase in LDs has been associated with the stimulation of interferon response against Zika for infection control [47].

We observed a significant increase in TGs in infected PNT1a cells at 5-dpi and a progressive decrease at 15-dpi. In contrast, monoacylglycerols (MG), subproducts of TG metabolism, and acylcarnitines presented an inverse trend. These alterations are in accordance with the accumulation of TG in LDs in the first stages of infection followed by the expected lipophagy promoted by the flavivirus. Moreover, since LDs accumulation is related to initial interferon activation, enhanced TGs levels on the first days of normal prostate cells infection could be linked to the observation of upregulation of interferon-related genes found by Izuagbe et al (2019) at 6-dpi [14]. While normal prostate cells do not energetically depend on FASN, DGAT, and accumulation of LDs, the competition for fatty acid biosynthesis and depletion of lipid storage may be significant and depreciative to prostate cancer cells. Acylcarnitines were found to decrease during the early days of infection in both PNT1a and PC-3. As the infection progresses, acylcarnitine's levels increase in PNT1a Zika-infected cells at 15-dpi, as a potential consequence of TG degradation to MG and FA observed with persistent infection. Acylcarnitines act as carriers of FAs to mitochondria for β-oxidation. In prostate cancer, miRNAs modulate enzymes involved in the transport of carnitines collaborating to control intense FA load to mitochondria

[48]. It has been shown that Zika infection interferes with mitochondria morphology potentially causing its dysfunction [6,30]. Therefore, the increase of acylcarnitines over time may reflect Zika's interference in mitochondrial function.

Considering the cell metabolic remodeling promoted by ZIKV, as it superposes to important characteristics of prostate normal and cancer cells basal metabolism, it is plausible to expect that these cells will behave metabolically different upon infection (Figure 3). In general, cell metabolic state of increased fatty acid synthesis, their storage as LDs, and metabolization by β-oxidation induced by ZIKV are similar to the cellular state expected from prostate cancer; this conflict for resources may be a factor for cell proliferation inhibition. Conversely, ZIKV may be benefited through prostate epithelial cells metabolism, by using citrate as a primary source for FA biogenesis. As the infection persists, we observed that PNT1a becomes more stressed, which perhaps contribute to cell malignancy, corroborating the trends of cancer upregulated pathways observed in previous studies of ZIKV persistence in prostate cells [14,15]. Overall, given the limitations of clinically available material to understand Zika's effect on the human prostate, in vitro studies shed light on potential mechanisms of cell metabolism remodeling upon infection, and its dependence on cell basal metabolic state.

SUPPLEMENTARY MATERIAL

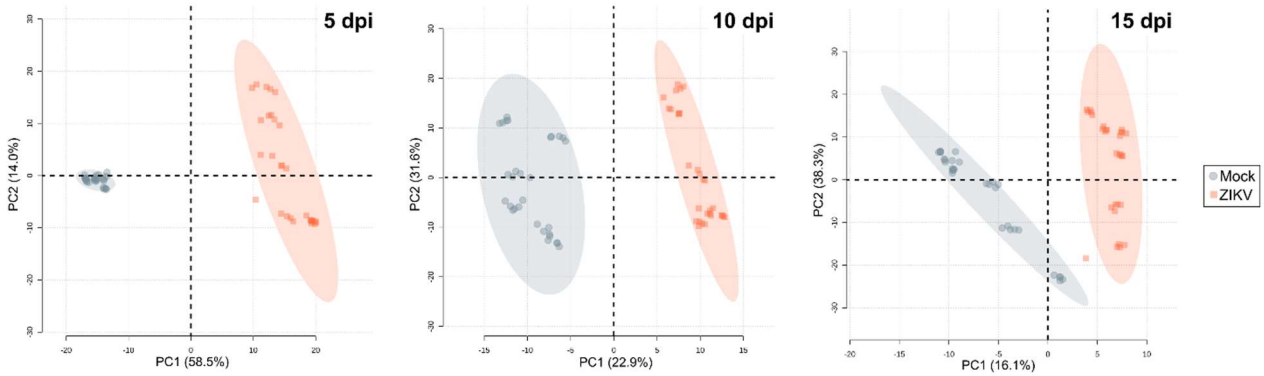

Figure S1. PLS-DA score plots at 5-, 10-, and 15-dpi timepoints showing the discrimination between PNT1a infected cells and mock cells by supervised multivariate analysis.

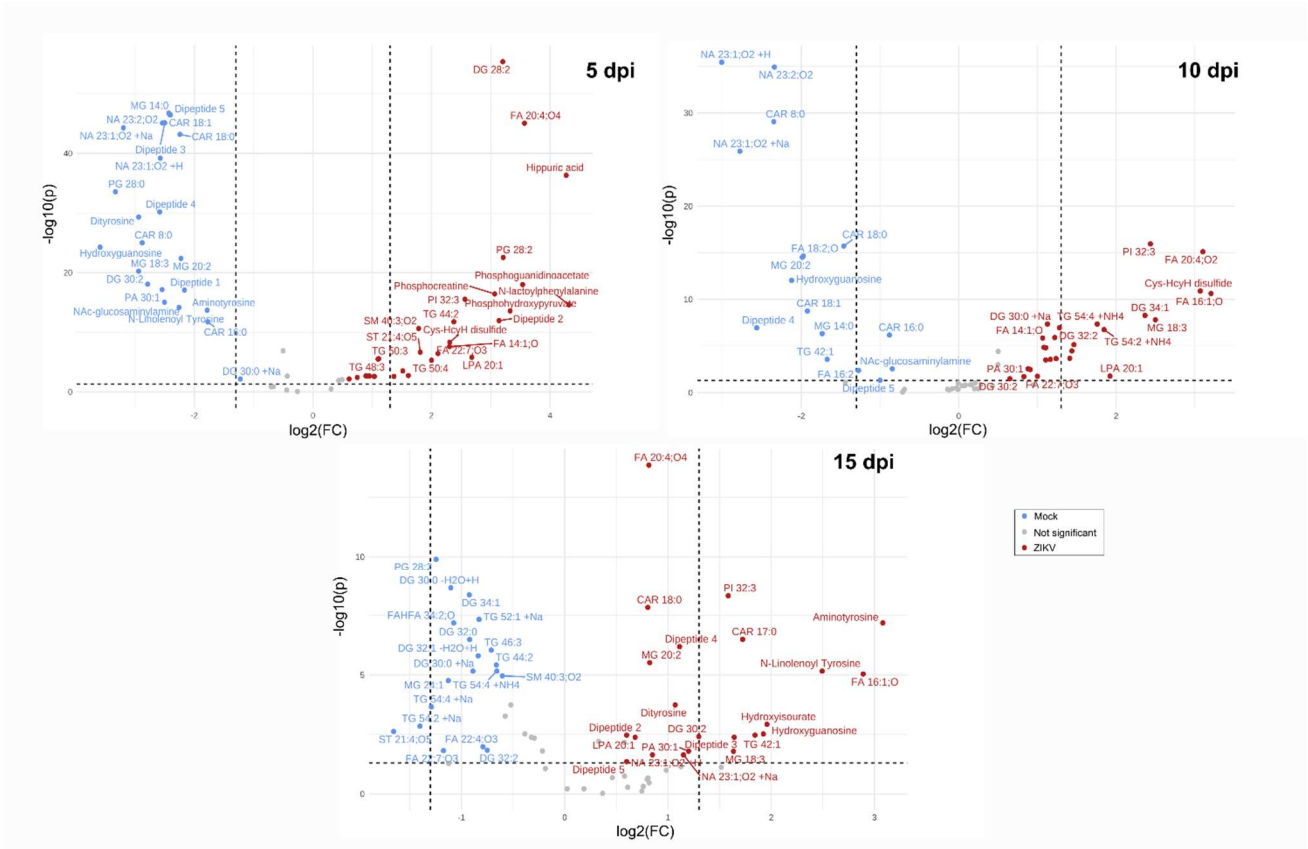

Figure S2. Volcano plots at 5-, 10-, and 15-dpi timepoints for PNT1a cells highlighting metabolites with FC > 1.5 and p-value < 0.05.

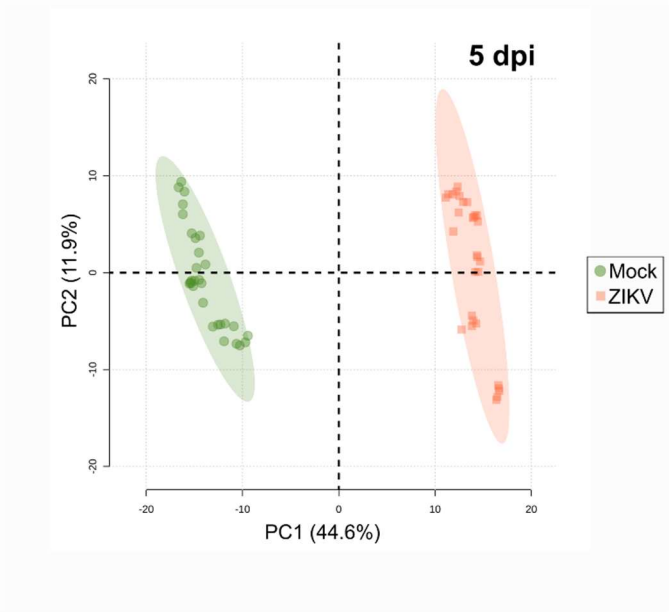

Figure S3. PLS-DA score plot at 5-dpi showing the discrimination between PC-3 infected cells and mock cells by supervised multivariate analysis.

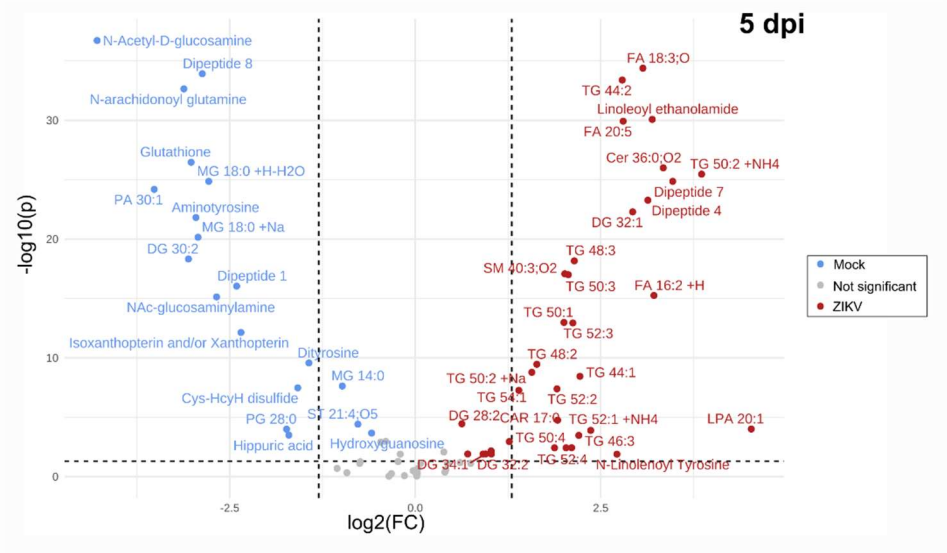

Figure S4. Volcano plot at 5-dpi for PC-3 cells highlighting metabolites with FC > 1.5 and p-value < 0.05.

Table S1. Annotated metabolites for PNT1a cells at 5-, 10-, and 15-dpi with ZIKV. Metabolites are subjected to isomers.

Class	Molecule	Adduct	Molecular Formula	Exact m/z	Error (ppm)	5-dpi		10-dpi		15-dpi	
						log_2FC	p-value	log_2FC	p-value	log_2FC	p-value
Amino acids and derivatives	Aminotyrosine	[M+K]+	C9H12N2O3	235.0473	2.98	-1.79	0.00	0.88	0.00	3.08	0.00
	Dipeptide 1	[M+H]+	C10H20N2O4	233.1495	0.43	-2.17	0.00	1.44	0.00	-1.12	0.05
	Dipeptide 2	[M+H]+	C8H15N3O4S	250.0846	4.00	3.14	0.00	-0.01	0.09	0.60	0.00
	Dipeptide 3	[M+H]+	C10H16N2O7	277.1031	-0.36	-2.50	0.00	-0.71	0.86	1.64	0.00
	Dipeptide 4	[M+NH4]+	C14H20N2O4	298.1757	1.34	-2.59	0.00	-2.57	0.00	1.11	0.00
	Dipeptide 5	[M+H]+	C11H23N5O3S	306.1581	4.25	-2.41	0.00	-1.00	0.05	0.60	0.04
	Dityrosine	[M+H-H2O]+	C18H20N2O6	343.1291	0.87	-2.94	0.00	0.91	0.00	1.07	0.00
	N- lactoyl phenylalanine	[M+K]+	C12H15NO4	276.0638	-1.81	4.32	0.00	0.95	0.15	0.75	0.76
Carnitines	CAR 16:0	[M+Na]+	C23H45NO4	422.3224	4.03	-1.77	0.00	-0.88	0.00	0.58	0.18
	CAR 17:0	[M+Na]+	C24H47NO4	436.3382	3.44	0.49	0.01	0.50	0.00	1.72	0.00
	CAR 18:0	[M+H]+	C25H49NO4	428.3722	2.80	-2.24	0.00	-1.46	0.00	0.81	0.00
	CAR 18:1	[M+H]+	C25H47NO4	426.3557	4.93	-2.41	0.00	-1.92	0.00	ND	ND
	CAR 8:0	[M+Na]+	C15H29NO4	310.2003	-4.51	-2.88	0.00	-2.35	0.00	0.46	0.21
Fatty acids	FA 14:1;O	[M+Na]+	C14H26O3	265.1782	-3.02	2.30	0.00	1.07	0.00	1.13	0.07
	FA 16:1;O	[M+Na]+	C16H30O3	293.2096	-3.07	ND	ND	3.21	0.00	2.89	0.00
	FA 16:2	[M+NH4]+	C16H28O2	270.2420	2.96	0.43	0.01	-1.27	0.00	0.02	0.61
	FA 18:2;O	[M+Na]+	C18H32O3	319.2252	-2.51	-0.43	0.00	-1.98	0.00	0.80	0.24
	FA 20:4;O2	[M+Na]+	C20H32O4	359.2183	2.78	-0.50	0.00	3.10	0.00	0.98	0.10
	FA 20:4;O4	[M+H]+	C20H32O6	369.2288	-4.60	3.57	0.00	0.21	0.09	0.82	0.00
	FA 22:4;O3	[M+Na]+	C22H36O5	403.2451	0.99	0.31	0.32	0.43	0.19	-0.79	0.01
	FA 22:7;O3	[M+H-H2O]+	C22H30O5	357.2064	0.56	2.11	0.00	1.00	0.02	-1.17	0.02
	FAHFA 34:2;O	[M+H]+	C34H64O4	537.4863	2.60	ND	ND	0.09	0.15	-1.07	0.00
Glycerolipids	DG 28:2	[M+Na]+	C31H56O5	531.4044	-4.52	3.20	0.00	-0.02	0.38	0.33	0.01

	DG 30:0	[M+H-H2O]+	C33H64O5	523.4705	4.01	0.61	0.01	-0.12	0.51	-1.10	0.00
	DG 30:0	[M+Na]+	C33H64O5	563.4627	3.37	-1.22	0.01	1.13	0.00	-0.89	0.00
	DG 30:2	[M+K]+	C33H60O5	575.4090	-3.13	-2.79	0.00	0.65	0.03	1.30	0.00
	DG 32:0	[M+H-H2O]+	C35H68O5	551.5016	4.17	0.75	0.00	-0.01	0.45	-0.92	0.00
	DG 32:1	[M+H-H2O]+	C35H66O5	549.4860	4.19	ND	ND	0.15	0.15	-0.84	0.00
	DG 32:1	[M+Na]+	C35H66O5	589.4784	3.05	-0.26	0.85	0.28	0.14	-0.22	0.02
	DG 32:2	[M+Na]+	C35H64O5	587.4631	2.55	-0.44	0.52	1.28	0.00	-0.75	0.01
	DG 34:1	[M+Na]+	C37H70O5	617.5095	3.24	-0.67	0.13	2.37	0.00	-0.92	0.00
	MG 14:0	[M+Na]+	C17H34O4	325.2338	3.38	-2.43	0.00	-1.74	0.00	0.58	0.01
	MG 18:3	[M+Na]+	C21H36O4	375.2493	3.46	-2.94	0.00	2.50	0.00	1.63	0.02
	MG 20:2	[M+NH4]+	C23H42O4	400.3410	2.75	-2.23	0.00	-1.99	0.00	0.82	0.00
	MG 24:1	[M+Na]+	C27H52O4	463.3741	3.67	-0.70	0.14	-0.03	0.31	-1.13	0.00
	TG 42:1	[M+H]+	C45H84O6	721.6377	-4.99	1.37	0.00	-1.67	0.00	1.84	0.00
	TG 44:2	[M+Na]+	C47H86O6	769.6283	4.42	2.38	0.00	-0.69	0.45	-0.66	0.00
	TG 46:3	[M+Na]+	C49H88O6	795.6441	4.02	0.91	0.00	-0.08	0.37	-0.71	0.00
	TG 48:3	[M+Na]+	C51H92O6	823.6756	3.64	1.10	0.00	0.07	0.19	-0.30	0.00
	TG 50:3	[M+Na]+	C53H96O6	851.7066	3.87	1.11	0.00	0.05	0.19	-0.32	0.00
	TG 50:4	[M+NH4]+	C53H94O6	844.7364	2.96	2.00	0.00	-0.14	0.45	-0.19	0.09
	TG 52:1	[M+NH4]+	C55H104O6	878.8132	4.44	0.95	0.00	1.46	0.00	-0.52	0.00
	TG 52:1	[M+Na]+	C55H104O6	883.7687	4.30	1.03	0.00	1.11	0.00	-0.83	0.00
	TG 52:4	[M+NH4]+	C55H98O6	872.7667	4.01	1.52	0.00	1.11	0.00	-0.39	0.00
	TG 54:2	[M+NH4]+	C57H106O6	904.8283	4.86	0.89	0.00	1.85	0.00	-0.58	0.00
	TG 54:2	[M+Na]+	C57H106O6	909.7850	3.52	ND	ND	ND	ND	-1.40	0.00
	TG 54:4	[M+NH4]+	C57H102O6	900.7974	4.44	ND	ND	1.76	0.00	-0.66	0.00
	TG 54:4	[M+Na]+	C57H102O6	905.7526	4.64	ND	ND	1.08	0.00	-1.29	0.00
Hexose	NAc-glucosaminylamine	[M+H-H2O]+	C8H16N2O5	203.1029	1.48	-2.50	0.00	-0.84	0.00	1.52	0.08
Metabolites	Hippuric acid	[M+K]+	C9H9NO3	218.0224	-4.59	4.27	0.00	0.50	0.00	0.37	0.95

	Hydroxyguanosine	[M+NH4]+	C10H13N5O6	317.1199	1.58	-3.59	0.00	-2.12	0.00	1.92	0.00
	Phosphocreatine	[M+Na]+	C4H10N3O5P	234.0256	-2.56	3.07	0.00	1.24	0.00	0.82	0.34
	Phosphoguanidinoacetate	[M+Na]+	C3H8N3O5P	220.0088	2.73	3.54	0.00	1.17	0.00	0.76	0.48
	Phosphohydroxypyruvate	[M+NH4]+	C3H5O7P	202.0113	-0.99	3.33	0.00	1.41	0.00	0.61	0.53
	Cys-HcyH disulfide	[M+H-H2O]+	C7H14N2O4S2	237.0361	2.95	2.31	0.00	3.07	0.00	0.81	0.21
N-acylamines	N-Linolenoyl Tyrosine	[M+K]+	C27H39NO4	480.2493	3.75	-2.26	0.00	-1.44	0.08	2.49	0.00
	N-stearoyl proline	[M+H]+	C23H43NO3	382.3298	4.71	-2.54	0.00	-2.34	0.00	0.19	0.61
	N-stearoyl valine	[M+H]+	C23H45NO3	384.3460	3.12	-2.58	0.00	-3.01	0.00	0.85	0.02
	N-stearoyl valine	[M+Na]+	C23H45NO3	406.3279	3.20	-3.20	0.00	-2.78	0.00	1.15	0.02
Phospholipids	LPA 20:1	[M+Na]+	C23H45O7P	487.2776	3.90	2.68	0.00	1.92	0.02	0.68	0.00
	PA 30:1	[M+H]+	C33H63O8P	619.4348	-2.42	-2.55	0.00	0.83	0.02	1.20	0.02
	PG 28:0	[M+H-H2O]+	C34H67O10P	649.4448	-0.62	-3.33	0.00	ND	ND	ND	ND
	PG 28:2	[M+Na]+	C34H63O10P	685.4077	-3.79	3.21	0.00	1.22	0.00	-1.25	0.00
	PI 32:3	[M+Na]+	C41H73O13P	827.4649	3.87	2.56	0.00	2.44	0.00	1.58	0.00
Purine	Hydroxyisourate	[M+Na]+	C6H6O8	207.0127	3.86	1.61	0.00	0.25	0.38	1.96	0.00
Sphingolipid	SM 40:3;O2	[M+H]+	C45H87N2O6P	783.6406	-3.96	1.78	0.00	0.16	0.15	-0.60	0.00
Sterol lipid	ST 21:4;O5	[M+H]+	C21H28O5	361.2013	-0.83	1.81	0.00	0.20	0.38	-1.66	0.00

Abbreviations: CAR – acylcarnitine; DG – diacylglycerol; FA – fatty acid; MG – monoacylglycerol; ND – Not detected; TG – triacylglycerol.

Table S2. Annotated metabolites for PNT1a and PC-3 cells at 5-dpi with ZIKV. Metabolites are subjected to isomers.

Class	**Molecule**	**Adduct**	**Molecular Formula**	**Exact m/z**	**Error (ppm)**	**PC-3**		**PNT1a**	
						log_2FC	**p-value**	**log_2FC**	**p-value**
Amino acids and derivatives	Aminotyrosine	[M+K]+	C9H12N2O3	235.0473	2.98	-2.96	0.00	-1.86	0.00
	Dipeptide 1	[M+H]+	C10H20N2O4	233.1495	0.43	-2.41	0.00	-2.28	0.00
	Dipeptide 2	[M+H]+	C8H15N3O4S	250.0846	4.00	-1.05	0.20	3.06	0.00
	Dipeptide 3	[M+H]+	C10H16N2O7	277.1031	-0.36	ND	ND	-2.65	0.00

	Dipeptide 4	[M+NH4]+	C14H20N2O4	298.1757	1.34	3.14	0.00	-2.74	0.00
	Dipeptide 5	[M+H]+	C11H23N5O3S	306.1581	4.25	-0.74	0.06	-2.56	0.00
	Dipeptide 6	[M+H-H2O]+	C10H20N2O3S	231.1159	3.46	3.47	0.00	0.54	0.00
	Dipeptide 7	[M+K]+	C11H14N2O3	261.0632	1.53	-2.87	0.00	ND	ND
	Dityrosine	[M+H-H2O]+	C18H20N2O6	343.1291	0.87	-1.43	0.00	-3.05	0.00
	N-lactoylphenylalanine	[M+K]+	C12H15NO4	276.0638	-1.81	1.02	0.01	4.20	0.00
Carnitines	CAR 16:0	[M+Na]+	C23H45NO4	422.3224	4.03	-0.23	0.05	-1.82	0.00
	CAR 17:0	[M+Na]+	C24H47NO4	436.3382	3.44	1.92	0.00	0.34	0.02
	CAR 18:0	[M+H]+	C25H49NO4	428.3722	2.8	-0.03	0.32	-2.38	0.00
	CAR 18:1	[M+H]+	C25H47NO4	426.3557	4.93	0.02	0.89	-2.56	0.00
	CAR 8:0	[M+Na]+	C15H29NO4	310.2003	-4.51	-0.15	0.84	-2.99	0.00
Fatty acids	FA 14:1;O	[M+Na]+	C14H26O3	265.1782	-3.02	0.40	0.42	2.09	0.00
	FA 16:2	[M+H]+	C16H30O4	287.2214	1.04	3.22	0.00	-0.09	0.10
	FA 18:2;O	[M+Na]+	C18H32O3	319.2252	-2.51	-0.40	0.00	-0.59	0.00
	FA 18:3;O	[M+H]+	C18H30O3	295.2265	1.02	3.07	0.00	0.25	0.02
	FA 20:4;O2	[M+Na]+	C20H32O4	359.2183	2.78	0.91	0.01	-0.64	0.00
	FA 20:4;O4	[M+H]+	C20H32O6	369.2288	-4.6	0.07	0.08	3.45	0.00
	FA 20:5	[M+H]+	C20H30O2	303.2313	1.98	2.80	0.00	0.76	0.00
	FA 22:4;O3	[M+Na]+	C22H36O5	403.2451	0.99	-0.47	0.00	0.14	0.50
	FA 22:7;O3	[M+H-H2O]+	C22H30O5	357.2064	0.56	0.03	0.21	2.05	0.00
Glycerolipids	DG 28:2	[M+Na]+	C31H56O5	531.4044	-4.52	0.63	0.00	3.07	0.00
	DG 30:0	[M+H-H2O]+	C33H64O5	523.4705	4.01	0.39	0.01	0.50	0.07
	DG 30:0	[M+Na]+	C33H64O5	563.4627	3.37	1.27	0.00	-1.38	0.00
	DG 30:2	[M+K]+	C33H60O5	575.409	-3.13	-3.06	0.00	-2.86	0.00
	DG 32:0	[M+H-H2O]+	C35H68O5	551.5016	4.17	-0.32	0.56	0.65	0.04
	DG 32:1	[M+Na]+	C35H66O5	589.4784	3.05	2.93	0.00	-0.32	0.88
	DG 32:2	[M+Na]+	C35H64O5	587.4631	2.55	1.03	0.01	-0.53	0.27
	DG 34:1	[M+Na]+	C37H70O5	617.5095	3.24	0.95	0.01	-0.82	0.02

	MG 14:0	[M+Na]+	C17H34O4	325.2338	3.38	-0.98	0.00	-2.59	0.00
	MG 18:0	[M+Na]+	C21H42O4	381.2964	2.89	-2.93	0.00	-0.89	0.00
	MG 18:3	[M+Na]+	C21H36O4	375.2493	3.46	-0.35	0.91	-3.04	0.00
	MG 20:2	[M+NH4]+	C23H42O4	400.341	2.75	0.03	0.50	-2.37	0.00
	MG 24:1	[M+Na]+	C27H52O4	463.3741	3.67	-0.75	0.08	-0.80	0.05
	TG 42:1	[M+H]+	C45H84O6	721.6377	-4.99	ND	ND	1.09	0.00
	TG 44:1	[M+Na]+	C47H88O6	771.6447	3.37	2.22	0.00	1.16	0.00
	TG 44:2	[M+Na]+	C47H86O6	769.6283	4.42	2.79	0.00	2.33	0.00
	TG 46:3	[M+Na]+	C49H88O6	795.6441	4.02	2.20	0.00	0.81	0.02
	TG 48:2	[M+Na]+	C51H94O6	825.6928	1.82	1.64	0.00	0.82	0.00
	TG 48:3	[M+Na]+	C51H92O6	823.6756	3.64	2.14	0.00	1.05	0.00
	TG 50:1	[M+Na]+	C53H100O6	855.7381	3.62	2.00	0.00	0.79	0.00
	TG 50:2	[M+Na]+	C53H98O6	853.7239	1.99	1.57	0.00	0.72	0.00
	TG 50:2	[M+NH4]+	C53H98O6	848.7689	1.53	3.86	0.00	3.58	0.00
	TG 50:3	[M+Na]+	C53H96O6	851.7066	3.87	2.06	0.00	1.06	0.00
	TG 50:4	[M+NH4]+	C53H94O6	844.7364	2.96	1.88	0.00	1.95	0.00
	TG 52:1	[M+NH4]+	C55H104O6	878.8132	4.44	2.37	0.00	0.86	0.02
	TG 52:1	[M+Na]+	C55H104O6	883.7687	4.3	ND	ND	0.95	0.02
	TG 52:2	[M+Na]+	C55H102O6	881.7569	3.86	1.91	0.00	1.77	0.00
	TG 52:3	[M+Na]+	C55H100O6	879.7412	3.07	2.12	0.00	2.05	0.00
	TG 52:4	[M+NH4]+	C55H98O6	872.7667	4.01	2.03	0.00	1.44	0.00
	TG 54:1	[M+NH4]+	C57H108O6	906.8424	6.62	1.40	0.00	-0.89	0.07
	TG 54:2	[M+NH4]+	C57H106O6	904.8283	4.86	2.11	0.00	0.80	0.02
Hexose	NAc-glucosamine	[M+H]+	C8H15NO6	222.0981	-4.05	-4.29	0.00	-2.54	0.00
	NAc-glucosaminylamine	[M+H-H2O]+	C8H16N2O5	203.1029	1.48	-2.68	0.00	-2.57	0.00
Metabolites	Hippuric acid	[M+K]+	C9H9NO3	218.0224	-4.59	-1.70	0.00	4.13	0.00
	Hydroxyguanosine	[M+NH4]+	C10H13N5O6	317.1199	1.58	-0.59	0.00	-3.69	0.00
	Phosphocreatine	[M+Na]+	C4H10N3O5P	234.0256	-2.56	0.71	0.01	2.95	0.00

	Phosphoguanidinoacetate	[M+Na]+	C3H8N3O5P	220.0088	2.73	0.41	0.27	3.42	0.00
	Phosphohydroxypyruvate	[M+NH4]+	C3H5O7P	202.0113	-0.99	0.75	0.08	3.19	0.00
	Cys-HcyH disulfide	[M+H-H2O]+	C7H14N2O4S2	237.0361	2.95	-1.58	0.00	2.16	0.00
	Glutathione	[M+H-H2O]+	C10H17N3O6S	290.0811	0.00	-3.02	0.00	ND	ND
	Isoxanthopterin and/or Xanthopterin	[M+H]+	C6H5N5O2	180.0510	3.33	-2.35	0.00	2.06	0.00
N-acylamines	Linoleoyl ethanolamide	[M+H]+	C20H37NO2	324.2895	0.62	3.19	0.00	0.54	0.00
	N-arachidonoyl glutamine	[M+Na]+	C25H40N2O4	455.2869	2.42	-3.12	0.00	ND	ND
	N-Linolenoyl Tyrosine	[M+K]+	C27H39NO4	480.2493	3.75	2.72	0.01	-2.40	0.00
	N-stearoyl proline	[M+H]+	C23H43NO3	382.3298	4.71	0.01	0.33	-2.69	0.00
	N-stearoyl valine	[M+H]+	C23H45NO3	384.346	3.12	0.01	0.49	-2.72	0.00
	N-stearoyl valine	[M+Na]+	C23H45NO3	406.3279	3.20	-0.20	0.01	-3.33	0.00
Phospholipids	LPA 20:1	[M+Na]+	C23H45O7P	487.2776	3.90	4.53	0.00	2.53	0.00
	PA 30:1	[M+H]+	C33H63O8P	619.4348	-2.42	-3.52	0.00	-2.63	0.00
	PG 28:0	[M+H-H2O]+	C34H67O10P	649.4448	-0.62	-1.73	0.00	-3.49	0.00
	PG 28:2	[M+Na]+	C34H63O10P	685.4077	-3.79	ND	ND	3.11	0.00
	PI 32:3	[M+Na]+	C41H73O13P	827.4649	3.87	0.60	0.07	2.38	0.00
Purine	Hydroxyisourate	[M+Na]+	C6H6O8	207.0127	3.86	0.43	0.08	1.30	0.00
Sphingolipids	SM 40:3;O2	[M+H]+	C45H87N2O6P	783.6406	-3.96	2.02	0.00	1.74	0.00
	Cer36:0;O2	[M+H-H2O]+	C36H73NO3	550.5553	1.82	3.34	0.00	2.09	0.00
Sterol lipid	ST 21:4;O5	[M+H]+	C21H28O5	361.2013	-0.83	-0.77	0.00	1.75	0.00

Abbreviations: CAR – acylcarnitine; DG – diacylglycerol; FA – fatty acid; MG – monoacylglycerol; ND – Not-detected; TG – triacylglycerol.

REFERENCES

[1] Dick GWA. Zika virus (II). Pathogenicity and physical properties. Trans R Soc Trop Med Hyg 1952;46. https://doi.org/10.1016/0035-9203(52)90043-6.

[2] Petersen LR, Jamieson DJ, Powers AM, Honein MA. Zika Virus (Review Article). New England Journal of Medicine 2016;374.

[3] Boeuf P, Drummer HE, Richards JS, Scoullar MJL, Beeson JG. The global threat of Zika virus to pregnancy: Epidemiology, clinical perspectives, mechanisms, and impact. BMC Med 2016;14. https://doi.org/10.1186/s12916-016-0660-0.

[4] Zhu Z, Gorman MJ, McKenzie LD, Chai JN, Hubert CG, Prager BC, et al. Zika virus has oncolytic activity against glioblastoma stem cells. Journal of Experimental Medicine 2017;214. https://doi.org/10.1084/jem.20171093.

[5] Chen Q, Wu J, Ye Q, Ma F, Zhu Q, Wu Y, et al. Treatment of human glioblastoma with a live attenuated Zika virus vaccine candidate. MBio 2018;9. https://doi.org/10.1128/mBio.01683-18.

[6] Garcez PP, Loiola EC, da Costa RM, Higa LM, Trindade P, Delvecchio R, et al. Zika virus: Zika virus impairs growth in human neurospheres and brain organoids. Science (1979) 2016;352. https://doi.org/10.1126/science.aaf6116.

[7] Kaid C, Goulart E, Caires-Júnior LC, Araujo BHS, Soares-Schanoski A, Bueno HMS, et al. Zika virus selectively kills aggressive human embryonal CNS tumor cells in vitro and in vivo. Cancer Res 2018;78. https://doi.org/10.1158/0008-5472.CAN-17-3201.

[8] Iannolo G, Sciuto MR, Cuscino N, Pallini R, Douradinha B, Ricci Vitiani L, et al. Zika virus infection induces MiR34c expression in glioblastoma stem cells: new perspectives for brain tumor treatments. Cell Death Dis 2019;10. https://doi.org/10.1038/s41419-019-1499-z.

[9] Liang Q, Luo Z, Zeng J, Chen W, Foo SS, Lee SA, et al. Zika Virus NS4A and NS4B Proteins Deregulate Akt-mTOR Signaling in Human Fetal Neural Stem Cells to Inhibit Neurogenesis and Induce Autophagy. Cell Stem Cell 2016;19. https://doi.org/10.1016/j.stem.2016.07.019.

[10] Dabaja MZ, Lima E de O, de Oliveira DN, Guerreiro TM, Melo CFOR, Morishita KN, et al. Metabolic alterations induced by attenuated Zika virus in glioblastoma cells. Cell Biosci 2018;8. https://doi.org/10.1186/s13578-018-0243-1.

[11] Paz-Bailey G, Rosenberg ES, Doyle K, Munoz-Jordan J, Santiago GA, Klein L, et al. Persistence of Zika Virus in Body Fluids — Final Report. New England Journal of Medicine 2018;379. https://doi.org/10.1056/nejmoa1613108.

[12] Spencer JL, Lahon A, Tran LL, Arya RP, Kneubehl AR, Vogt MB, et al. Replication of Zika virus in human prostate cells: A potential source of sexually transmitted virus. Journal of Infectious Diseases 2018;217. https://doi.org/10.1093/infdis/jix436.

[13] Oliveira DBL, Durigon GS, Mendes ÉA, Ladner JT, Andreata-Santos R, Araujo DB, et al. Persistence and intra-host genetic evolution of zika virus infection in symptomatic adults: A special view in the male reproductive system. Viruses 2018;10. https://doi.org/10.3390/v10110615.

[14] Izuagbe RE. A prostate cell line model of persistent Zika virus infection. Master of Applied Science. Queensland University of Technology, 2019.

[15] Machado FC, Bittar C, Rahal P, Calmon MF. Identification of differentially expressed miRNAs in human cells infected with different Zika virus strains. Arch Virol 2021;166. https://doi.org/10.1007/s00705-021-05051-9.

[16] Byers NM, Fleshman AC, Perera R, Molins CR. Metabolomic insights into human arboviral infections: Dengue, chikungunya, and zika viruses. Viruses 2019;11. https://doi.org/10.3390/v11030225.

[17] Eidelman E, Twum-Ampofo J, Ansari J, Siddiqui MM. The metabolic phenotype of prostate cancer. Front Oncol 2017;7. https://doi.org/10.3389/fonc.2017.00131.

[18] Cutruzzolà F, Giardina G, Marani M, Macone A, Paiardini A, Rinaldo S, et al. Glucose metabolism in the progression of prostate cancer. Front Physiol 2017;8. https://doi.org/10.3389/fphys.2017.00097.

[19] Elia I, Schmieder R, Christen S, Fendt SM. Organ-specific cancer metabolism and its potential for therapy. Handb Exp Pharmacol, vol. 233, 2016. https://doi.org/10.1007/164_2015_10.

[20] Liu Y. Fatty acid oxidation is a dominant bioenergetic pathway in prostate cancer. Prostate Cancer Prostatic Dis 2006;9. https://doi.org/10.1038/sj.pcan.4500879.

[21] Xu H, Chen Y, Gu M, Liu C, Chen Q, Zhan M, et al. Fatty acid metabolism reprogramming in advanced prostate cancer. Metabolites 2021;11. https://doi.org/10.3390/metabo11110765.

[22] Meertens L, Labeau A, Dejarnac O, Cipriani S, Sinigaglia L, Bonnet-Madin L, et al. Axl Mediates ZIKA Virus Entry in Human Glial Cells and Modulates Innate Immune Responses. Cell Rep 2017;18. https://doi.org/10.1016/j.celrep.2016.12.045.

[23] Silva-Filho JL, de Oliveira LG, Monteiro L, Parise PL, Zanluqui NG, Polonio CM, et al. Gas6 drives Zika virus-induced neurological complications in humans and congenital syndrome in immunocompetent mice. Brain Behav Immun 2021;97. https://doi.org/10.1016/j.bbi.2021.08.008.

[24] Sharp TM, Fischer M, Muñoz-Jordán JL, Paz-Bailey G, Erin Staples J, Gregory CJ, et al. Dengue and zika virus diagnostic testing for patients with a clinically compatible illness and risk for infection with both viruses. MMWR Recommendations and Reports 2019;68. https://doi.org/10.15585/MMWR.RR6801A1.

[25] Kuivanen S, Bespalov MM, Nandania J, Ianevski A, Velagapudi V, de Brabander JK, et al. Obatoclax, saliphenylhalamide and gemcitabine inhibit Zika virus infection in vitro and differentially affect cellular signaling, transcription and metabolism. Antiviral Res 2017;139. https://doi.org/10.1016/j.antiviral.2016.12.022.

[26] Melo CFOR, Navarro LC, de Oliveira DN, Guerreiro TM, Lima E de O, Delafiori J, et al. A machine learning application based in random forest for integrating mass spectrometry-based metabolomic data: A simple screening

method for patients with Zika virus. Front Bioeng Biotechnol 2018;6. https://doi.org/10.3389/fbioe.2018.00031.

[27] Delafiori J, Lima E de O, Dabaja MZ, Dias-Audibert FL, de Oliveira DN, Melo CFOR, et al. Molecular signatures associated with prostate cancer cell line (PC-3) exposure to inactivated Zika virus. Sci Rep 2019;9. https://doi.org/10.1038/s41598-019-51954-8.

[28] Nunes E da C, de Filippis AMB, Pereira TDES, Faria NR da C, Salgado Á, Santos CS, et al. Untargeted metabolomics insights into newborns with congenital zika infection. Pathogens 2021;10. https://doi.org/10.3390/pathogens10040468.

[29] Pang Z, Chong J, Li S, Xia J. Metaboanalystr 3.0: Toward an optimized workflow for global metabolomics. Metabolites 2020;10. https://doi.org/10.3390/metabo10050186.

[30] Chen Q, Gouilly J, Ferrat YJ, Espino A, Glaziou Q, Cartron G, et al. Metabolic reprogramming by Zika virus provokes inflammation in human placenta. Nat Commun 2020;11. https://doi.org/10.1038/s41467-020-16754-z.

[31] Faria NR da C, Chaves-Filho AB, Alcantara LCJ, de Siqueira IC, Calcagno JI, Miyamoto S, et al. Plasma lipidome profiling of newborns with antenatal exposure to zika virus. PLoS Negl Trop Dis 2021;15. https://doi.org/10.1371/journal.pntd.0009388.

[32] Catala A, Stone M, Busch MP, D'Alessandro A. Reprogramming of red blood cell metabolism in Zika virus–infected donors. Transfusion (Paris) 2022;62. https://doi.org/10.1111/trf.16851.

[33] Zhan X, Wang X, Desiderio DM. Mass spectrometry analysis of nitrotyrosine-containing proteins. Mass Spectrom Rev 2015;34. https://doi.org/10.1002/mas.21413.

[34] Campolo N, Issoglio FM, Estrin DA, Bartesaghi S, Radi R. 3-Nitrotyrosine and related derivatives in proteins: Precursors, radical intermediates and impact in function. Essays Biochem 2020;64. https://doi.org/10.1042/EBC20190052.

[35] Ohtake S, Kawahara T, Ishiguro Y, Takeshima T, Kuroda S, Izumi K, et al. Oxidative stress marker 8-hydroxyguanosine is more highly expressed in prostate cancer than in benign prostatic hyperplasia. Mol Clin Oncol 2018. https://doi.org/10.3892/mco.2018.1665.

[36] Motrich RD, Salazar FC, Breser ML, Mackern-Oberti JP, Godoy GJ, Olivera C, et al. Implications of prostate inflammation on male fertility. Andrologia 2018;50. https://doi.org/10.1111/and.13093.

[37] Oono K, Ohtake K, Watanabe C, Shiba S, Sekiya T, Kasono K. Contribution of Pyk2 pathway and reactive oxygen species (ROS) to the anti-cancer effects of eicosapentaenoic acid (EPA) in PC3 prostate cancer cells. Lipids Health Dis 2020;19. https://doi.org/10.1186/s12944-019-1122-4.

[38] Tang DG, La E, Kern J, Kehrer JP. Fatty acid oxidation and signaling in apoptosis. Biol Chem 2002;383. https://doi.org/10.1515/BC.2002.046.

[39] Pauls SD, Rodway LA, Winter T, Taylor CG, Zahradka P, Aukema HM. Anti-inflammatory effects of α-linolenic acid in M1-like macrophages are associated with enhanced production of oxylipins from α-linolenic and linoleic acid. Journal of Nutritional Biochemistry 2018;57. https://doi.org/10.1016/j.jnutbio.2018.03.020.

[40] Subbarayan V, Xu XC, Kim J, Yang P, Hoque A, Sabichi AL, et al. Inverse relationship between 15-lipoxygenase-2 and PPAR-γ gene expression in normal epithelia compared with tumor epithelia. Neoplasia 2005;7. https://doi.org/10.1593/neo.04457.

[41] Mitra R, Le TT, Gorjala P, Goodman OB. Positive regulation of prostate cancer cell growth by lipid droplet forming and processing enzymes DGAT1 and ABHD5. BMC Cancer 2017;17. https://doi.org/10.1186/s12885-017-3589-6.

[42] Martín-Acebes MA, Vázquez-Calvo Á, Saiz JC. Lipids and flaviviruses, present and future perspectives for the control of dengue, Zika, and West Nile viruses. Prog Lipid Res 2016;64. https://doi.org/10.1016/j.plipres.2016.09.005.

[43] Mwaliko C, Nyaruaba R, Zhao L, Atoni E, Karungu S, Mwau M, et al. Zika virus pathogenesis and current therapeutic advances. Pathog Glob Health 2021;115. https://doi.org/10.1080/20477724.2020.1845005.

[44] Cloherty APM, Olmstead AD, Ribeiro CMS, Jean F. Hijacking of lipid droplets by hepatitis C, dengue and zika viruses-from viral protein moonlighting to extracellular release. Int J Mol Sci 2020;21. https://doi.org/10.3390/ijms21217901.

[45] Heaton NS, Perera R, Berger KL, Khadka S, LaCount DJ, Kuhn RJ, et al. Dengue virus nonstructural protein 3 redistributes fatty acid synthase to sites of viral replication and increases cellular fatty acid synthesis. Proc Natl Acad Sci U S A 2010;107. https://doi.org/10.1073/pnas.1010811107.

[46] Leier HC, Weinstein JB, Kyle JE, Lee JY, Bramer LM, Stratton KG, et al. A global lipid map defines a network essential for Zika virus replication. Nat Commun 2020;11. https://doi.org/10.1038/s41467-020-17433-9.

[47] Monson EA, Crosse KM, Duan M, Chen W, O'Shea RD, Wakim LM, et al. Intracellular lipid droplet accumulation occurs early following viral infection and is required for an efficient interferon response. Nat Commun 2021;12. https://doi.org/10.1038/s41467-021-24632-5.

[48] Valentino A, Calarco A, di Salle A, Finicelli M, Crispi S, Calogero RA, et al. Deregulation of MicroRNAs mediated control of carnitine cycle in prostate cancer: Molecular basis and pathophysiological consequences. Oncogene 2017;36. https://doi.org/10.1038/onc.2017.216.

4.2 Capítulo 2

Artigo publicado na revista *Scientific Reports (open access)*

Delafiori, J., Lima, E. de O., Dabaja, M. Z., Dias-Audibert, F. L., de Oliveira, D. N., Melo, C. F. O. R. et al. Molecular signatures associated with prostate cancer cell line (PC-3) exposure to inactivated Zika virus. Sci Rep. 2019, 9: 15351. https://doi.org/10.1038/s41598-019-51954-8

Molecular signatures associated with prostate cancer cell line (PC-3) exposure to inactivated Zika virus

Jeany Delafiori[1], Estela de Oliveira Lima[2], Mohamed Ziad Dabaja[1], Flávia Luísa Dias-Audibert[1], Diogo Noin de Oliveira[1], Carlos Fernando Odir Rodrigues Melo[1], Karen Noda Morishita[1], Geovana Manzan Sales[1], Ana Lucia Tasca Gois Ruiz[3,4], Gisele Goulart da Silva[4], Marcelo Lancellotti[5], and Rodrigo Ramos Catharino[1,*]

1 Innovare Biomarkers Laboratory, Faculty of Pharmaceutical Sciences, University of Campinas (UNICAMP), Campinas, São Paulo, Brazil

2 Medical School, São Paulo State University (UNESP), Botucatu, São Paulo, Brazil

3 Faculty of Pharmaceutical Sciences, University of Campinas (UNICAMP), Campinas, São Paulo, Brazil

4 Department of Physiological Sciences, Piracicaba Dental School, University of Campinas (UNICAMP), Piracicaba, São Paulo, Brazil

5 Laboratory of Biotechnology, Faculty of Pharmaceutical Sciences, University of Campinas (UNICAMP), Campinas, São Paulo, Brazil

*Corresponding author: rodrigo.catharino@fcf.unicamp.br

ABSTRACT

The recent outbreak of Zika virus (ZIKV) infection associated with microcephaly cases has elicited much research on the mechanisms involved in ZIKV-host cell interactions. It has been described that Zika virus impairs cell growth, raising a hypothesis about its oncolytic potential against cancer cells. ZIKV tumor cell growth inhibition was later confirmed for glioblastoma. It was also demonstrated that an inactivated ZIKV prototype (ZVp) based on bacterial outer membrane vesicles has antiproliferative activity upon other cancer cell lines, such as PC-3 prostate cancer cell. This study aims at understanding the pathways that might be involved with the antiproliferative effect of Zika virus against prostate cancer cells. A metabolomic approach based on high-resolution mass spectrometry analysis led to the identification of 21 statistically relevant markers of PC-3 cells treated with ZVp. The markers were associated with metabolic alterations that trigger lipid remodeling, endoplasmic reticulum stress, inflammatory mediators, as well as disrupted porphyrin and folate metabolism. These findings highlight molecular signatures of ZVp-induced response that may be involved on cellular pathways triggered by its antiproliferative effect. To our knowledge, this is the first reported metabolomic assessment of ZIKV effect on prostate cancer cells, a promising topic for further research.

Keywords: prostate cancer; PC-3; zika virus; ZIKV; virus-host interactions; oxidative stress; PI3K/AKT; metabolomics; mass spectrometry; lipid metabolism; endoplasmic reticulum stress.

INTRODUCTION

The recent outbreak of Zika virus infection associated with microcephaly cases on South and Central America emerged the need for understanding the mechanisms involved in ZIKV-host cell interaction[1]. It was observed that the tropism of ZIKV to neuronal cells leads to consequent impairment of stem cells differentiation, neuronal growth, cellular cycle arrest, and cell death[2,3]. Zika virus-mediated cell death has also been associated with increased expression of pro-

apoptotic and autophagic pathways such as dysregulation on PI3K-Akt pathway and caspase-3[2,4]. As other flaviviruses, ZIKV uses host cell enzymatic machinery and orchestrate a reorganization of lipid metabolism to promote viral replication and processing of its own proteins[5,6]. ZIKV is composed of three structural proteins (capsid (C), precursor membrane (prM), and envelope protein (E)) and seven nonstructural proteins (NS1, NS2A, NS2B, NS3, NS4A, NS4B e NS5)[7]. Among these, NS4A and NS4B were reported as key elements involved in growth restriction through Akt/mTOR stress-response pathway, since their interactions with Akt and mTOR inactivation lead to autophagy[4,7,8]. Markers related to impaired Akt/mTOR signaling have been associated with ZIKV-host interaction and was identified in the serum of infected patients, in a new proposed approach for Zika diagnosis[9,10].

In addition to neural tissue, the confirmation of ZIKV transmission through sexual contact suggested viral tropism to reproductive tract cells[1,11]. Kumar et al. (2018) demonstrated that Sertoli cells are susceptible to ZIKV, and replication is persistent in the male reproductive tract[11]. Moreover, ZIKV was able to infect testis of mice, leading to an important increase in Reactive Oxygen Species (ROS) and consequently to testicular oxidative stress and impaired spermatogenesis[12]. In addition, men infected with ZIKV presented prostatitis and hematospermia, suggesting prostate infection and inflammation[13]. Human prostate epithelial adenocarcinoma (LNCaP) has also shown permissiveness to infection and ZIKV replication, thus confirming cellular tropism to prostate malignant cells. All this data, therefore, suggest human prostate as a ZIKV reservoir on sexual transmission through semen[13,14].

Given the ZIKV tropism to various cell types, and its ability of interrupting cell growth, a hypothesis was raised about its oncolytic potential. In vitro[15,16] and in vivo[17] experiments were conducted to confirm the antiproliferative activity of Zika against glioblastoma tumor cells. Zhu et al. (2017) demonstrated that ZIKV preferentially targets glioblastoma stem cells, differently from another neurotropic flavivirus, the West Nile Virus, WNV, which kills both normal and tumor cells[17]. Due to potential virus virulence latency on CNS[18], Dabaja et al. (2018) evaluated metabolic alterations in glioblastoma cells induced by a ZIKV prototype (ZVp), which also demonstrated cytopathic effects. This prototype based on inactivated

ZIKV particles fused with Outer Membrane Vesicles (OMV) from Neisseria meningitidis demonstrated significant immune response and great potential for tumor management[16,19]. Additionally to the cytopathic effect demonstrated in glioblastoma cells, ZVp has also shown tropism and antiproliferative effects against the PC-3 androgen-independent human prostate cancer cell line[16], whose mechanisms are yet to be elucidated.

Prostate cancer etiology, progression and therapy responsiveness have been associated with oxidative stress, DNA instability and aberrant DNA methylation[20,21]. Defense mechanisms against ROS are used as a survival strategy by tumor cells[22]. However, increased ROS, ER stress, cell cycle arrest and DNA damage are also strategies used in anticancer therapy through approaches such as radiotherapy and chemotherapy[23]. One study demonstrated that PC-3 and DU-145 cells differed significantly in their radiosensitivity due to variations in basal and induced Nrf2 (Nuclear Factor Erythroid 2-Related Factor-2) expression levels[24].This basic leucine zipper transcription factor modulates cell inflammatory and immune response by inducing the transcription of antioxidant enzymes, which have a role in maintenance of cancer cell survival and disease progression[22]. However, despite indications of Nrf2 overexpression in malignant cells[22,25], several authors demonstrated evidence that cytoprotective enzymes are downregulated in prostate cancer, partially due to hypermethylation of CpG sites in the Nrf2 gene[21,26,27]; thus, the role of Nrf2 on the susceptibility of prostate cancer to oxidative stress remains controversial.

Accordingly, impairments in the cytoprotective activity of Nrf2, blockage of PI3K/Akt/mTOR signaling, and the interaction of ZIKV proteins with key pathways might be used as strategies to increase cancer cell susceptibility to oxidative stress and, consequently, inhibit tumor cell growth[22,25,26,28]. Given the interaction of Zika virus with pathways that play a role on ROS homeostasis[4,8,29] and promote lipid metabolism modifications[5,30], we investigated the metabolic alterations induced by ZVp on the PC-3 prostate cancer cell line. Employing a metabolomic approach based on high-resolution mass spectrometry, statistically discriminant biomarkers for PC-3 treated ZVp were selected and structurally proposed as an attempt to correlate the antiproliferative effect reported in the literature with molecular signatures.

METHODS

Zika virus prototype (ZVp) production

The Brazilian ZIKV strain (BeH823339, GenBank KU729217) was kindly provided by Professor Doctor Edison Durigon (Biomedical Sciences Institute, University of São Paulo). This strain was isolated from an infected patient in 2015 during the Zika outbreak in the State of Ceará (Brazil) and used for ZVp production. N. meningitidis (C2135), Aedes albopictus (C6/36) and glial cell (M059J) lines were obtained from INCQS—FIOCRUZ (National Institute for Quality Control—Oswaldo Cruz Foundation, Rio de Janeiro, RJ and Cell Bank).

Culture and infection of C6/36 cells with ZIKV strain was used to replicate the virus after cell confluence achieved 70%. C6/26 culture and infection followed the procedure reported by Melo et al.[60]. After viral cytopathic effect (CPE) reached 75%, aliquots of 1 mL of ZIKV were stored at −80 °C.

Intending to obtain Outer Membrane Vesicles (OMVs), Neisseria meningitidis was chosen as the microorganism to provide OMVs. For that, this bacterial species was grown at 37 °C under 5% of CO^2 in agar GCB (Difco). N. meningitidis OMVs were isolated according to Alves et al.[61] and stored at − 80 °C before use.

The product OMV fused Zika virus was obtained from M059J cells culture. These cells were infected with ZIKV strain, then OMV particles were added, and the culture were submitted to agitation, inducing ZIKV-OMV fusion. The supernatants containing OMV-ZIKV fused particle (ZVp) were formed, collected, inactivated at 56 °C for 1 h and characterized for the parameters of size, polydispersity index (PDI), and electric charge potential using a Zetasizer Nano equipment (Malvern Instruments Ltd., Grovewood Road, Malvern, United Kingdom). In addition, a Nano Tracking Analysis (NanoSign Equipment, Malvern Instruments Ltd., Grovewood Road, Malvern, United Kingdom) was used to determine particles per frame and particles per mL (concentration). The tests performed for ZVp characterization and results is described by Martins et al. (2018) procedure[19].

PC-3 cell culture and ZVp test

PC-3 human prostate cancer cell line was gently provided by Frederick Cancer Research & Development Center, National Cancer Institute, Frederick, MA, USA. Cell cultures growth was performed accordingly to the procedure established by Roman Jr et al.[62]. Briefly, 5 mL of RPMI-1640 supplemented with 5% of fetal bovine serum (RPMI/FBS 5% Gibco®, USA) and 1% penicillin: streptomycin (Nutricell®, Brazil, 1000 U/mL) at 37 °C with 5% CO_2 was used for PC-3 cells grow until confluence of 80%. For the experiments, PC-3 cells were used between passages 5 to 12.

Tests using PC-3 cell line and Zika virus prototype (ZVp) were similar to those applied for Glioblastoma cells reported by Dabaja et al.[16]. Briefly, PC-3 cells were transferred to 96-well plates (100 µL.well^{-1}, inoculation density: 4.5×10^4 cell. mL^{-1}). To achieve statistical significance, 10 wells were used to culture the PC-3 cells for the control test, and 10 wells to culture PC-3 cells exposed to ZVp at a concentration of 5.9×10^7 ZVp.mL^{-1} (diluted in cell medium) for 24 h at 37 °C and 5% CO_2. The chosen ZVp concentration, condition, and timepoint were previously determined by GI50 data (concentration for 50% of maximal inhibition of cell proliferation) obtained from an antiproliferative assay performed by Dabaja et al.[16]. The control group was maintained at the same conditions, except by the exposure to ZVp aliquot.

Sample preparation

After trypsinization, 200 µL PC-3 prostate cancer cells exposed and non-exposed to ZVp were transferred to a 2 mL plastic tube and stored at −80 °C until analysis. The sample preparation procedure was performed according to Melo et al.[9]. Briefly, 20-µL aliquots of each sample were added to a plastic tube containing 200 µL of tetrahydrofuran and vortexed for 30 seconds at room temperature. After agitation, the extract was diluted with methanol (1000 µL q.s.), homogenized and centrifuged at 3200 rpm for 5 minutes for protein precipitation. Subsequently, 20 µL of each supernatant was diluted in 980 µL of methanol and separated in

two aliquots of 500 µL each and ionized separately with the addition of 0.1% formic acid (positive ion mode) and 0.1% ammonium hydroxide (negative ion mode) for HRMS analysis.

High resolution mass spectrometry analysis (HRMS)

Each solution was directly infused in high resolution mass spectrometer ESI-LTQ-XL Orbitrap Discovery (Thermo Scientific, Bremen, Germany) with a nominal resolution of 30,000 (FWHM). Spectral data were acquired using the following parameters: flow rate of 10 µL.min^{-1}, capillary temperature at 280 °C, 5 kV spray voltage and sheath gas at 10 arbitrary units. Each sample had 10 technical replicates acquired in the mass range of 400–1100 *m/z* and analyzed using XCalibur software (v. 2.4, Thermo Scientific, San Jose, CA).

Statistical analysis and structural proposals

To investigate the induced alterations of ZVp on PC-3 cell model a Partial Least Square Discriminant Analysis (PLS-DA) was performed using the online software MetaboAnalyst 4.0 (www.metaboanalyst.ca)[63]. A guided selection of molecules *m/z* is established by the observation of VIP (Variable Importance in Projection) scores, that translate the impact of selected features in the proposed model. Only biomarkers with VIP scores equal to, or greater than, 2.2 were evaluated. Prediction accuracy during training test with 2000 permutations was used to assess model significance on both ion modes. A VIP heat map of the selected markers using the Euclidean's distance measurement and Ward's clustering algorithm was built to illustrate the distribution of the most important biomarkers among groups.

The identity of statistically relevant markers was assessed through comparison of high-resolution *m/z* marker (mass error <2 ppm) with available metabolomic databases such as HMDB v.4.0 (Human Metabolome database—www.hmdb.ca), METLIN (Scripps Center for Metabolomics, La Jolla, CA) and Lipid MAPS (University of California, San Diego, CA—www.lipidmaps.org). Tandem MS experiments were used for confirmatory purpose, being acquired in

the same instrument, using Helium as the collision gas, with energies for collision-induced dissociation (CID) ranging from 20–50 (arbitrary units). Spectra were compared with theoretical mass fragmentation of Mass Frontier software (v. 6.0, Thermo Scientific, San Jose, CA).

RESULTS

In order to evaluate the metabolic alterations upon inactivated Zika virus exposure, we treated the PC-3 human prostate cancer androgen-independent cell line with ZVp. After 24 hours of incubation, the cellular extracts of non-exposed and exposed cells were directly infused in a high-resolution mass spectrometer for data analysis on positive and negative ion modes.The acquired mass spectra data were submitted to multivariate statistical analysis (PLS-DA) for group comparison. PLS-DA is a supervised regression analysis, widely used in metabolomics to assess association among sample groups. The principle is based on linear combinations of data variables and further extraction from mass spectrometry raw data features that discriminate sample clustering. Results disposed in Fig. 1 showed remarkable separation between cells exposed to ZVp treatment versus non-exposed cells on both positive and negative ionization modes. The statistical separation among groups confirms the existence of discriminative analytes associated with ZVp-induced metabolic cell alterations. The model was statistically significant on both ion modes ($p < 0.001$) through validation with prediction accuracy during training permutation test (see Additional File, Fig. S1).

Based on variable importance in projection (VIP) score values greater or equal to 2.2, molecules that metabolically discriminated Group 2 from Group 1 were elected. A heat map analysis (See Additional File, Fig. S2) demonstrated the distribution of the most relevant markers among samples. On the positive ion mode, we were able to identify 10 biomarkers for the ZVp-treated condition, while 11 biomarkers were elucidated on the negative ion mode. Characterization was performed cross-checking data from high-resolution mass spectrometry and metabolomics databases. Proposed chemical structures are described in Table 1.

It was possible to correlate biomarkers' function with the recent finds on the antiproliferative effect of Zika virus on prostate cancer cell16. Some molecules, identified on Table 1, are involved on cell mechanisms impaired during viral exposure, while others suggest altered pathways that might lead to prostate cancer cell death. Among them, we found changes on the lipidomic cell profile of phospholipids and ceramides, inflammatory mediators, N-glycan biosynthesis precursors, porphyrin and folate, whose importance is briefly illustrated in Figs 2 and 3. Supported by literature information, we were able to infer the significance of these molecules on PC-3 prostate cancer cell line metabolism disrupted by viral influence and the role of ZIKV interactions with metabolic pathways of host cells.

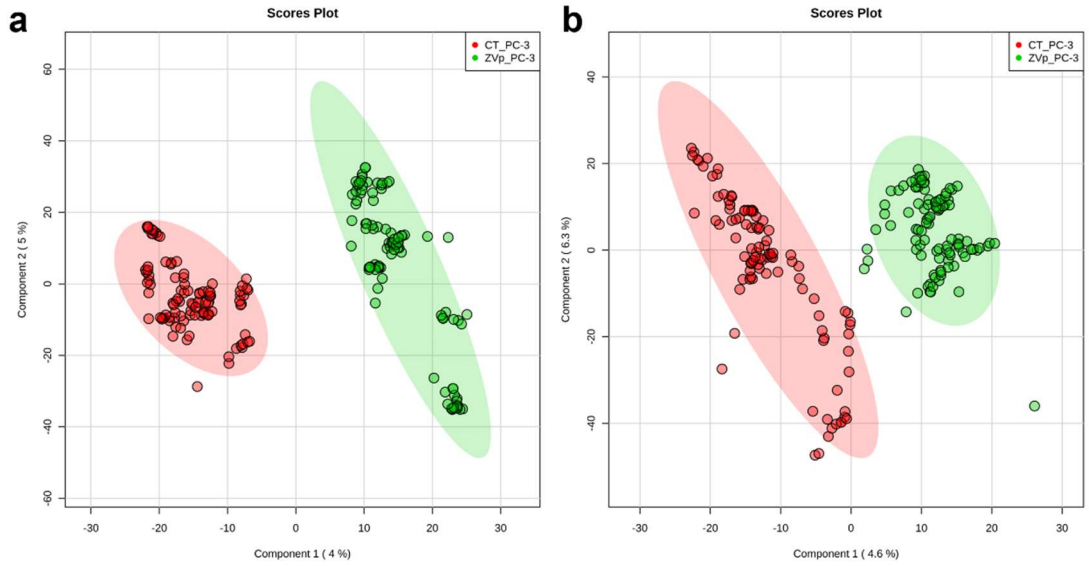

Figure 1. Partial Least Square-Discriminant Analysis (PLS-DA) score plot model showing separation between PC-3 cells control (red) and PC-3 cells exposed to ZVp (green) clustering with data on positive ion mode (a) and negative ion mode (b).

Table 1. Proposed chemical markers elected by PLS-DA VIP scores ≥2.2 from PC-3 prostate cancer cells exposed to Zika virus prototype on both positive and negative ion mode.

Compound	Adduct	Experimental Mass	Theoretical Mass	Error (ppm)	ID[1]	MSMS
Positive Ion Mode						
PGH_2-EA	$[M + K]^+$	432.2505	432.2511	1.39	74984	415, 386, 372
CerP(32:1)[b]	$[M + H]^+$	590.4555	590.4544	−1.86	103039	544, 309, 281, 573, 558, 232
N-Acetyl-D-glucosaminyl diphosphodolichol	$[M + Na]^+$	610.2145	610.2153	1.31	6251	355, 266, 464, 371, 221, 284
Azelaoyl PAF	$[M + H - H_2O]^+$	634.4436	634.4448	1.89	62938	573, 624, 587, 520
GlcCer (30:1)[b]	$[M + H]^+$	644.5105	644.5096	−1.39	7222	612,626, 598, 459, 532, 516
PE(P-32:0)[b]	$[M + H - H_2O]^+$	658.5186	658.5176	−1.52	62174[a]	640, 627, 613, 459
PE(P-34:4)[b]	$[M + H - H_2O]^+$	678.4872	678.4863	−1.33	62157[a]	633, 622, 660, 647, 481/482, 558, 532, 586
PE-NMe(32:0)[b]	$[M + H - H_2O]^+$	688.5292	688.5281	−1.59	40733[a]	671, 566, 431/432, 641, 342, 463, 656
PE(P-32:1)[b]	$[M + H]^+$	702.5445	702.5432	−1.85	62178[a]	684, 670, 656, 333, 459, 365, 644
PE(38:5)[b]	$[M + H]^+$	766.5394	766.5381	−1.70	60376[a]	720, 706, 747, 734, 548, 569, 485
Negative Ion Mode						
HO-$PGF_{2\alpha}$ or HO-PGE_1[c]	$[M + Cl]^-$	405.2042	405.2049	1.73	36117[a] or 36196[a]	337, 369, 387, 367, 373, 361
Dihomo-$PGF_{2\alpha}$ or Dihomo-PGE_1 or Isoprostanes[c]	$[M + Cl]^-$	417.2408	417.2413	1.19	36206[a] or 36171[a]	297, 373, 289, 399
Dolichol phosphate D-mannose	$[M - H]^-$	425.1939	425.1946	1.64	5925	283,367, 379, 255, 313, 407
PG(14:0)[b]	$[M - H]^-$	455.2421	455.2415	−1.31	80000[a]	397, 423, 339, 437, 409,387
PG(12:0)[b]	$[M + Cl]^-$	477.1662	477.1661	1.87	4086[a]	415, 459, 433, 417, 409, 441, 449

PA(20:1)[b]	$[M + Cl]^-$	499.2606	499.2597	−1.80	82345[a]	383, 373, 311, 261, 431, 441, 481, 453, 463
PI(12:0)[b]	$[M - H]^-$	515.2272	515.2263	−1.75	81172	447, 397, 399, 401, 457, 478, 497
5-Methyltetrahydropteroy *l*-tri-glutamate	$[M - H_2O - H]^-$	621.2276	621.2269	−1.13	3684	584, 505, 353, 563, 603, 612
Isocoproporphyrin or Coproporphyrin (I, II, III or IV) [c]	$[M - H_2O - H]^-$	635.2518	635.2506	−1.89	5665[a]	599, 577, 617
Dehydroisocoproporphyrin	$[M - H]^-$	651.2471	651.2460	−1.68	6570	571, 633, 615, 607, 593, 583
Coproporphyrinogen (I or III)[c]	$[M + Cl]^-$	695.2863	695.2853	−1.44	63930 or 80	653, 677, 665, 659, 637, 569

[1]METLIN ID; [a]Representative ID for the class; [b]Carbon number: double bond; [c]Not specified molecules with the same *m/z* and similar fragmentation profile.

CerP-Ceramide phosphate; GlcCer-Glucosylceramide; PAF-Platelet activating factor; PC-Phosphatidylcholine; PE-Phosphatidylethanolamine; PI-Phosphatidylinositol; PG-Phosphatidylglycerol; HO-PGF2α-Hydroxy Prostaglandin F2α; HO-PGE1-Hydroxy Prostaglandin E1; PGH2-EA - Prostaglandin H2-Ethanolamine.

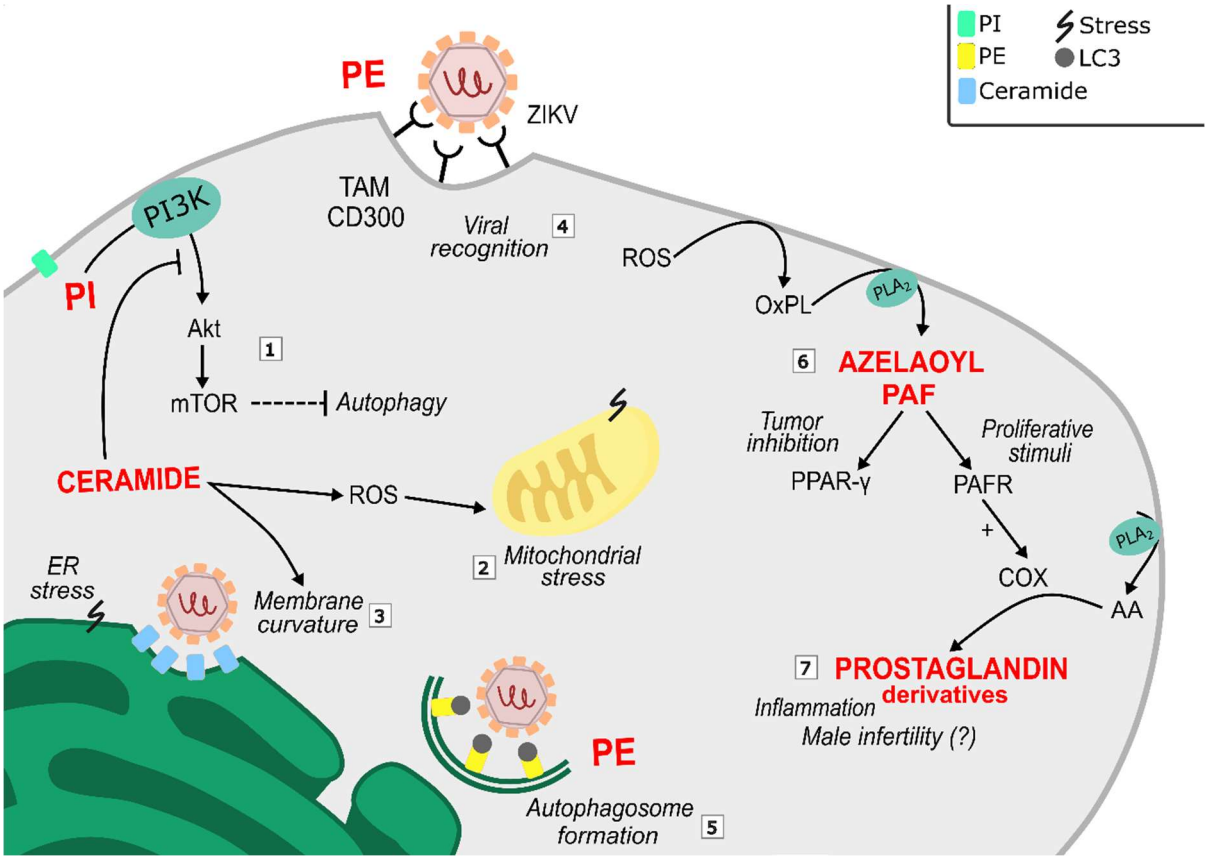

Figure 2. Lipid metabolism alterations induced by ZVp on prostate cancer cells (PC-3 line) mediate increased levels of: phosphatidylinositol, a marker of ZIKV interaction with autophagic pathway (1); ceramides, that contribute to autophagy (1), mitochondrial stress (2) and membrane curvature (3); and phosphatidylethanolamine, which assist on particle recognition (4) and autophagosome formation (5). Zika virus stresses prostate cancer cells leading to high levels of ROS and consequently the presence of oxidized molecules (6) and inflammatory mediators (7). Together, all these factors may contribute to trigger cellular stress and prostate cancer cell death. Abbreviations: AA – arachidonic acid; COX – cyclooxygenase; ER – Endoplasmic reticulum; OxPL – Oxidized phospholipids; PAF – Platelet Activating Factor; PAFR – PAF receptor; PE – Phosphatidylethanolamine; PI – Phosphatidylinositol; ROS – Reactive Oxygen Species.

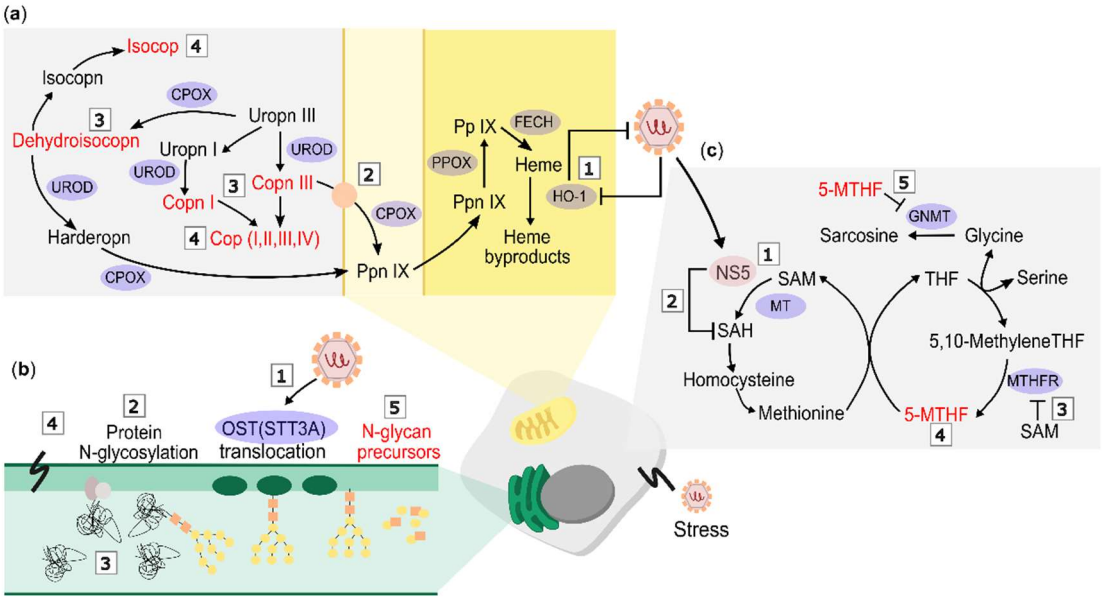

Figure 3. Proposed interaction of ZIKV moieties with pathways involved on (**a**) porphyrin homeostasis, (**b**) protein glycosylation process and (**c**) one-carbon metabolism, leading to the presence of elected biomarkers (in red). (**a**) Heme formation is dependent of an influx of porphyrins to mitochondria which is coordinated by the action of CPOX and UROD enzymes on porphyrin precursors. However, ZIKV interaction with HO-1 enzyme (1) may interfere on heme degradation process. Disturbances on heme metabolism eventually affect porphyrins mitochondrial transport through ABCB6 (2) resulting on porphyrin accumulation (3) represented by Copn (I and II) and Dehidroisocopn and its oxidation products (4) illustrated by Cop (I, II, III and IV) and Isocop; (**b**) ZIKV may interact with OST complex displayed on endoplasmic reticulum (ER) (1), which has an important role on the N-glycan translocation, impairing on host cell protein glycosylation (2). This interaction may lead to misfolded protein formation (3) and ER stress (4) contributing to N-glycan precursors accumulation (5); and (**c**) SAM is an essential methyl donor for methylation processes and its availability impact on the one carbon metabolism molecules abundance. Possible ZIKV NS5 moieties interference on SAM (1) and SAH (2) impact SAM availability and regulation of MTHFR (3), leading to 5-MTHF accumulation (4). As consequence, 5-MTHF negatively control GNMT activity (5), decreasing sarcosine production and promoting a better prognosis to prostate cancer cells. Abbreviations: Cop – Coproporphyrin; Copn – Coproporphyrinogen; DehydroisoPn – Dehydroisocoproporphyrin; HarderoPn – Harderoporphyrinogen; Isocop –

Isocoproporphyrin; Isocopn – Isocoproporphyrinogen; Ppn – Protoporphyrinogen; Pp – Protoporphyrin; Uropn – Uroporphyrinogen; CPOX – Coproporphyrinogen Oxidase; UROD – Uroporphyrinogen Decarboxylase; PPOX – Protoporphyrinogen Oxidase; FECH – Ferrochelatase; HO-1 – Heme Oxygenase; OST – Oligosaccharyltransferase; GNMT – Glycine N-Methyltransferase; 5-MTHF – 5-Methyltetrahydrofolate; THF – Tetrahydrofolate; MTHFR – Methylenetetrahydrofolate Reductase; SAM – S-Adenosylmethionine; SAH – S-Adenosylhomocysteine; MT – Methyltransferase.

DISCUSSION

Viral replication is a mechanism closely dependent on host cell factors. To achieve this purpose, flaviviruses, including ZIKV, promote a reorganization of lipid metabolism and the endoplasmic reticulum (ER) membrane to favor replication[30]. ZIKV, particularly, promotes alterations on general lipid metabolism[5]. In this context, although the proposed ZVp is a particle with inactivated ZIKV, i.e. there is no actual infection and/or replication, key active or binding moieties from molecules that trigger certain pathways may remain intact, even after thermal inactivation; therefore, some lipid classes may play fundamental roles in the interaction with viral antigens and express mediators of cellular response upon contact with ZVp.

Ceramide phosphate (32:1) m/z 590.4555 and Glucosylceramide (30:1) m/z 644.5105 were identified as chemical markers for the ZVp-exposed condition. Increased basal levels of ceramides are known to have effects over cell fate regulation, and are also associated with cell stress conditions[31]. During infection of pathogenic flaviviruses (e.g. Dengue Virus (DENV) and WNV), increased ceramide levels have been reported, especially due to their role on viral assembly by membrane vesiculation[32]. Arboleda et al. (2009) highlighted the potential of increased of ceramide levels to induce mitochondrial dysfunction and neuronal cells death through autophagy mediated by the PI3K/Akt pathway[31] (See Fig. 2). Thus, the induction of increased levels of ceramides has been used as an anticancer strategy, given its ability to promote the activation of cancer cell death through apoptosis and autophagic responses[33].

Other lipids elected by our analysis play an important structural role on cell membranes. Phosphatidylethanolamines (PE), Phosphatidylserines (PS), Phosphatidylinositol (PI), Phosphatidylcholine (PC) Phosphatidic acid (PA) and Phosphatidylglycerol (PG) are abundant lipids on cellular membranes, and therefore are on front of cell-cell and cell-pathogen interactions[30]. Statistically relevant metabolic markers for PC-3 cells exposed to ZVp condition were identified as five PEs with m/z 658.5186 PE(P-32:0), m/z 678.4872 PE(P-34:4), m/z 688. 5292 PE-NMe(32:0), m/z 702.5445 PE(P-32:1) and m/z 766.5394 PE(38:5) on positive ion mode. Being a product of PS decarboxylation, both PE and PS play roles on ZIKV facilitating viral entry on normal conditions[5]. Furthermore, the increase of intracellular PE positively regulates autophagy in mammalian cells. Autophagic membranes are enriched in PE, and this molecule also participates as an anchor to LC3 autophagic protein. Hamel et al. (2015) demonstrated the expressed co-localization of ZIKV viral envelope and cytosolic LC3, suggesting the role of this protein on a ZIKV-induced autophagic process[34]. Thus, the lipidation of LC3 to promote autophagosome membrane formation is a process dependent on PE abundance[35], suggesting that the excess of PE may contribute to ZIKV-mediated cell death.

Different anionic phospholipids [m/z 499.2609 PA(20:1), m/z 477.1662 PG(12:0), m/z 455.2421 PG(14:0) and m/z 515.2274 PI(12:0)] were also elected by the statistical model. Anionic lipids such as PA and lysoPA favor membrane curvature by the action of flipases, and this rearrangement may promote better interaction of membrane phospholipids with flavivirus' molecules[36]. Phosphatidylinositols in particular had their association with ZIKV previously reported in metabolomic studies[9,16], corroborating to our findings. When evaluating the cytostatic impact of inactivated ZIKV on glioblastoma cells, Dabaja et al. (2018) observed PI and phosphatidylinositol phosphate (PIP) as biomarkers[16]. In addition, Melo et al. (2017) reported several alterations on PIP and PIP2 metabolites in the serum of patients infected with ZIKV strain[9], which suggests that the interaction with ZVp may be sufficient to promote cell alterations. Phosphatidylinositol phosphates are important precursors in PI3K/Akt pathway, which leads to mTORC1 inhibition of autophagic processes and cell survival. The upregulation of this pathway significantly contributes to prostate

cancer cell proliferation, migration and invasion. Due to previously reported ZIKV NS4A and NS4B blockage of Akt signaling, the presence of PIs derivatives is expected, and may highlight the molecular signatures of an autophagic fate[4,9,10].

Cell death may also be triggered by caspase 3 activation in neuroprogenitor cells[2], a stimulus that may promote generation of platelet-activating factor (PAF) as counteraction for tumor cell repopulation. PAF, nonetheless, presents dual functions: (i) as a contributor to tumorigenesis, and (ii) as a promoter of cell death, participating in a complex regulation process[37]. In ZVp-treated PC-3 cells, a PAF derivative, Azelaoyl-PAF m/z 634.4436, was identified as a candidate biomarker. Azelaoyl-PAF is formed by the action of PLA2 on oxidized phospholipids (OxPLs) truncated in sn-2 position due ROS damage[38]. Azelaoyl-PAF, an OxPL, stimulates PAF receptor (PAFR) and behaves as an agonist of PPAR-γ, a common receptor on normal tissues and prostate adenocarcinoma cell lines, as well as a reported tumor growth inhibitor. While the interaction with PAFR leads to NF-κB activation and consequently induction of COX and prostaglandins to a pro-inflammatory process and cell resistance[37], a PPAR-γ agonist may induce prostate cancer growth inhibition[39].

The PLA2 gene has been indicated as a potential therapeutic target in prostate cancer[37,40,41]. Therefore, OxPLs and highly expressed PLA2 influence the production of downstream arachidonic acid derivatives, such as prostaglandins by the action of COX enzymes. We found three *m/z* correlated to prostaglandin biomarkers: *m/z* 405.2042 for Hydroxy Prostaglandins F2α (OH-PGF2α) or E1 (OH-PGE1), *m/z* 417.2413 Dihomo Prostaglandins F2α, E1 or Isoprostane analogs and *m/z* 432.2505 for Prostaglandin H2 – Ethanolamine (PGH2-EA). On human seminal fluid OH-PGE1 and OH-PGE2 are the major prostaglandins, with PGE1, PGE2, PGF1α and PGF2α and OH-PGF also reported[41]. While PGE2 promotes cancer development, PGE1 exerts antiproliferative activity, which implies that the ratio between these two opposing metabolites is critical to cancer progression[40]. While there is little knowledge about the cellular effects of hydroxylated prostaglandins, some studies tried to correlate their presence on human seminal fluid with spermatozoa motility. OH-PGF is associated to decreased sperm motility while OH-PGE exerts the opposite effect[42]. It has been reported that ZIKV-infected men presented a significant

decrease in spermatozoa number and motility, which suggests that Zika virus is a risk factor to impaired male fertility[13,43]. Moreover, the presence of isoprostane analogs from F2α family and E1 derivatives as biomarkers indicates extensive oxidative stress, since these molecules are associated with lipid peroxidation in several diseases including prostate cancer[44,45]. Their election as biomarkers suggests elevation on ROS levels in ZVP-treated condition. Altogether, the fine control of prostaglandins, hydroxy prostaglandins and isoprostanes in prostate cancer cell treated with ZVP may be an explanation to male infertility during ZIKV infection[13,42,43,44].

Porphyrin derivatives, Isocoproporphyrin or Coproporphyrin isomers (I, II, III or IV) *m/z* 635.2519, Dehydroisocoproporphyrin *m/z* 651.2474 and Coproporphyrinogen isomers (I or III) *m/z* 695.2863 were also found as biomarkers. Free porphyrin metabolites may cause cell damage through oxidative stress; accordingly, the cell engages a well-coordinated heme biosynthesis through heme negative feedback and a fine control of porphyrin derivatives by degradation enzymes and transporters[46]. Heme oxygenase (HO-1) is a stress response enzyme, induced by Nrf2 signaling and inflammation, responsible to transform heme derivatives in biliverdin, carbon monoxide and ferrous iron[25]. HO-1 exhibits antiviral activity against several flavivirus, such as DENV, Hepatitis C (HCV) and ZIKV. However, recently it was observed that ZIKV could limit HO-1 antiviral activity in a translational or post-translational manner, impairing HO-1 efficacy, a real possibility given the role of ZIKV on ER stress[29,47]. Thus, the capacity of HO-1 modulation by ZIKV may implicate in viral persistence and alterations on heme metabolism[29,48]. However, molecules and mechanisms involved in this interaction remain unknown. Lined up with metabolic interference of virus molecules, Nakano et al. (2018) discovered that HCV suppresses intracellular protoporphyrin IX (Pp IX), elevates excretion of coproporphyrinogen III (Copn III), higher levels of Pp IX exporter (FLVCR1 and ABCG2) transcription and decreases expression of mitochondrial coproporphyrinogen III importer (ABCB6), altering porphyrin metabolism[48]. Therefore, the observed porphyrins may be resulted from disturbances in heme degradation, biosynthesis, and transport. A porphyrin synthesis scheme is simplified in Fig. 3.

Moreover, a fundamental outer membrane transporter of porphyrin to mitochondria for heme synthesis is ABCB6, and its expression responds to intracellular porphyrin levels[49]. The markers elucidate the spontaneous oxidation of Coproporphyrinogens to Coproporphyrin isomers. The presence of these autoxidation products may occur due to porphyrin precursor accumulation. We hypothesize that an impairment on heme degradation through HO-1 by ZIKV molecules may eventually increase mitochondrial concentrations of heme, causing negative feedback on ABCB6 importer, and consequently accumulation of porphyrin precursors. Excess of porphyrin may photosensitize cancer cells, triggering elevation of ROS and cell death[46]. Since this is a complex and important system for cell homeostasis, further experiments need to be addressed to confirm the role of ZIKV on porphyrin metabolism of prostate cancer cells.

Regarding the autophagic process, cytoplasmic vacuolation and ER-derived autophagosome formation is evidence of response to ZIKV particles[34,47]. The previously discussed lipid remodeling[5] induced by ZIKV, as well as the excess use of N-linked glycosylation enzymes for cancer cell protein glycosylation are factors that may trigger an ER stress response[30]. N-acetyl-D-glucosaminyldiphosphodolichol *m/z* 610.2145 and Dolichol phosphate D-mannose *m/z* 425.1939, precursors of N-glycan biosynthesis, were identified as biomarkers of ZVp-treated condition. Glycosylation is the most ordinary and versatile posttranslational protein modification, which regulates protein folding and function[50]. The formation of N-glycan structures starts on ER through a series of glycosylation generating the N-glycan core (See Fig. 3). The translocation of N-glycans to translated proteins occurs via the oligosaccharyltransferase complex (OST), composed of STT3A and STT3B subunits[50,51]. Cancer cells present a differentiated pattern of glycosylation through a process highly dependent on glucosyltransferases, ER function and integrity; the importance of this process is such, that protein glycosylation inhibition has been reported as an alternative chemotherapeutic strategy[51]. An OST inhibitor has been reported as a strategy to flavivirus infection blockage, suggesting that ZIKV molecules interact with host cell machinery[6,52]. In fact, ZIKV E protein glycosylation and infectivity is assisted by STT3A expression[52]. Therefore, considering these findings, an increase in N-glycan precursors may appear as a result of ZIKV and PC-3 cell

interaction with either N-glycosylation machinery or ER stress. Thus, the interaction between ZIKV and N-glycosylation enzymes, in addition to ROS-mediated ER stress, may lead to the accumulation of misfolded protein and consequently ER function impairment and pro-apoptotic signaling[50].

Moreover, some ZIKV non-structural proteins interact with host biomolecules on methylation steps[53,54]. The availability of methyl donors requires intracellular folate from a functional one-carbon metabolism[55]. 5-Methyltetrahydropteroyl tri-L-glutamate (5-MTHF) *m/z* 621.2276, a folate derivative, was found as a ZVp-treated biomarker; the same molecule was previously described by Dabaja et al. (2018) during glioblastoma antiproliferative assessment[16], corroborating the importance of this finding. This molecule participates in the conversion of methionine to S-Adenosylmethionine (SAM), homocysteine to methionine, and as downregulation factor for Glycine N-methyltransferase (GNMT)[55]. For instance, 5-MTHF formation is regulated by precursor availability and SAM levels, which in high levels exerts inhibitory effects on MTHF reductase[55] (See Fig. 3). Coloma et al. (2016) reported that the non-structural protein NS5 has homology to methyltransferases and may sequestrate SAM as methyl donor[53]. Moreover, NS5 may bind to S-Adenosylhomocysteine (SAH) blocking the regeneration of homocysteine and consequently remethylation of methionine and SAM[54]. SAM is used in prostate cancer cells for glycine methylation into sarcosine via GNMT; high levels of sarcosine were found to be a biomarker of prostate cancer progression[56]. The inhibition of GNMT results in decreased sarcosine, diminished proliferation and a better prognosis of prostate cancer[56,57]. All these factors may implicate on modifications of intracellular levels of SAM in one-carbon metabolism and, consequently, 5-MTHF accumulation. Furthermore, changes in DNA methylation of genes in developing cells and human neural cells suggest that one-carbon metabolism is a key pathway on microcephaly[58,59]. Given the basal prostate cancer cell aberrant methylation and ZIKV interaction with folate metabolism, ZVp may interfere on DNA instability, thereby controlling cell fate.

All abovementioned biomarkers were proposed to be involved with the effects of Zika prototype on PC-3 prostate cancer cell line; remarkably, they pointed to ZVp-host lipid remodeling and interaction of ZIKV moieties with key

pathways for cell homeostasis, namely the regulation of cytoprotective enzymes, autophagic signaling and ROS induced stress, raising new hypotheses about the role of ZIKV as an oncolytic virus and a promoter of male infertility. The metabolomics approach applied herein has allowed not only the observation of a handful of non-obvious biomarkers, but also their related pathways, which are being correlated to Zika for the first time. Our findings suggest, therefore, the involvement of several pathways with the antiproliferative effect of Zika virus against prostate cancer contributing to a promising topic for future research; this also reinforces the importance of studies with broader, untargeted metabolomics/ lipidomics approaches, as most of these pathways might not have been identified by targeted biomolecular assays. Finally, to the best our knowledge, these molecular signatures were the first reported for prostate cancer cells exposed to inactivated ZIKV particles.

SUPPLEMENTARY MATERIAL

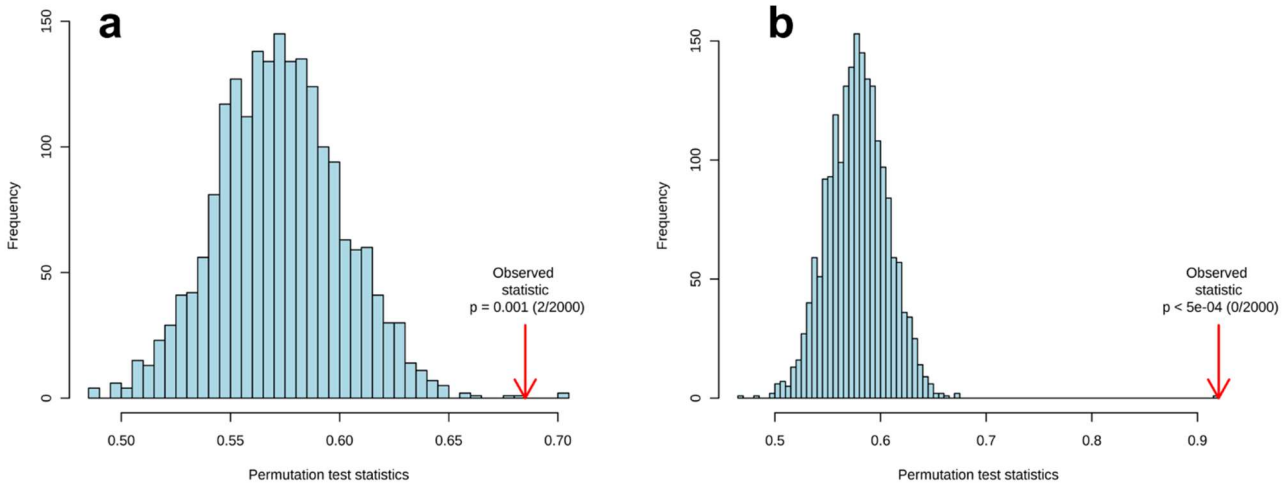

Figure S1. Permutation tests based on prediction accuracy during training for PLS-DA statistical validation. (a) p-value < 0.001 (2/2000) on positive ion mode; (b) p-value < 5e-04 (0/2000) on negative ion mode.

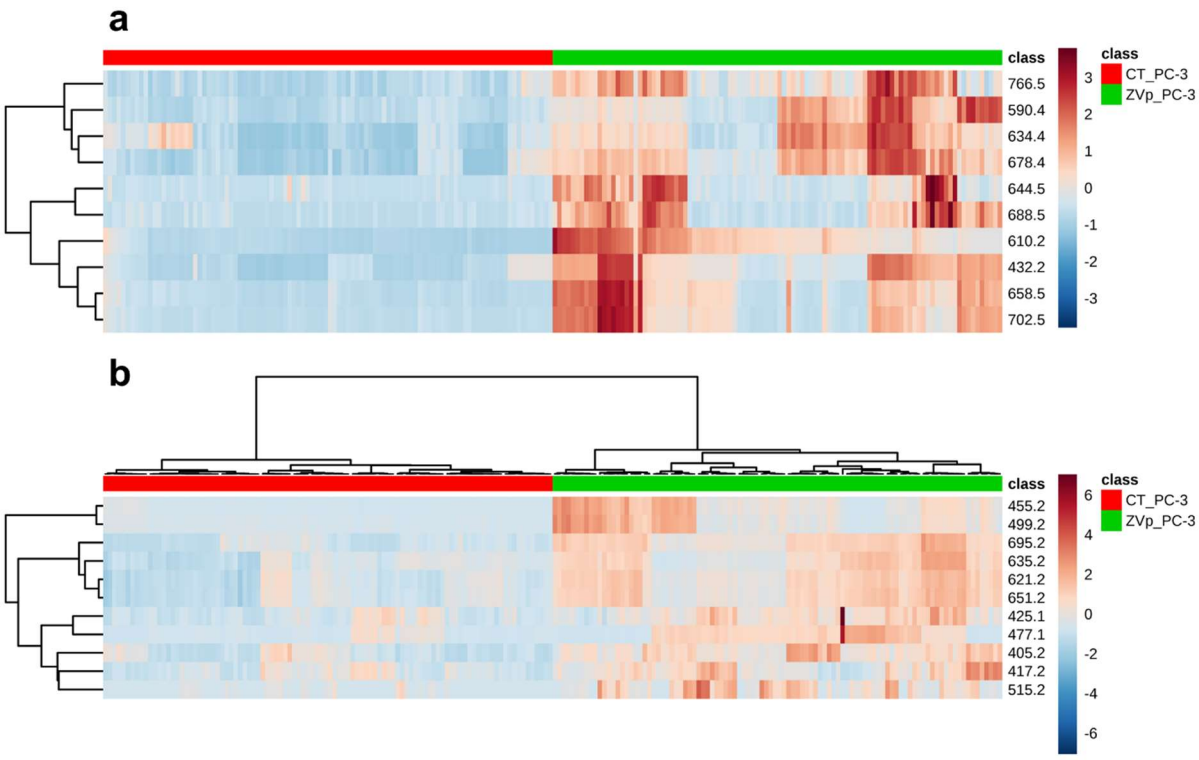

Figure S2. Heatmap analysis of selected markers distribution (a) on positive and (b) on negative ion mode.

REFERENCES

1. Boeuf, P., Drummer, H. E., Richards, J. S., Scoullar, M. J. & Beeson, J. G. The global threat of Zika virus to pregnancy: epidemiology, clinical perspectives, mechanisms, and impact. BMC medicine 14, 112, https://doi.org/10.1186/s12916-016-0660-0 (2016).
2. Tang, H. et al. Zika virus infects human cortical neural progenitors and attenuates their growth. Cell stem cell 18, 587–590, https://doi.org/10.1016/j.stem.2016.02.016 (2016).
3. Li, C. et al. Zika virus disrupts neural progenitor development and leads to microcephaly in mice. Cell stem cell 19, 120–126, https://doi.org/10.1016/j.stem.2016.04.017 (2016).
4. Liang, Q. et al. Zika virus NS4A and NS4B proteins deregulate Akt-mTOR signaling in human fetal neural stem cells to inhibit neurogenesis and induce autophagy. Cell stem cell 19, 663–671, https://doi.org/10.1016/j.stem.2016.07.019 (2016).

5. Martin-Acebes, M. A., Vazquez-Calvo, A. & Saiz, J.-C. Lipids and flaviviruses, present and future perspectives for the control of dengue, Zika, and West Nile viruses. Progress in lipid research 64, 123–137, doi:10.1016/j.plipres.2016.09.005 (2016).
6. Pérez-García, L. A., Martínez-Duncker, I. & Montes, H. M. M. The Endoplasmic Reticulum Alpha-Glycosidases as Potential Targets for Virus Control. Current Protein and Peptide Science 18, 1090–1097, https://doi.org/10.2174/1389203717666160813161729 (2017).
7. Li, G. et al. Characterization of cytopathic factors through genome-wide analysis of the Zika viral proteins in fission yeast. Proceedings of the National Academy of Sciences 114, E376–E385, https://doi.org/10.1073/pnas.1619735114 (2017).
8. Lee, I. et al. Probing Molecular Insights into Zika Virus–Host Interactions. Viruses 10, 233, https://doi.org/10.3390/v10050233 (2018).
9. Melo, C. F. O. et al. Serum metabolic alterations upon Zika infection. Frontiers in microbiology 8, 1954 (2017).
10. Melo, C. F. et al. Corrigendum: Serum metabolic alterations upon Zika infection. Frontiers in microbiology 8, https://doi.org/10.3389/fmicb.2017.02373 (2017).
11. Kumar, A. et al. Human Sertoli cells support high levels of Zika virus replication and persistence. Scientific reports 8, 5477, https://doi.org/10.1038/s41598-018-23899-x (2018).
12. Simanjuntak, Y. et al. Ebselen alleviates testicular pathology in mice with Zika virus infection and prevents its sexual transmission. PLoS pathogens 14, e1006854, https://doi.org/10.1371/journal.ppat.1006854 (2018).
13. Stassen, L., Armitage, C., van der Heide, D., Beagley, K. & Frentiu, F. Zika virus in the male reproductive tract. Viruses 10, 198, https://doi.org/10.3390/v10040198 (2018).
14. Spencer, J. L. et al. Replication of Zika virus in human prostate cells: a potential source of sexually transmitted virus. The Journal of infectious diseases 217, 538–547, https://doi.org/10.1093/infdis/jix436 (2017).
15. Lima, Ed. O. et al. MALDI imaging detects endogenous digoxin in glioblastoma cells infected by Zika virus—Would it be the oncolytic key?

Journal of Mass Spectrometry 53, 257–263, https://doi.org/10.1002/jms.4058 (2018).

16. Dabaja, M. Z. et al. Metabolic alterations induced by attenuated Zika virus in glioblastoma cells. Cell & Bioscience 8, 47, https://doi.org/10.1186/s13578-018-0243-1 (2018).
17. Zhu, Z. et al. Zika virus has oncolytic activity against glioblastoma stem cells. Journal of Experimental Medicine 214, 2843–2857, https://doi.org/10.1084/jem.20171093 (2017).
18. Chimelli, L. et al. Persistence of Zika virus after birth: clinical, virological, neuroimaging, and neuropathological documentation in a 5-month infant with congenital Zika syndrome. Journal of Neuropathology & Experimental Neurology 77, 193–198, https://doi.org/10.1093/jnen/nlx116 (2018).
19. Martins, P. et al. Outer membrane vesicles from Neisseria Meningitidis (Proteossome) used for nanostructured Zika virus vaccine production. Scientific reports 8, 8290, https://doi.org/10.1038/s41598-018-26508-z (2018).
20. Paschos, A., Pandya, R., Duivenvoorden, W. & Pinthus, J. Oxidative stress in prostate cancer: changing research concepts towards a novel paradigm for prevention and therapeutics. Prostate cancer and prostatic diseases 16, 217, https://doi.org/10.1038/pcan.2013.13 (2013).
21. Majumdar, S., Buckles, E., Estrada, J. & Koochekpour, S. Aberrant DNA methylation and prostate cancer. Current genomics 12, 486–505, https://doi.org/10.2174/138920211797904061 (2011).
22. Moon, E. J. & Giaccia, A. Dual roles of NRF2 in tumor prevention and progression: possible implications in cancer treatment. Free Radical Biology and Medicine 79, 292–299, https://doi.org/10.1016/j.freeradbiomed.2014.11.009 (2015).
23. Milkovic, L., Zarkovic, N. & Saso, L. Controversy about pharmacological modulation of Nrf2 for cancer therapy. Redox biology 12, 727–732, https://doi.org/10.1016/j.redox.2017.04.013 (2017).
24. Jayakumar, S., Kunwar, A., Sandur, S. K., Pandey, B. N. & Chaubey, R. C. Differential response of DU145 and PC3 prostate cancer cells to ionizing radiation: role of reactive oxygen species, GSH and Nrf2 in

radiosensitivity. Biochimica et Biophysica Acta (BBA)-General Subjects 1840, 485–494, https://doi.org/10.1016/j.bbagen.2013.10.006 (2014).

25. No, J. H., Kim, Y.-B. & Song, Y. S. Targeting nrf2 signaling to combat chemoresistance. Journal of cancer prevention 19, 111, https://doi.org/10.15430/JCP.2014.19.2.111 (2014).
26. Yu, S. et al. Nrf2 expression is regulated by epigenetic mechanisms in prostate cancer of TRAMP mice. PloS one 5, e8579, https://doi.org/10.1371/journal.pone.0008579 (2010).
27. Frohlich, D., McCabe, M., Arnold, R. & Day, M. The role of Nrf2 in increased reactive oxygen species and DNA damage in prostate tumorigenesis. Oncogene 27, 4353, https://doi.org/10.1038/onc.2008.79 (2008).
28. Chen, H. et al. The PI3K/AKT pathway in the pathogenesis of prostate cancer. Front Biosci (Landmark Ed) 21, 1084–1091, https://doi.org/10.2741/4443 (2016).
29. El Kalamouni, C. et al. Subversion of the Heme Oxygenase-1 Antiviral Activity by Zika Virus. Viruses 11, 2, https://doi.org/10.3390/v11010002 (2019).
30. Strating, J. R. & van Kuppeveld, F. J. Viral rewiring of cellular lipid metabolism to create membranous replication compartments. Current opinion in cell biology 47, 24–33, https://doi.org/10.1016/j.ceb.2017.02.005 (2017).
31. Arboleda, G., Morales, L. C., Benítez, B. & Arboleda, H. Regulation of ceramide-induced neuronal death: cell metabolism meets neurodegeneration. Brain research reviews 59, 333–346, https://doi.org/10.1016/j.brainresrev.2008.10.001 (2009).
32. Leier, H. C., Messer, W. B. & Tafesse, F. G. Lipids and pathogenic flaviviruses: An intimate union. PLoS pathogens 14, e1006952, https://doi.org/10.1371/journal.ppat.1006952 (2018).
33. Morad, S. A. & Cabot, M. C. Ceramide-orchestrated signalling in cancer cells. Nature Reviews Cancer 13, 51, https://doi.org/10.1038/nrc3398 (2013).
34. Hamel, R. et al. Biology of Zika virus infection in human skin cells. Journal of virology 89, 8880–8896, https://doi.org/10.1128/JVI.00354-15 (2015).

35. Rockenfeller, P. et al. Phosphatidylethanolamine positively regulates autophagy and longevity. Cell death and differentiation 22, 499, https://doi.org/10.1038/cdd.2014.219 (2015).
36. Kooijman, E. E., Chupin, V., de Kruijff, B. & Burger, K. N. Modulation of membrane curvature by phosphatidic acid and lysophosphatidic acid. Traffic 4, 162–174, https://doi.org/10.1034/j.1600-0854.2003.00086.x (2003).
37. Dando, I. et al. Oncometabolites in cancer aggressiveness and tumour repopulation. Biological Reviews, https://doi.org/10.1111/brv.12513 (2019).
38. Long, J. Z. & Cravatt, B. F. The metabolic serine hydrolases and their functions in mammalian physiology and disease. Chemical reviews 111, 6022–6063, https://doi.org/10.1021/cr200075y (2011).
39. Mueller, E. et al. Effects of ligand activation of peroxisome proliferator-activated receptor γ in human prostate cancer. Proceedings of the National Academy of Sciences 97, 10990–10995, https://doi.org/10.1073/pnas.180329197 (2000).
40. Xu, Y. & Qian, S. Y. Anti-cancer activities of ω-6 polyunsaturated fatty acids. Biomedical journal 37, 112, https://doi.org/10.4103/2319-4170.131378 (2014).
41. Bylund, J. Cytochrome P450 enzymes in oxygenation of prostaglandin endoperoxides and arachidonic acid: Cloning, expression and catalytic properties of CYP4F8 and CYP4F21, Acta Universitatis Upsaliensis (2000).
42. Gottlieb, C., Svanborg, K., Eneroth, P. & Bygdeman, M. Effect of prostaglandins on human sperm function in vitro and seminal adenosine triphosphate content. Fertility and sterility 49, 322–327, https://doi.org/10.1016/S0015-0282(16)59723-4 (1988).
43. Joguet, G. et al. Effect of acute Zika virus infection on sperm and virus clearance in body fluids: a prospective observational study. The Lancet Infectious Diseases 17, 1200–1208, https://doi.org/10.1016/S1473-3099(17)30444-9 (2017).

44. Brys, M. et al. Relationship of urinary isoprostanes to prostate cancer occurence. Molecular and cellular biochemistry 372, 149–153, https://doi.org/10.1007/s11010-012-1455-z (2013).
45. Jadoon, S. & Malik, A. A Comprehensive Review Article on Isoprostanes as Biological Markers. Biochem Pharmacol (Los Angel) 7, https://doi.org/10.4172/2167-0501.1000246 (2018).
46. Yang, X., Palasuberniam, P., Kraus, D. & Chen, B. Aminolevulinic acid-based tumor detection and therapy: molecular mechanisms and strategies for enhancement. International journal of molecular sciences 16, 25865–25880, https://doi.org/10.3390/ijms161025865 (2015).
47. Monel, B. et al. Zika virus induces massive cytoplasmic vacuolization and paraptosis-like death in infected cells. The EMBO journal 36, 1653–1668, https://doi.org/10.15252/embj.201695597 (2017).
48. Nakano, T., Moriya, K., Koike, K. & Horie, T. Hepatitis C virus core protein triggers abnormal porphyrin metabolism in human hepatocellular carcinoma cells. PloS one 13, e0198345, https://doi.org/10.1371/journal.pone.0198345 (2018).
49. Krishnamurthy, P. C. et al. Identification of a mammalian mitochondrial porphyrin transporter. Nature 443, 586, https://doi.org/10.1038/nature05125 (2006).
50. Xu, C. & Ng, D. T. Glycosylation-directed quality control of protein folding. Nature reviews Molecular cell biology 16, 742, https://doi.org/10.1038/nrm4073 (2015).
51. Kurosu, M. Inhibition of N-glycosylation towards novel anti-cancer chemotherapeutics. Journal of molecular pharmaceutics & organic process research 6, https://doi.org/10.4172/2329-9053.1000141 (2018).
52. Mossenta, M., Marchese, S., Poggianella, M., Campos, J. S. & Burrone, O. Role of N-glycosylation on Zika virus E protein secretion, viral assembly and infectivity. Biochemical and biophysical research communications 492, 579–586, https://doi.org/10.1016/j.bbrc.2017.01.022 (2017).
53. Coloma, J., Jain, R., Rajashankar, K. R., García-Sastre, A. & Aggarwal, A. K. Structures of NS5 methyltransferase from Zika virus. Cell reports 16, 3097–3102, https://doi.org/10.1016/j.celrep.2016.08.091 (2016).

54. Zhao, B. et al. Structure and function of the Zika virus full-length NS5 protein. Nature communications 8, 14762, https://doi.org/10.1038/ncomms14762 (2017).
55. Litwack, G. Folic acid and folates. Vol. 79 (Academic Press, 2008).
56. Song, Y. H., Shiota, M., Kuroiwa, K., Naito, S. & Oda, Y. The important role of glycine N-methyltransferase in the carcinogenesis and progression of prostate cancer. Modern Pathology 24, 1272, https://doi.org/10.1038/modpathol.2011.76 (2011).
57. Heger, Z. et al. Prostate tumor attenuation in the nu/nu murine model due to anti-sarcosine antibodies in folate-targeted liposomes. Scientific reports 6, 33379, https://doi.org/10.1038/srep33379 (2016).
58. Janssens, S. et al. Zika virus alters DNA methylation of neural genes in an organoid model of the developing human brain. MSystems 3, e00219–00217, https://doi.org/10.1128/mSystems.00219-17 (2018).
59. Dean, W., Lucifero, D. & Santos, F. DNA methylation in mammalian development and disease. Birth Defects Research Part C: Embryo Today: Reviews 75, 98–111, https://doi.org/10.1002/bdrc.20037 (2005).
60. Melo, C. F. O. R. et al. A lipidomics approach in the characterization of Zika-infected mosquito cells: potential targets for breaking the transmission cycle. PloS one 11, e0164377, https://doi.org/10.1371/journal.pone.0164377 (2016).
61. Alves, D., Mattos, I., Hollanda, L. & Lancellotti, M. Use of mesoporous silica Sba-15 and Sba-16 in association of outer membrane vesicles-Omv from Neisseria meningitidis. Journal of Vaccines and Vaccination, https://doi.org/10.4172/2157-7560.1000196 (2013).
62. Roman Junior, W. A. et al. Antiproliferative effects of pinostrobin and 5, 6-dehydrokavain isolated from leaves of Alpinia zerumbet. Revista Brasileira de Farmacognosia 27, 592–598, https://doi.org/10.1016/j.bjp.2017.05.007 (2017).
63. Chong, J. et al. MetaboAnalyst 4.0: towards more transparent and integrative metabolomics analysis. Nucleic acids research 46, W486–W494 (2018).

4.3 Resultados complementares

Utilizando as células PNT1a nos tempos 5, 10 e 15 dias agrupadas tanto nas condições de controle quanto expostas ao ZIKV, avaliou-se o uso de algoritmos de Machine Learning para ranqueamento de marcadores discriminantes conforme método publicado por Delafiori et al. (2021)(20).

Os dados de espectrometria de massas coletados para os marcadores identificados foram divididos em duas partições: treinamento (70%) e teste (30%) sendo testados diferentes algoritmos (*PLS - Partial Least Square, RF – Random Forest; GDTB – Gradient Tree Boosting; ADA – ADA Boosting*). A projeção da separação entre os grupos foi feita através de ajuste recursivo por MCC (*Matthew Correlation Coeficient*) e a importância de cada valor de *m/z* avaliada por meio do ΔJ. A importância é dada por uma função de distribuição cumulativa; por exemplo, a distribuição cumulativa de um dado valor de *m/z* no grupo controle (negativo) é comparada com a distribuição cumulativa do mesmo valor de *m/z* no grupo exposto ao ZIKV (positivo) através do teste de hipótese de Kolmogorov-Smirnov para determinar se as distribuições são iguais. Se o teste falha (distribuições diferentes), um valor de ΔJ é atribuído, sendo valores positivos marcadores do grupo exposto (ZIKV) e negativos marcadores do grupo controle (exemplo Figura 5).

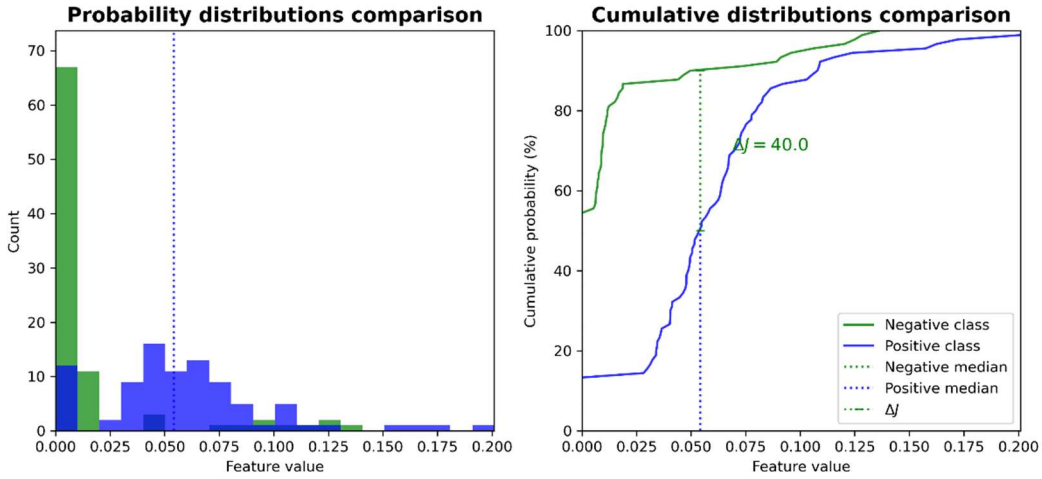

Figura 5. Exemplo de função de distribuição cumulativa para valor de *m/z* 436.3 com atribuição de ΔJ.

Dentre os algoritmos testados, o modelo gerado com o algoritmo PLS apresentou melhor performance, com especificidade e sensibilidade acima de 90% utilizando-se os primeiros 9 marcadores ranqueados (Tabelas 1 e 2).

Tabela 1. Métricas do ranqueamento de marcadores para cada algoritmo. Valores correspondem à porcentagem média e desvio.

Algorítmo	**ADA**	**PLS**	**RF**	**GDTB**
Exatidão	90.4 ± 4.6	92.9 ± 7.6	84.6 ± 5.1	88.4 ± 4.1
Precisão	88.7 ± 9.7	92.2 ± 10.1	78.4 ± 6.4	84.5 ± 9.11
Sensibilidade	94.8 ± 7.7	95.5 ± 10.5	96.5 ± 8.26	96.5 ± 6.8
Especificidade	86.0 ± 12.6	90.3 ± 13.0	72.7 ± 9.3	80.3 ± 12.33
MCC	0.8 ± 0.1	0.9 ± 0.1	0.7 ± 0.1	0.8 ± 0.1

Tabela 2. Lista dos 9 marcadores ranqueados pelo algoritmo PLS.

Ordem	***m/z***	**Molécula**	**Aduto**	**Fórmula Molecular**	**Erro (ppm)**	**ΔJ (%)**
0	426.3	CAR 18:1	[M+H]+	C24H47NO4	4.9	-50.0
1	359.2	FA 20:4;O2	[M+Na]+	C20H32O4	2.8	35.6
2	382.3	N-estearoil prolina	[M+H]+	C23H43NO3	4.7	-50.0
3	436.3	CAR 17:0	[M+Na]+	C24H47NO4	3.4	40.0
4	218.0	Ácido hipúrico	[M+K]+	C9H9NO3	-4.6	23.3
5	369.2	FA 20:4;O4	[M+H]+	C20H32O6	-4.6	32.2
6	237.0	Cys-HCys dissulfito	[M+H-H2O]+	C7H14N2O4S2	3.0	28.9
7	384.3	N-estearoil valina	[M+H]+	C23H45NO3	3.1	-17.8
8	233.1	Dipeptídeo 1	[M+H]+	C10H20N2O4	0.4	-36.7

CAR – acilcarnitina; FA – ácido graxo; Cys-HCys - Cisteína-homocisteína.

A projeção em PCA demonstra a separação dos grupos controle e infectado por ZIKV, destacando as amostras que se apresentaram classificadas como verdadeiro positivas (TP – azul), falso positivas (FP - preto), verdadeiro negativas (TN – verde) e falso negativas (FN - vermelho) na Figura 6. O mapa

de calor presente na Figura 7 mostra a distribuição das massas selecionadas entre as amostras.

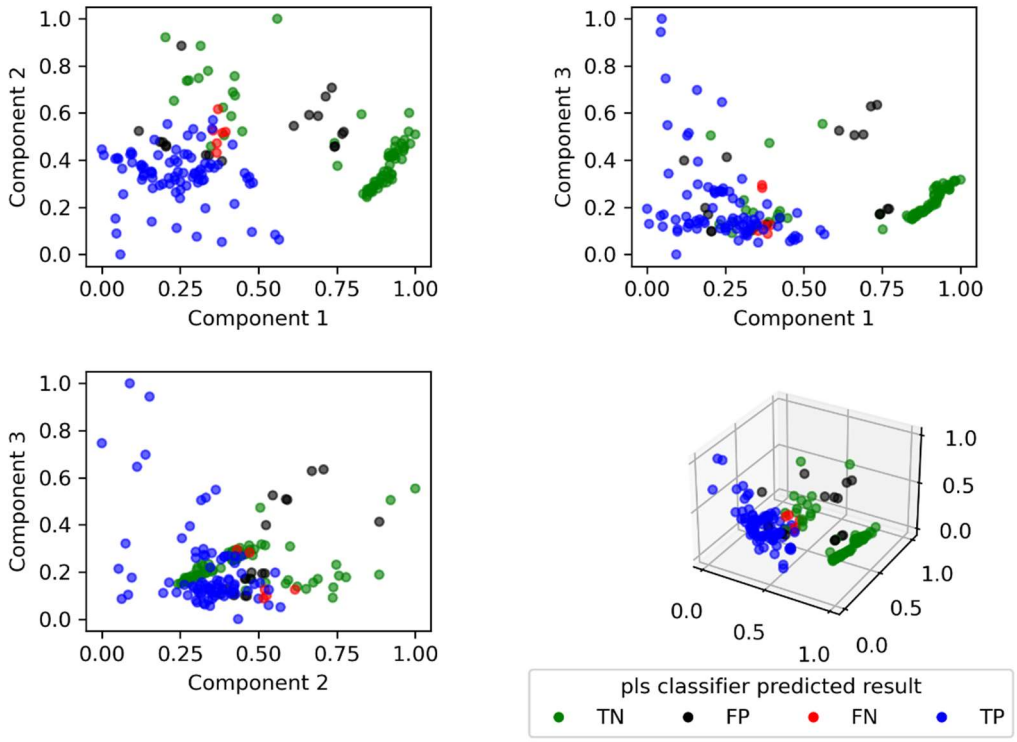

Figura 6. Projeção de PCA com a classificação das amostras realizada pelo algoritmo PLS.

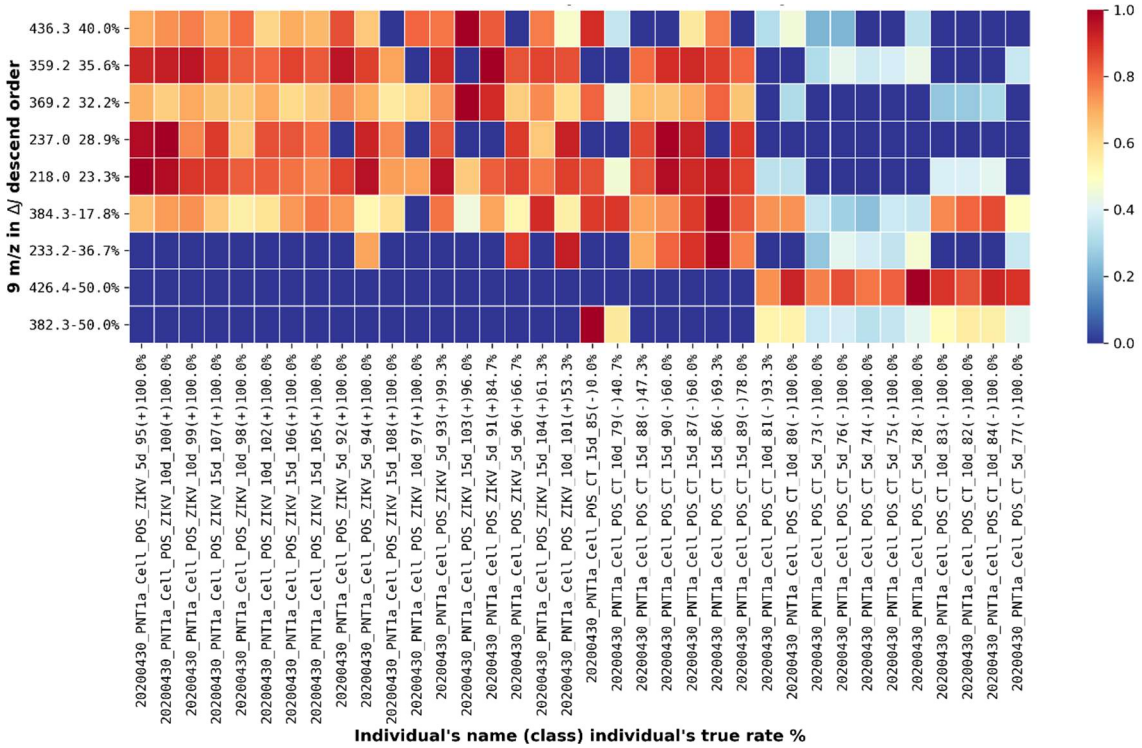

Figura 7. Mapa de calor com os metabólitos ranqueados pelo valor de ΔJ.

Conforme destacado no Capítulo 1, o aumento do metabólito acilcarnitina, aqui ranqueado como principal marcador, foi progressivo ao longo do tempo de infecção persistente em células da próstata. Elevados níveis de carnitina estão associados ao aumento no aporte de ácidos graxos para β-oxidação mitocondrial, condizente com o metabolismo pró-lipólise apresentado pelos flavivirus (24,26,27).

5. DISCUSSÃO GERAL

Durante a epidemia de 2016, o ZIKV demonstrou rápida disseminação e associação com sintomas neurológicos, como a síndrome congênita por Zika (1). Nos primeiros anos, diversos pesquisadores juntaram esforços em estudos para o desenvolvimento de medidas de contenção e diagnóstico. Tais medidas foram fundamentais para alertar a população sobre os riscos e a necessidade da diferenciação da infecção por Zika de outras arboviroses como Dengue e Chikungunya (4). Mesmo com o passar da epidemia e com as dificuldades associadas ao seu diagnóstico clínico, estudos direcionados para a investigação dos mecanismos de infecção humana pelo Zika se extenderam, reforçando sua importância clínica e epidemiológica.

O papel do sistema reprodutor masculino na infecção por ZIKV tem sido explorado aos poucos. Dificuldades na obtenção de amostras de urina e sêmen de homens infectados por ZIKV é um importante gargalo no entendimento da fisiopatologia da doença e do potencial comprometimento temporário ou a longo prazo da fertilidade (37,42,45). Entretanto, experimentos *in vivo* com modelos animais, e *in vitro* têm explorado a permissividade das células do sistema reprodutor ao ZIKV (37–39). Embora não esteja envolvida na produção de gametas, a próstata apresenta função indireta na reprodução através da produção do fluido prostático que compõe o sêmen. Esse fluido é rico em zinco, citrato e proteínas, auxiliando na proteção, nutrição e transporte dos espermatozóides (54). Dessa forma, alterações no funcionamento e metabolismo das células da próstata por inflamações transitórias ou crônicas podem comprometer seu desempenho (90).

Neste estudo, foi possível demonstrar que as células epiteliais da próstata respondem à infecção pelo ZIKV em baixa multiplicidade mantendo normalmente sua proliferação quando submetidas à infecção persistente por 15 dias. Embora não tenha sido observado efeito antiproliferativo, o metabolismo das células encontrou-se diferencialmente alterado nos 3 tempos observados, caracterizados pelo aumento ou diminuição progressiva de determinados metabólitos. Destaca-se a tendência ao aumento de hidróxiguanosina, ditirosina e aminotirosina com o decorrer da infecção. Essas moléculas estão relacionadas a presença de estresse oxidativo, evidenciando o estado metabólico celular

provocado pela condição de infecção persistente. Ambas ditirosina e aminotirosina são resultado da nitrogenação de resíduos de aminoácido tirosina em proteínas, podendo levar a sinalizações de morte celular por estresse (91,92). Além disso, a hidróxiguanosina é um marcador de dano de DNA/RNA, mostrando que a infecção persistente pode estar associada a processos carcinogênicos a longo prazo (93). Em contrapartida, a fosfocreatina foi detectada em diminuição progressiva. Essa molécula atua como fonte de energia para funções de alta demanda energética, estando presente em altas concentrações no fluido seminal; sua diminuição também é associada ao câncer de próstata (hidrolisada pela enzima ácido prostático fosfatase) (94,95). Em relação aos marcadores lipídicos observa-se que inicialmente triacilgliceróis mantém-se praticamente inalterados ou aumentados em relação ao controle, o que condiz com o aumento da biogênese de lipídeos promovida por flavivírus; entretanto, ocorre uma diminuição dessas espécies com o tempo, acompanhado do aumento dos nívels de monoacilglicerois e acilcarnitinas. Tais observações comprovam o aumento e acúmulo inicial de lipídeos complexos seguido da tendência à lipólise e à oxidação de ácido graxos, em acordo com registros anteriores sobre a ação de flavivirus (23,24,26–28). Adicionalmente, acilcarnitina foi apontada como principal marcador de infecção persistente por algoritmos de ML. Portanto, através dos marcadores anotados pode-se sugerir que na infecção persistente de células normais da próstata ocorre um aumento de demanda energética e estresse oxidativo com o tempo de infecção pelo ZIKV.

Em contraste com as células epiteliais, células de adenocarcinoma da próstata de estágio metastático são mais susceptíveis aos efeitos antiproliferativos do ZIKV. Dentre os marcadores observados, destaca-se o aumento de ácido eicosapentaenoico (FA 20:5), o qual já foi reportado como inibidor da fosforilação de proteínas envolvidas com sinalização de morte celular, além da indução da superprodução de espécies reativas de oxigênio (96). Tal observação é acompanhada por significante redução dos níveis de glutationa, a qual possui função antioxidativa (90). A diferença de resposta entre células normais e células tumorais da próstata evidencia que o efeito da infecção persistente é dependente do tipo celular. Uma vez que células normais, embora estressadas pela infecção, não sucumbem à morte celular como as células

tumorais, tais evidências reforçam e apontam para o efeito oncolítico induzido pelo ZIKV em células de alta proliferação.

Embora células normais e tumorais da próstata se comportem de forma diferente em relação à proliferação frente à infecção pelo ZIKV, o direto uso do vírus, sem modificações, como forma de terapia tumoral é controverso e limitado. A ausência de morte celular na infecção prolongada não elimina a extensa alteração metabólica provocada pela infecção viral. Inflamações crônicas são fatores contribuintes no desenvolvimento de tumores a partir de células normais. Consequentemente, modificações estruturais na partícula viral são necessárias para seu uso como terapia.

Estudos anteriores demonstraram a possibilidade do uso de partículas de Zika modificadas como terapias tumorais. Em estudo realizado por Chen et al. (2018) com células de glioblastoma, um protótipo de vírus atenuado desencadou resposta imune antiviral e de inflamação, diminuindo a proliferação do tumor (32). Já Martins et al (2018) conjugou a partícula viral com vesículas de membrana extracelular (OMV) de *Neisseria meningitidis* para a criação de uma vacina (33). Além de promover resposta imune contra o vírus da Zika em modelos animais, em estudo de Dabaja et al. 2018 tal protótipo (ZVp) apresentou efeito citostático em linhagens tumorais como glioblastoma (U-251), câncer de ovário (OVCAR-03) e de próstata (PC-3) (33,50). Neste projeto, as alterações metabólicas induzidas pelo protótipo ZVp em células PC-3 que desencadeiam o efeito antiproliferativo foram investigadas através da metabolômica. Dentre os marcadores elucidados observa-se alterações no metabolismo lipídico, com a presença do aumento relativo de fosfolipídeos e ceramidas, assim como marcadores de processos inflamatórios, precursores da síntese de N-glicanos, porfirinas e derivados de folato. O aumento de ceramidas está relacionado com o estresse celular e indução de disfunção mitocondrial, além de ter sido reportado como um ativador de processos autofágicos e apoptóticos em células cancerosas (97). Outros lipídeos, como fosfatidiletanolamina e fosfatidilinositol são abundantes em membranas celulares, e encontram-se aumentados na condição exposta ao ZVp. Fosfatidiletanolaminas intracelulares participam de processos autofágicos através de ancoragem com a proteína LC3 (98), enquanto que fosfatidilinositóis são importantes precursores da via PI3K/Akt também

envolvida na autofagia (10). Também foram observados aumento nos níveis de porfirinas, que quando acumuladas induzem aumento de estresse oxidativo (99), precursores de N-glicanos, que podem estar relacionados à disfunção de retículo endoplasmático na glicosilação de proteínas (100), e um derivado de folato, envolvido na manutenção do metabolismo do carbono e processos de metilação (101). De forma geral, os biomarcadores encontrados estão relacionados com extenso remodelamento lipídico e alterações celulares envolvendo estresse oxidativo e efeitos antiproliferativos que justificam a observação de efeito citostático do ZVp em células PC-3.

6. CONCLUSÃO

Infecções virais são conhecidas por desencadear intenso remodelamento lipídico e metabólico nas células do hospedeiro. A forma com que isso ocorre é dependente do tipo celular e vírus investigado, levando a um número fatorial de metabólitos que podem estar envolvidos nas manifestações da doença. Nesse estudo, a análise metabolômica associada a uma técnica sensível e robusta como a espectrometria de massas permitiu a análise exploratória e não direcionada do metaboloma celular. A análise do fenótipo de células epiteliais (PNT1a) e de câncer de próstata (PC-3) sob a influência do vírus da Zika levou à identificação de potenciais marcadores de infecção. Em células PNT1a foi possível determinar que o ZIKV promove infecção persistente mediada por alterações nos níveis de glicerolipídios, acilcarnitinas, ácido graxos e oxilipinas, e pequenos metabólitos resultantes do estresse oxidativo e mediadores de progressão tumoral. Já as células PC-3 mostraram-se mais susceptíveis aos efeitos antiproliferativos do ZIKV apontando para o potential oncolítico do vírus em células tumorais da próstata. Como recorte do metabolismo das células PC-3 sob infecção pelo ZIKV, observa-se o aumento de ácido graxo e oxilipina com efeitos antiproliferativos em conjunto à diminuição de molécula protetora no estresse oxidativo, o que justifica o fenótipo observado. Devido à limitação no emprego de patógeno virulento como terapia tumoral, neste estudo as alterações metabólicas induzidas por um protótipo (ZVp) foram avaliadas, as quais apontam o envolvimento de lipídeos e metabólitos envolvidos na sinalização de morte celular. Em conjunto, os metabólitos identificados neste estudo corroboram e agregam à literatura informações metabólicas relacionadas ao fenótipo de células da próstata sob efeito do Zika e reforçam a dualidade de benefícios e precauções necessárias no potencial uso do Zika como terapia.

7. REFERÊNCIAS

1. Petersen LR, Jamieson DJ, Powers AM, Honein MA. Zika Virus (Review Article). New England Journal of Medicine. 2016;374(16):1552–63.

2. Hennessey M, Fischer M, Staples JE. Zika Virus Spreads to New Areas - Region of the Americas, May 2015-January 2016. American Journal of Transplantation. 2016;16(3):1031–4.

3. Boeuf P, Drummer HE, Richards JS, Scoullar MJL, Beeson JG. The global threat of Zika virus to pregnancy: Epidemiology, clinical perspectives, mechanisms, and impact. BMC Med. 2016;14(1):1–9.

4. Landry ML, St George K. Laboratory diagnosis of zika virus infection. Arch Pathol Lab Med. 2017;141(1):60–7.

5. Cao-Lormeau VM, Blake A, Mons S, Lastère S, Roche C, Vanhomwegen J, et al. Guillain-Barré Syndrome outbreak associated with Zika virus infection in French Polynesia: A case-control study. The Lancet. 2016;387(10027):1531–9.

6. Garcez PP, Nascimento JM, de Vasconcelos JM, Madeiro Da Costa R, Delvecchio R, Trindade P, et al. Zika virus disrupts molecular fingerprinting of human neurospheres. Sci Rep. 2017;7:1–10.

7. Tang H, Hammack C, Ogden SC, Wen Z, Qian X, Li Y, et al. Zika virus infects human cortical neural progenitors and attenuates their growth. Cell Stem Cell. 2016;18(5):587–90.

8. Li C, Xu D, Ye Q, Hong S, Jiang Y, Liu X, et al. Zika Virus Disrupts Neural Progenitor Development and Leads to Microcephaly in Mice. Cell Stem Cell. 2016;19(1):120–6.

9. Garcez PP, Loiola EC, da Costa RM, Higa LM, Trindade P, Delvecchio R, et al. Zika virus: Zika virus impairs growth in human neurospheres and brain organoids. Science (1979). 2016;352(6287):816–8.

10. Liang Q, Luo Z, Zeng J, Chen W, Foo SS, Lee SA, et al. Zika Virus NS4A and NS4B Proteins Deregulate Akt-mTOR Signaling in Human Fetal

Neural Stem Cells to Inhibit Neurogenesis and Induce Autophagy. Cell Stem Cell. 2016;19(5):663–71.

11. Cugola FR, Fernandes IR, Russo FB, Freitas BC, Dias JLM, Guimarães KP, et al. The Brazilian Zika virus strain causes birth defects in experimental models. Nature. 2016;534(7606):267–71.

12. Lee I, Bos S, Li G, Wang S, Gadea G, Desprès P, et al. Probing molecular insights into Zika virus–host interactions. Viruses. 2018;10(5):233.

13. el Ghouzzi V, Bianchi FT, Molineris I, Mounce BC, Berto GE, Rak M, et al. ZIKA virus elicits P53 activation and genotoxic stress in human neural progenitors similar to mutations involved in severe forms of genetic microcephaly and p53. Cell Death Dis. 2016;7(10):e2440.

14. Ferreira RO, Garcez PP. Dissecting the Toxic Effects of Zika Virus Proteins on Neural Progenitor Cells. Neuron. 2019;101(6):989–91.

15. Rosa-Fernandes L, Cugola FR, Russo FB, Kawahara R, de Melo Freire CC, Leite PEC, et al. Zika virus impairs neurogenesis and synaptogenesis pathways in human neural stem cells and neurons. Front Cell Neurosci. 2019;13:64.

16. Islam MS, Khan MAAK, Murad MW, Karim M, Islam ABMMK. In silico analysis revealed Zika virus miRNAs associated with viral pathogenesis through alteration of host genes involved in immune response and neurological functions. J Med Virol. 2019;91(9):1584–94.

17. Carbaugh DL, Baric RS, Lazear HM. Envelope Protein Glycosylation Mediates Zika Virus Pathogenesis. J Virol. 2019;93(12):e00113-19.

18. Monel B, Compton AA, Bruel T, Amraoui S, Burlaud-Gaillard J, Roy N, et al. Zika virus induces massive cytoplasmic vacuolization and paraptosis-like death in infected cells. EMBO J. 2017;36(12):1653–68.

19. Alfano C, Gladwyn-Ng I, Couderc T, Lecuit M, Nguyen L. The unfolded protein response: A key player in zika virus-associated congenital microcephaly. Front Cell Neurosci. 2019;13:94.

20. Delafiori J, Navarro LC, Siciliano RF, de Melo GC, Busanello ENB, Nicolau JC, et al. Covid-19 Automated Diagnosis and Risk Assessment through Metabolomics and Machine Learning. Anal Chem. 2021;93(4):2471–9.

21. Melo CFOR, Navarro LC, de Oliveira DN, Guerreiro TM, Lima E de O, Delafiori J, et al. A machine learning application based in random forest for integrating mass spectrometry-based metabolomic data: A simple screening method for patients with Zika virus. Front Bioeng Biotechnol. 2018;6:31.

22. Melo CFOR, Delafiori J, de Oliveira DN, Guerreiro TM, Esteves CZ, Lima E de O, et al. Serum metabolic alterations upon ZIKA infection. Front Microbiol. 2017;8:1954.

23. Byers NM, Fleshman AC, Perera R, Molins CR. Metabolomic insights into human arboviral infections: Dengue, chikungunya, and zika viruses. Viruses. 2019;11(3):225.

24. Martín-Acebes MA, Vázquez-Calvo Á, Saiz JC. Lipids and flaviviruses, present and future perspectives for the control of dengue, Zika, and West Nile viruses. Prog Lipid Res. 2016;64:123–37.

25. Mansuy JM, Dutertre M, Mengelle C, Fourcade C, Marchou B, Delobel P, et al. Zika virus: High infectious viral load in semen, a new sexually transmitted pathogen? Lancet Infect Dis. 2016;16(4):405.

26. Leier HC, Weinstein JB, Kyle JE, Lee JY, Bramer LM, Stratton KG, et al. A global lipid map defines a network essential for Zika virus replication. Nat Commun. 2020;11(1):1–5.

27. Cloherty APM, Olmstead AD, Ribeiro CMS, Jean F. Hijacking of lipid droplets by hepatitis C, dengue and zika viruses-from viral protein moonlighting to extracellular release. Int J Mol Sci. 2020;21(21):7901.

28. Monson EA, Crosse KM, Duan M, Chen W, O'Shea RD, Wakim LM, et al. Intracellular lipid droplet accumulation occurs early following viral infection and is required for an efficient interferon response. Nat Commun. 2021;12(1):1–7.

29. Tang DG, La E, Kern J, Kehrer JP. Fatty acid oxidation and signaling in apoptosis. Biol Chem. 2002;383:425–42.

30. Diop F, Vial T, Ferraris P, Wichit S, Bengue M, Hamel R, et al. Zika virus infection modulates the metabolomic profile of microglial cells. PLoS One. 2018;13(10):e0206093.

31. Larocca RA, Abbink P, Peron JPS, Zanotto PMDA, Iampietro MJ, Badamchi-Zadeh A, et al. Vaccine protection against Zika virus from Brazil. Nature. 2016;536(7617):474–8.

32. Chen Q, Wu J, Ye Q, Ma F, Zhu Q, Wu Y, et al. Treatment of human glioblastoma with a live attenuated Zika virus vaccine candidate. mBio. 2018;9(5):e01683-18.

33. Martins P, Machado D, Theizen TH, Guarnieri JPO, Bernardes BG, Gomide GP, et al. Outer membrane vesicles from neisseria meningitidis (proteossome) used for nanostructured Zika virus vaccine production. Sci Rep. 2018;8(1):1–10.

34. Shaily S, Upadhya A. Zika virus: Molecular responses and tissue tropism in the mammalian host. Rev Med Virol. 2019;29(4):e2050.

35. Miner JJ, Diamond MS. Zika Virus Pathogenesis and Tissue Tropism. Cell Host Microbe. 2017;21(2):134–42.

36. Meertens L, Labeau A, Dejarnac O, Cipriani S, Sinigaglia L, Bonnet-Madin L, et al. Axl Mediates ZIKA Virus Entry in Human Glial Cells and Modulates Innate Immune Responses. Cell Rep. 2017;18(2):324–33.

37. Spencer JL, Lahon A, Tran LL, Arya RP, Kneubehl AR, Vogt MB, et al. Replication of Zika virus in human prostate cells: A potential source of sexually transmitted virus. Journal of Infectious Diseases. 2018;217(4):538–47.

38. Machado FC, Bittar C, Rahal P, Calmon MF. Identification of differentially expressed miRNAs in human cells infected with different Zika virus strains. Arch Virol. 2021;166(6):1681–9.

39. Izuagbe RE. A prostate cell line model of persistent Zika virus infection [Master of Applied Science]. [Brisbane]: Queensland University of Technology; 2019.

40. Kumar A, Jovel J, Lopez-Orozco J, Limonta D, Airo AM, Hou S, et al. Human sertoli cells support high levels of zika virus replication and persistence. Sci Rep. 2018;8(1):1–11.

41. Ma W, Li S, Ma S, Jia L, Zhang F, Zhang Y, et al. Zika Virus Causes Testis Damage and Leads to Male Infertility in Mice. Cell. 2016;167(6):1511–24.

42. Oliveira DBL, Durigon GS, Mendes ÉA, Ladner JT, Andreata-Santos R, Araujo DB, et al. Persistence and intra-host genetic evolution of zika virus infection in symptomatic adults: A special view in the male reproductive system. Viruses. 2018;10(11):615.

43. Kaid C, Goulart E, Caires-Júnior LC, Araujo BHS, Soares-Schanoski A, Bueno HMS, et al. Zika virus selectively kills aggressive human embryonal CNS tumor cells in vitro and in vivo. Cancer Res. 2018;78(12):3363–74.

44. Ball EE, Pesavento PA, van Rompay KKA, Keel MK, Singapuri A, Gomez-Vazquez JP, et al. Zika virus persistence in the male macaque reproductive tract. PLoS Negl Trop Dis. 2022 Jul 5;16(7):e0010566.

45. Paz-Bailey G, Rosenberg ES, Doyle K, Munoz-Jordan J, Santiago GA, Klein L, et al. Persistence of Zika Virus in Body Fluids — Final Report. New England Journal of Medicine. 2018;379(13):198.

46. Armitage EG, Barbas C. Metabolomics in cancer biomarker discovery: Current trends and future perspectives. J Pharm Biomed Anal. 2014;87:1–11.

47. Vitiello GAF, Ferreira WAS, Cordeiro de Lima VC, Medina T da S. Antiviral Responses in Cancer: Boosting Antitumor Immunity Through Activation of Interferon Pathway in the Tumor Microenvironment. Front Immunol. 2021;12:5126.

48. Vähä-Koskela MJV, Heikkilä JE, Hinkkanen AE. Oncolytic viruses in cancer therapy. Cancer Lett. 2007 Sep;254(2):178–216.

49. Mazar J, Li Y, Rosado A, Phelan P, Kedarinath K, Parks GD, et al. Zika virus as an oncolytic treatment of human neuroblastoma cells requires CD24. PLoS One. 2018;13(7):.e0200358.

50. Dabaja MZ, Lima E de O, de Oliveira DN, Guerreiro TM, Melo CFOR, Morishita KN, et al. Metabolic alterations induced by attenuated Zika virus in glioblastoma cells. Cell Biosci. 2018;8(1):1–9.

51. Zhu Z, Gorman MJ, McKenzie LD, Chai JN, Hubert CG, Prager BC, et al. Zika virus has oncolytic activity against glioblastoma stem cells. Journal of Experimental Medicine. 2017;214(10):2843–57.

52. Li H, Hu Y, Huang J, Feng Y, Zhang Z, Zhong K, et al. Zika virus NS5 protein inhibits cell growth and invasion of glioma. Biochem Biophys Res Commun. 2019;516(2):515–20.

53. Iannolo G, Sciuto MR, Cuscino N, Pallini R, Douradinha B, Ricci Vitiani L, et al. Zika virus infection induces MiR34c expression in glioblastoma stem cells: new perspectives for brain tumor treatments. Cell Death Dis. 2019;10(4):1–10.

54. Eidelman E, Twum-Ampofo J, Ansari J, Siddiqui MM. The metabolic phenotype of prostate cancer. Front Oncol. 2017;7:131.

55. Cutruzzolà F, Giardina G, Marani M, Macone A, Paiardini A, Rinaldo S, et al. Glucose metabolism in the progression of prostate cancer. Front Physiol. 2017;8:97.

56. Elia I, Schmieder R, Christen S, Fendt SM. Organ-specific cancer metabolism and its potential for therapy. In: Handbook of Experimental Pharmacology. 2016. p. 321–53.

57. Andersen MK, Krossa S, Høiem TS, Buchholz R, Claes BSR, Balluff B, et al. Simultaneous Detection of Zinc and Its Pathway Metabolites Using MALDI MS Imaging of Prostate Tissue. Anal Chem. 2020;92(4):3171–9.

58. Liu Y. Fatty acid oxidation is a dominant bioenergetic pathway in prostate cancer. Prostate Cancer Prostatic Dis. 2006;9(3):230–4.

59. Xu H, Chen Y, Gu M, Liu C, Chen Q, Zhan M, et al. Fatty acid metabolism reprogramming in advanced prostate cancer. Metabolites. 2021;11(11):765.

60. Sung H, Ferlay J, Siegel RL, Laversanne M, Soerjomataram I, Jemal A, et al. Global cancer statistics 2020: GLOBOCAN estimates of incidence and mortality worldwide for 36 cancers in 185 countries. CA Cancer J Clin. 2021;71(3):209–49.

61. Stewart RW, Lizama S, Peairs K, Sateia HF, Choi Y. Screening for prostate cancer. Semin Oncol. 2017 Feb;44(1):47–56.

62. Litwin MS, Tan HJ. The diagnosis and treatment of prostate cancer: A review. JAMA - Journal of the American Medical Association. 2017;317(24):2532–42.

63. Epstein JI, Egevad L, Amin MB, Delahunt B, Srigley JR, Humphrey PA. The 2014 international society of urological pathology (ISUP) consensus conference on gleason grading of prostatic carcinoma definition of grading patterns and proposal for a new grading system. American Journal of Surgical Pathology. 2016;40(2):244–52.

64. Bilusic M, Madan RA, Gulley JL. Immunotherapy of prostate cancer: Facts and hopes. Clinical Cancer Research. 2017;23(22):6764–70.

65. Nuhn P, de Bono JS, Fizazi K, Freedland SJ, Grilli M, Kantoff PW, et al. Update on Systemic Prostate Cancer Therapies: Management of Metastatic Castration-resistant Prostate Cancer in the Era of Precision Oncology. Eur Urol. 2019;75(1):88–99.

66. Crawford ED, Heidenreich A, Lawrentschuk N, Tombal B, Pompeo ACL, Mendoza-Valdes A, et al. Androgen-targeted therapy in men with prostate cancer: evolving practice and future considerations. Prostate Cancer Prostatic Dis. 2019;22(1):24–38.

67. Mamas M, Dunn WB, Neyses L, Goodacre R. The role of metabolites and metabolomics in clinically applicable biomarkers of disease. Arch Toxicol. 2011;85(1):5–17.

68. Kaddurah-Daouk R, Kristal BS, Weinshilboum RM. Metabolomics: A global biochemical approach to drug response and disease. Annu Rev Pharmacol Toxicol. 2008;48:653–83.

69. Dettmer K, Aronov PA, Hammock BD. Mass spectrometry-based metabolomics. Mass Spectrom Rev. 2007 Jan;26(1):51–78.

70. Sussulini A. Metabolomics: From Fundamentals to Clinical Applications. 1st ed. Vol. 965. Springer; 2017. 1–350 p.

71. Schrimpe-Rutledge AC, Codreanu SG, Sherrod SD, McLean JA. Untargeted Metabolomics Strategies—Challenges and Emerging Directions. J Am Soc Mass Spectrom. 2016;27(12):1897–905.

72. Gross JH. Mass spectrometry: A textbook: Second edition. Mass Spectrometry: A Textbook: Second Edition. 2011.

73. Breiman L. Random Forests. Mach Learn. 2001;45(1):5–32.

74. Kourou K, Exarchos TP, Exarchos KP, Karamouzis M v., Fotiadis DI. Machine learning applications in cancer prognosis and prediction. Comput Struct Biotechnol J. 2015;13:8–17.

75. Trock BJ. Application of metabolomics to prostate cancer. Urologic Oncology: Seminars and Original Investigations. 2011;29(5):572–81.

76. Lima AR, Bastos M de L, Carvalho M, Guedes de Pinho P. Biomarker discovery in human prostate cancer: An update in metabolomics studies. Transl Oncol. 2016;9(4):357–70.

77. Andersen MK, Høiem TS, Claes BSR, Balluff B, Martin-Lorenzo M, Richardsen E, et al. Spatial differentiation of metabolism in prostate cancer tissue by MALDI-TOF MSI. Cancer Metab. 2021;9(1):1–13.

78. Liang Q, Liu H, Xie L xiang, Li X, Zhang AH. High-throughput metabolomics enables biomarker discovery in prostate cancer. RSC Adv. 2017;7(5):2587–93.

79. de Hoffmann E, Stroobant V. Mass Spectrometry: Principles and applications. 3rd Edition. John Wiley & Sons; 2007.

80. Fenn JB, Mann M, Meng CK, Wong SF, Whitehouse CM. Electrospray ionization for mass spectrometry of large biomolecules. Vol. 246, Science. 1989.

81. Cunsolo V, Muccilli V, Saletti R, Foti S. Mass spectrometry in food proteomics: a tutorial. Journal of Mass Spectrometry. 2014;49(9):768–84.

82. Bairoch A. The cellosaurus, a cell-line knowledge resource. Journal of Biomolecular Techniques. 2018;29(2):25.

83. Kaighn ME, Narayan KS, Ohnuki Y, Lechner JF, Jones LW. Establishment and characterization of a human prostatic carcinoma cell line (PC-3). Invest Urol. 1979;17(1):16–23.

84. Ikediobi ON, Davies H, Bignell G, Edkins S, Stevens C, O'Meara S, et al. Mutation analysis of 24 known cancer genes in the NCI-60 cell line set. Mol Cancer Ther. 2006;5(11):2606–12.

85. Melo CFOR, de Oliveira DN, de Oliveira Lima E, Guerreiro TM, Esteves CZ, Beck RM, et al. A lipidomics approach in the characterization of zika-infected mosquito cells: Potential targets for breaking the transmission cycle. PLoS One. 2016;11(10):e0164377.

86. Alves DA, Mattos IB, Hollanda LM, Lancellotti M. Use of mesoporous silica SBa-15 and SBa-16 in association of outer membrane vesicles - OMV from Neisseria meningitidis. J Vaccines Vaccin. 2013;4:6.

87. Junior WAR, Gomes DB, Zanchet B, Schönell AP, Diel KAP, Banzato TP, et al. Antiproliferative effects of pinostrobin and 5,6-dehydrokavain isolated from leaves of Alpinia zerumbet. Revista Brasileira de Farmacognosia. 2017 Sep;27(5):592–8.

88. Chong J, Xia J. Using MetaboAnalyst 4.0 for Metabolomics Data Analysis, Interpretation, and Integration with Other Omics Data. In: Methods in Molecular Biology. Springer; 2020. p. 337–60.

89. Delafiori J, Lima E de O, Dabaja MZ, Dias-Audibert FL, de Oliveira DN, Melo CFOR, et al. Molecular signatures associated with prostate cancer cell line (PC-3) exposure to inactivated Zika virus. Sci Rep. 2019;9(1):1–10.

90. Motrich RD, Salazar FC, Breser ML, Mackern-Oberti JP, Godoy GJ, Olivera C, et al. Implications of prostate inflammation on male fertility. Andrologia. 2018;50(11):e13093.

91. Campolo N, Issoglio FM, Estrin DA, Bartesaghi S, Radi R. 3-Nitrotyrosine and related derivatives in proteins: Precursors, radical intermediates and impact in function. Essays Biochem. 2020;64(1):111–33.

92. Zhan X, Wang X, Desiderio DM. Mass spectrometry analysis of nitrotyrosine-containing proteins. Mass Spectrom Rev. 2015;34(4):423–48.

93. Ohtake S, Kawahara T, Ishiguro Y, Takeshima T, Kuroda S, Izumi K, et al. Oxidative stress marker 8-hydroxyguanosine is more highly expressed in prostate cancer than in benign prostatic hyperplasia. Mol Clin Oncol. 2018;9(3):302–4.

94. Hassan MI, Aijaz A, Ahmad F. Structural and functional analysis of human prostatic acid phosphatase. Expert Rev Anticancer Ther. 2010;10(7):1055–68.

95. Wyss M, Kaddurah-Daouk R. Creatine and creatinine metabolism. Physiol Rev. 2000;80(3):1107–213.

96. Oono K, Ohtake K, Watanabe C, Shiba S, Sekiya T, Kasono K. Contribution of Pyk2 pathway and reactive oxygen species (ROS) to the anti-cancer effects of eicosapentaenoic acid (EPA) in PC3 prostate cancer cells. Lipids Health Dis. 2020;19(1):1–12.

97. Morad SAF, Cabot MC. Ceramide-orchestrated signalling in cancer cells. Nat Rev Cancer. 2013;13(1):51–65.

98. Rockenfeller P, Koska M, Pietrocola F, Minois N, Knittelfelder O, Sica V, et al. Phosphatidylethanolamine positively regulates autophagy and longevity. Cell Death Differ. 2015;22(3):499–508.

99. Yang X, Palasuberniam P, Kraus D, Chen B. Aminolevulinic acid-based tumor detection and therapy: Molecular mechanisms and strategies for enhancement. Int J Mol Sci. 2015;16(10):25865–80.

100. Xu C, Ng DTW. Glycosylation-directed quality control of protein folding. Nat Rev Mol Cell Biol. 2015;16(12):742–52.

101. Litwack G. Folic Acid and Folates. 1st ed. Vol. 79. Academic Press; 2008. 1–480 p.

ANEXO 1

Cadastro no Sistema Nacional de Gestão do Patrimônio Genético e do Conhecimento Tradicional Associado (SisGen)

Ministério do Meio Ambiente
CONSELHO DE GESTÃO DO PATRIMÔNIO GENÉTICO
SISTEMA NACIONAL DE GESTÃO DO PATRIMÔNIO GENÉTICO E DO CONHECIMENTO TRADICIONAL ASSOCIADO

Comprovante de Cadastro de Acesso
Cadastro nº AB1FDB9

A atividade de acesso ao Patrimônio Genético, nos termos abaixo resumida, foi cadastrada no SisGen, em atendimento ao previsto na Lei nº 13.123/2015 e seus regulamentos.

Número do cadastro:	AB1FDB9
Usuário:	Rodrigo Ramos Catharino
CPF/CNPJ:	214.063.228-14
Objeto do Acesso:	Patrimônio Genético
Finalidade do Acesso:	Pesquisa

Espécie
Oropouche orthobunyavirus
Zika virus

Título da Atividade:	Metabolômica na era das deonças infecciosas virais emergentes: abordagens para investigação fisiopatológica, diagnóstica e de novos alvos moleculares

Equipe	
Jeany Delafiori	INDEPENDENTE
Natalia Mor	Independente
Rodrigo Ramos Catharino	UNICAMP

Data do Cadastro:	11/03/2021 09:36:38
Situação do Cadastro:	Concluído

Conselho de Gestão do Patrimônio Genético
Situação cadastral conforme consulta ao SisGen em 9:37 de 11/03/2021.

SISTEMA NACIONAL DE GESTÃO DO PATRIMÔNIO GENÉTICO E DO CONHECIMENTO TRADICIONAL ASSOCIADO - SISGEN

ANEXO 2

Permissão de inclusão de artigo em tese – *Journal of Proteome Research*

1/9/23, 3:03 PM Rightslink® by Copyright Clearance Center

CCC RightsLink

Home | Help | Live Chat | Sign in | Create Account

Unraveling the Metabolic Alterations Induced by Zika Infection in Prostate Epithelial (PNT1a) and Adenocarcinoma (PC-3) Cell Lines

ACS Publications
Most Trusted. Most Cited. Most Read.

Author: Jeany Delafiori, Alessandra V. de S. Faria, Arthur N. de Oliveira, et al
Publication: Journal of Proteome Research
Publisher: American Chemical Society
Date: Jan 1, 2023

Copyright © 2023, American Chemical Society

Quick Price Estimate

This service provides permission for reuse only. If you do not have a copy of the portion you are using, you may copy and paste the content and reuse according to the terms of your agreement. Please be advised that obtaining the content you license is a separate transaction not involving RightsLink.

Permission for this particular request is granted for print and electronic formats, and translations, at no charge. Figures and tables may be modified. Appropriate credit should be given. Please print this page for your records and provide a copy to your publisher. Requests for up to 4 figures require only this record. Five or more figures will generate a printout of additional terms and conditions. Appropriate credit should read: "Reprinted with permission from {COMPLETE REFERENCE CITATION}. Copyright {YEAR} American Chemical Society." Insert appropriate information in place of the capitalized words.

I would like to... reuse in a Thesis/Dissertatio | Format Print and Electronic
Requestor Type Author (original work) | Select your currency USD - $
Portion Full article | Quick Price Click Quick Price
QUICK PRICE CONTINUE

To request permission for a type of use not listed, please contact the publisher directly.

Declaração sobre direito autoral

Declaro que segundo as políticas de direitos autorais da revista *Journal of Proteome Research* é permitida a reprodução do artigo submetido/aceito/publicado em tese e dissertação de forma impressa ou eletronicamente na versão original ou traduzida.

Reprinted with permission from Delafiori, J., Faria, A. V. de S., de Oliveira, A. N., Sales, G. M., Dias-Audibert, F. L., Catharino, R. R. Unraveling the

metabolic alterations induced by Zika infection in prostate epithelial (PNT1a) and adenocarcinoma (PC-3) cell lines. J. Proteome Res. 2023, 22, 193-203. https://doi.org/10.1021/acs.jproteome.2c00630. Copyright 2023 American Chemical Society

ANEXO 3

Permissão de inclusão de artigo em tese – *Scientific Reports*

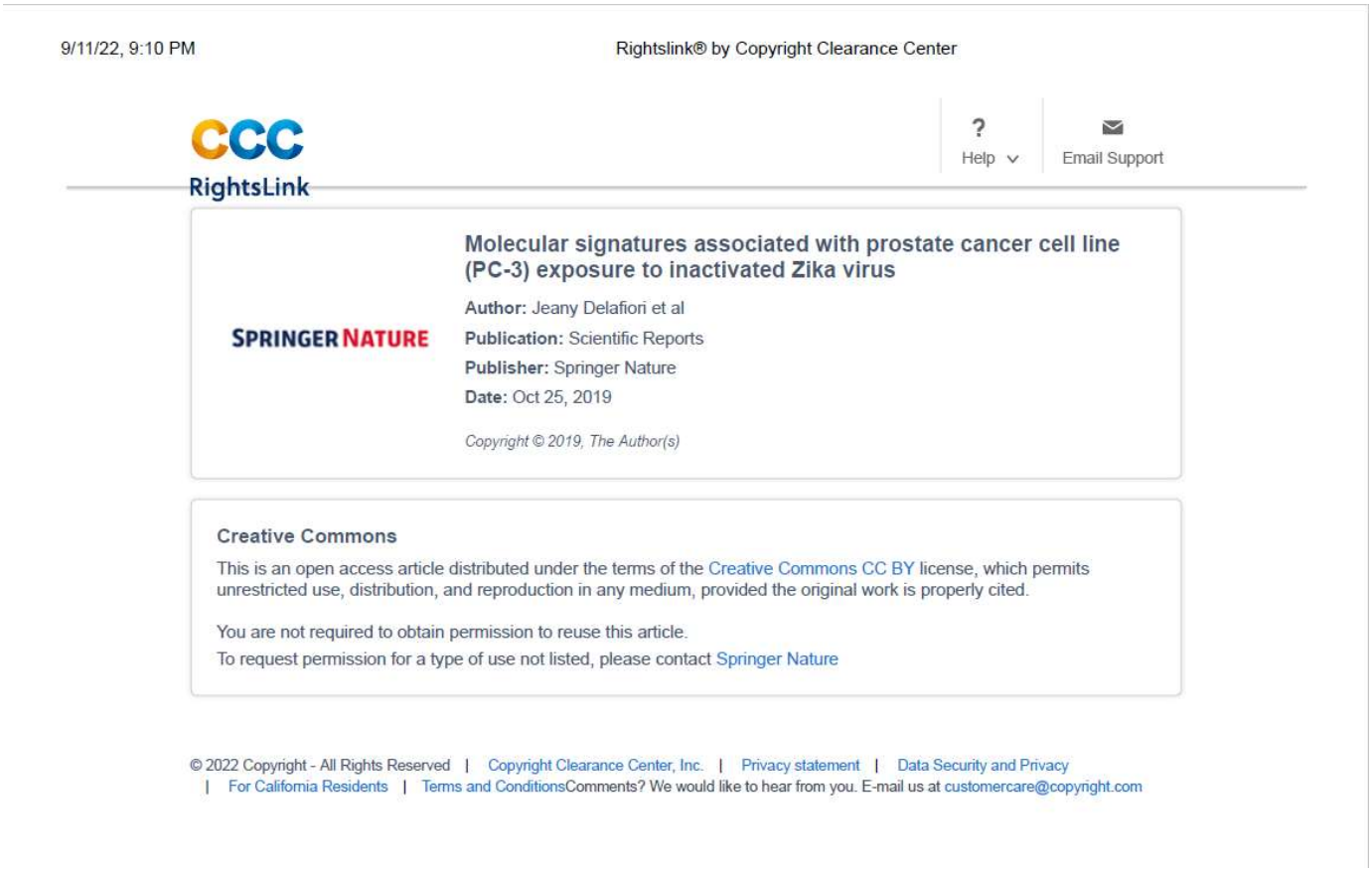

9/11/22, 9:10 PM Rightslink® by Copyright Clearance Center

RightsLink

Help Email Support

SPRINGER NATURE

Molecular signatures associated with prostate cancer cell line (PC-3) exposure to inactivated Zika virus

Author: Jeany Delafiori et al
Publication: Scientific Reports
Publisher: Springer Nature
Date: Oct 25, 2019

Copyright © 2019, The Author(s)

Creative Commons

This is an open access article distributed under the terms of the Creative Commons CC BY license, which permits unrestricted use, distribution, and reproduction in any medium, provided the original work is properly cited.

You are not required to obtain permission to reuse this article.
To request permission for a type of use not listed, please contact Springer Nature

Declaração sobre direito autoral

Declaro que segundo as políticas de direitos autorais da revista *Scientific Reports,* o artigo foi publicado em regime aberto (*Open Access),* não necessitando autorização para reprodução nesta tese.